Surface waves modelling and analysis in media of increasing degrees of complexity

Ludovic Bodet

Sorbonne Université - Faculté des Sciences et Ingénierie

Mémoire d'Habilitation à Diriger des Recherches, présenté en soutenance le 01/10/2019 devant le jury composé de :

Stéphane GARAMBOIS (Université Grenoble Alpes)	Rapporteur
Cyrille FAUCHARD (CEREMA)	Rapporteur
Jean-François SEMBLAT (ENSTA Paristech)	Rapporteur
Odile ABRAHAM (IFSTTAR)	Examinatrice
Alexis MAINEULT (CNRS-Sorbonne Université)	Examinateur

Surface waves modelling and analysis in media of increasing degrees of complexity

L. Bodet[a]

[a] *Sorbonne Université, CNRS, EPHE, UMR 7619 METIS, 4 place Jussieu, 75252 Paris 05, France*
ludovic.bodet@sorbonne-universite.fr

Abstract

Seismic surface waves analysis has become a relatively standard tool for a wide range of applications in Earth sciences, mainly to evaluate soils and rocks shear properties and to image near-surface heterogeneities. The underlying theories, the data processing workflows and interpretation methods are quite similar whatever the scales of interest (from global seismology to ultrasonic non-destructive testing). In each domain, the acquisition techniques are rapidly evolving with the development of innovative sensors enabling: wireless 3-components surveys; dense arrays; distributed measurements; continuous monitoring etc. In the meantime, most operational analysis tools remain based on the approximations that the wavefields mainly involve plain waves and that the probed media are elastic and stratified with smooth geometries compared to recorded wavelengths. Even if numerical modelling and data processing methods have made huge progresses in the last ten years (for instance with the democratisation of massively parallel computing platforms), addressing theoretical and methodological issues related to near-surface seismic prospecting is difficult as soon as the 3D nature of the Earth and its high degree of heterogeneity have to be taken into account, which is quite frequent, though! More than 15 years ago, we suggested the use of laboratory physical modelling and laser-Doppler small-scale surveys to complement numerical studies and to perform experimental benchmarks –and sometimes validations– of surface-wave processing and inversion techniques. In this manuscript we show how, since then, we developed this approach on 3D physical models of increasing degrees of complexity, in order to study seismic-wave propagation in unconsolidated and porous media, so as to target near-surface environmental, geological and geotechnical applications. We also provide guidelines for practitioners regarding the operational use and limits of surface-wave methods, e.g.: their ability to track compaction and rigidity anomalies in natural or artificial soils; the possible interpretation of near-surface seismic measurements in terms of spatio-temporal variations of water content. We also suggest alternative approaches to be addressed in the near future according to recent instrumental and computational developments cited supra.

Cite as: Bodet, L., 2019. Surface waves modelling and analysis in media of increasing degrees of complexity. Habilitation à Diriger des Recherche, English manuscript, 108 pages, Sorbonne Université.

Keywords: Signal processing, inverse problems, geophysics, seismic methods, guided waves, physical modelling, granular media

Status [Habilitation defended (2019/10/01) / Final manuscript, full English version, February 2020]

Contents

Acknowledgments

My first thought is for the one who gave me the real trigger (not to say a kick in the [...]) to prepare this HDR and whom I will never be able to thank as I would have liked.

Thank you so much to the one who actually gave me that kick (*ouch*) and supported me (*sorry about that*) during the questioning phases (this kind of retrospective work actually shows you every little things you didn't do, or did wrong, as well as every stupid and unproductive tasks you shouldn't have accepted... or that you should have dashed off without any professionalism instead of consciously achieving them).

I would also like to thank the committee who did me the honor of agreeing to read the manuscript and act as the jury of my defense, which I will remember as a very good moment.

Thank you to the colleagues and friends who came to attend [...] and did me the great honor to participate and animate the crucial post-defense informal buffet.

Finally, many thanks to the students and colleagues who contributed, in one way or another, to the projects presented in the following. To them, I dedicate one of my favorite quotes about applied geophysics:

- Volunteer #1: *'This new program's incredible. A few more years development and we won't even have to dig anymore'.*
- Dr. Alan Grant: *'Where's the fun in that?'.*

— quoting Michael Crichton and David Koepp

Short introduction and outline of the manuscript

'The real problem with colleagues preparing their HDR is they think they have to actually write it...', quoting J.-M. M. (2018)

About me (as of Februray 2020)

My background

After undergraduate studies in Physics in Poiters and Earth sciences in Rennes (France), I received a M.S. degree in Geophysics from the Institut de Physique du Globe de Paris (2000). I worked during two years as an engineering geophysicist in Fugro France S.A. (marine geophysics). In 2005, I received a Ph.D. in applied geophysics from the Université and Ecole Centrale de Nantes, France, after three years at the Laboratoire Central des Ponts et Chaussées (the 'French institute of science and technology for transport, development and networks' –now Gustave Eiffel University) and the Bureau de Recherches Géologiques et Minières (the French Geological Survey).

I was recruited as an Associate Professor (Maître de Conférences), first in Le Mans (2006-2010) then at Sorbonne Université (campus Pierre et Marie Curie, Paris). My research interests include physical modelling of wave propagation and seismic imaging (surface waves), granular media, signal processing and inverse problems in geophysics. I co-supervised 6 Ph.D. students and was PI and co-PI of several academic and industrial research projects. I am currently involved in French, international (EU, USA) programs in which I develop seismic-based approaches in near-surface geophysics applied to environmental sciences and civil engineering.

As written above, I am a "Maître de conférences" of the French academic system, which means I spend two-thirds of my time [1] dealing with collective administrative responsibilities, management of pedagogical projects and teams as wel as, of course, teaching (at Bachelor and Master's level approximately 240 hours per year). I am giving lectures, practicals and supervising field trips about: geophysics; signal processing; inverse problems; numerical modelling; basics of hydrogeology and applied geology...

Motivations (very brief foreword mainly for non-French and/or non-academic readers)

This "Diplôme d'Habilitation à Diriger les Recherches" actually is a higher education-sanctioned degree which, if I briefly and approximately translate the French law text (see www.legifrance.gouv.fr),

1. More details about my teaching and administrative activities in a detailed version of my resume available upon request.

'recognize the candidate's high scientific level, the originality of his approach in a field of science, his ability to master a research strategy in a sufficiently broad scientific or technological field and his ability to supervise young researchers'. It does not change much for me except I do not need any more to have a full professor co-supervising the PhD students working on the projects I am responsible for. In addition, I will be at higher rank in the councils and will be able to be in PhD committees as reviewer. Oh and yes, I am also now authorized to apply to full professor positions, having been evaluated by the National University Council!

Outline of the manuscript

My main research interests involve physical modelling and experiments, in the laboratory or on the field, for the study, the development and the validation of numerical methods, processing techniques or inversion tools dedicated to the characterisation of physical properties of natural or artificial environments in Earth sciences. My activity is divided in three main topics illustrated through three specific chapters in the following manuscript [2]. As suggested by is title, the natural link between these topics is the study and use of surface waves. Each chapter however can be considered independently, with associated introduction and general conclusions and perspectives.

Physical modelling of wave propagation using acoustic techniques and laser interferometry

The first chapter quickly introduces the use of small-scale laboratory models and laser-Doppler experiments as I developed it during my PhD thesis (Bodet, 2005). Its introduction is based on material available in Bodet et al. (2005, 2009a) and its main text mainly describes the way I applied the approach in Le Mans to study seismic-wave propagation in unconsolidated granular materials and then suggested alternative physical modelling tools (more particularly in the framework of projects funded by Région Pays de la Loire). It partly reproduces results available in Bodet et al. (2009b, 2010b, 2012); Dhemaied (2011); Dhemaied et al. (2011); Bergamo (2012); Bergamo et al. (2014); Bodet et al. (2014b); Pasquet et al. (2016a); Martin et al. (2018).

Analysis of guided seismic wave dispersion for multi-scale geophysical imaging

The second chapter illustrates this topic with the partial reproduction of internal reports (Bodet et al., 2014c, 2017) from industrial research contracts with SNCF Réseau, on the geophysical investigation of railways embankments with the help of Master's students whose results were presented in Rhamania (2015); Kyrkou (2016); Wacquier (2017); Heraibi (2019). This chapter was consequently in French and translated to a paper currently in preparation for submission.

Seismic methods as tools to study the Critical Zone

The third chapter presents the concepts and methodologies I have been developing, for the last 10 years, in order to include seismic methods in the hydrogeophysics' toolbox, in cooperation with my Master and PhD students in Le Mans and Paris, more particularly thanks to projects funded by Université Pierre et Marie Curie/Sorbonne Université, CNRS (INSU), as well as by the PIREN-Seine and CRITEX programs. The main text of this chapter partly reproduces contributions available in Duranteau (2010); Ezersky et al. (2013); Pasquet et al. (2015a,b); Pasquet and Bodet (2017); Schneider (2017); Dangeard et al. (2017b, 2018); Dangeard (2019); Dangeard et al. (2019).

2. Details about associated cooperations, funded projects, supervised students and published articles or reports can be found in a detailed version of my resume available upon request.

Chapter 1

Seismic-wave propagation in small-scale laboratory models

1.1. Introduction

1.1.1. Bridging the gap between numerical simulations and field data

Theoretical and experimental developments in acoustics have always been helpful to geophysicists investigating the propagation of mechanical waves through the Earth, whatever the scale of interest. Acoustics, non-destructive evaluation (NDE), exploration seismic and seismology obviously share common issues that can be addressed in parallel thanks to the development of innovative measurement devices and laboratory physical experiments (Blum et al., 2011a,b,c). Since the 1990s, laser-based ultrasonic techniques have been finding a wide range of applications in these domains, as anticipated by Scruby (1989), and have been providing appropriate tools for studying seismic-wave propagation. Among several interesting aspects, the main advantage of lasers is their non-contacting character, which makes it possible to generate mechanical waves or to record particle motion at the surface of many different types of materials, without any coupling. Additionally, these measurement devices allow for very fine resolutions and present high-density sampling abilities. Their use proved to be efficient in the physical modelling of seismic-wave propagation at various scales, providing a wide range of applications in NDE (Ruiz and Nagy, 2004; Lu et al., 2011; Abraham et al., 2012; Garnier et al., 2012; van Wijk and Hitchman, 2017), near-surface geophysics (Bodet et al., 2005, 2009a; Bretaudeau et al., 2011, 2013; Bergamo et al., 2014), exploration seismic (Campman et al., 2004, 2005; Blum et al., 2011c; de Cacqueray et al., 2011, 2013) or seismology (Nishizawa et al., 1997; Spetzler et al., 2002; van Wijk and Levshin, 2004; Hejazi Nooghabi et al., 2017).

Laboratory experiments involving lasers have been for instance chosen to study the propagation of seismic waves in random heterogeneous media, when numerical models may fail to depict the actual complexity of Earth materials (Nishizawa et al., 1997; Sivaji et al., 2002; Spetzler et al., 2002; Scales and Malcolm, 2003; Nishizawa and Kitagawa, 2007). Some of the previously cited studies involve actual Earth materials, such as granite in Nishizawa et al. (1997), but not only. Artificial media such as metals, polymers or resins, which can be perfectly controlled in terms of homogeneity, mechanical properties and shape, have been used to build specific 'physical models' dedicated to particular studies. Scales and van Wijk (1999) have for instance performed laboratory experiments to study multiple scattering of ultrasonic surface waves using an aluminium block presenting a

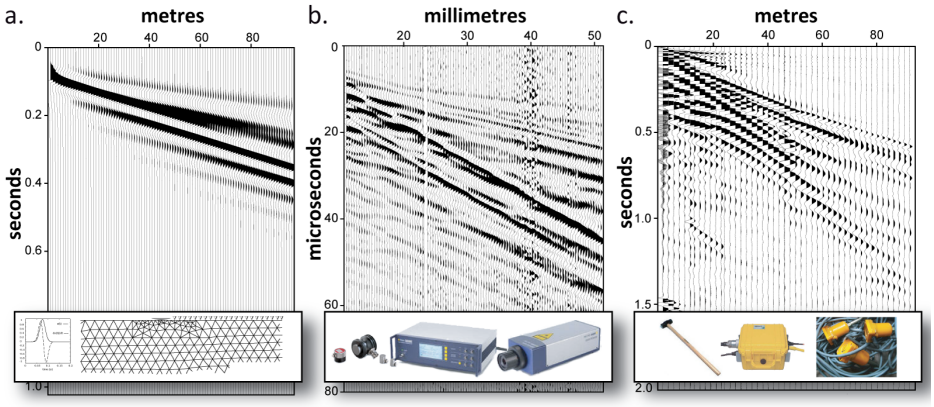

Figure 1.1: *'Studies of elastic wave propagation in the laboratory fits in between theoretical and numerical methods [(a)] on the one hand, and field-scale (seismic) experiments [(c)] . Laboratory data [(b)] has the real-life problems of noise, but has the advantage of doing controlled experiments [...] Laboratory studies of ultrasonic wave propagation can serve as either scaled modelling of challenges in seismic imaging, or as a way to investigate fundamental advancements in wave propagation. Particularly non-contacting laser ultrasonics provides tremendous opportunities [...]' quoting Thomas E. Blum and Kasper van Wijk from their communication at SEG annual meeting, 2010 (Blum and van Wijk, 2010).*

specific previously carved groove pattern at its surface. However, such experiments must not be considered as a mere alternative to numerical modelling (Fig. 1.1). Interestingly, the controlled character of Scales and van Wijk (1999) experiments made it possible to numerically reproduce their set-up. This actually gave the opportunity to highlight complementarities between numerical and physical modelling approaches (van Wijk et al., 2004) and to provide interesting insights for surface-wave seismology (van Wijk and Levshin, 2004).

Laboratory physical modelling and laser experiments can be similarly proposed to tackle theoretical and methodological issues related to the exploration seismic domain, more particularly when experimental validations of processing or inversion techniques are required. In this context, lasers are mainly used to reproduce typical field seismic acquisition set-ups at the laboratory scale (Hayashi and Nishizawa, 2001; Campman et al., 2004, 2005; Bodet et al., 2005, 2009a; Dewangan et al., 2006; Kaslilar, 2007; de Cacqueray et al., 2011). Most of the time, the controlled character of both the geometry and mechanical properties of specifically designed 'small-scale physical models' makes it possible to address, using real data, the efficiency, robustness or limitations of studied methods. The aluminium blocks mentioned earlier have for instance served Campman et al. (2004, 2005) to validate a wavefield-based imaging method to suppress surface waves scattered directly beneath the receivers, thanks to a simple circular hole dug at the surface of the medium. The same model was later used by Kaslilar (2007) for similar purposes. A homogeneous aluminium block was also used to study near-offset effects on Rayleigh-wave dispersion measurements and to validate numerical observations by Bodet et al. (2009a).

Increasing degrees of complexity can be chosen for the models construction. Multi-layered models made of acrylic, gabbro and mortar, have been built by Hayashi and Nishizawa (2001) in order to illustrate the behaviour of surface waves under controlled experimental conditions and test emerging dispersion analysis methods. Similar models have been built by Bodet et al. (2005) to

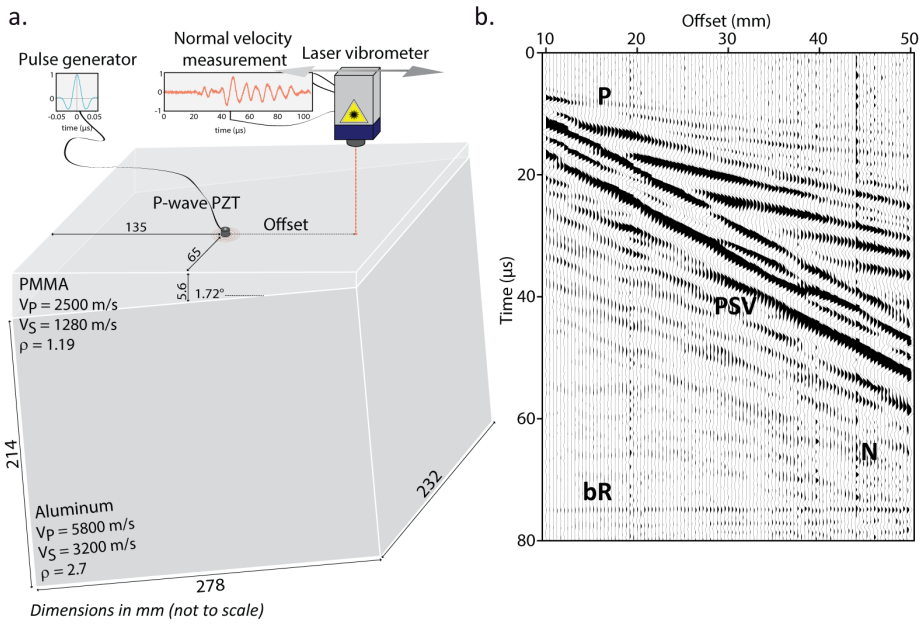

Figure 1.2: *A layered model with PMMA glued on an aluminium block. (a) The laser basically scans the surface excited by a piezoelectric transducer source and particle normal velocities are recorded at each offset along a linear section (the source remaining still). Both the mechanical properties and geometries/dimensions of the physical model (PM) are almost perfectly controlled. So are the source signal and non-contacting records along the simulated seismic line. (b) Yet, such simulations provide realistic 3D data (with typical P- and PSV-wave trains), for instance thanks to the strong noise level and scattering (N) due to dirt on the reflective tape, bad coupling of the PMMA or even identified air bubbles in the glue layer (see Fig. 1.3a,b and c). 'Artificial events', such as the bottom reflected arrivals (bR), may appear unrealistic compared to real data though... These experiments were used by Bodet et al. (2005, 2009a) to benchmark processing and inversion techniques with real data on controlled models, thus bridging the gap between 'too perfect –or only 2D– numerical simulations' and 'too poorly controlled' field studies (Fig. 1.1).*

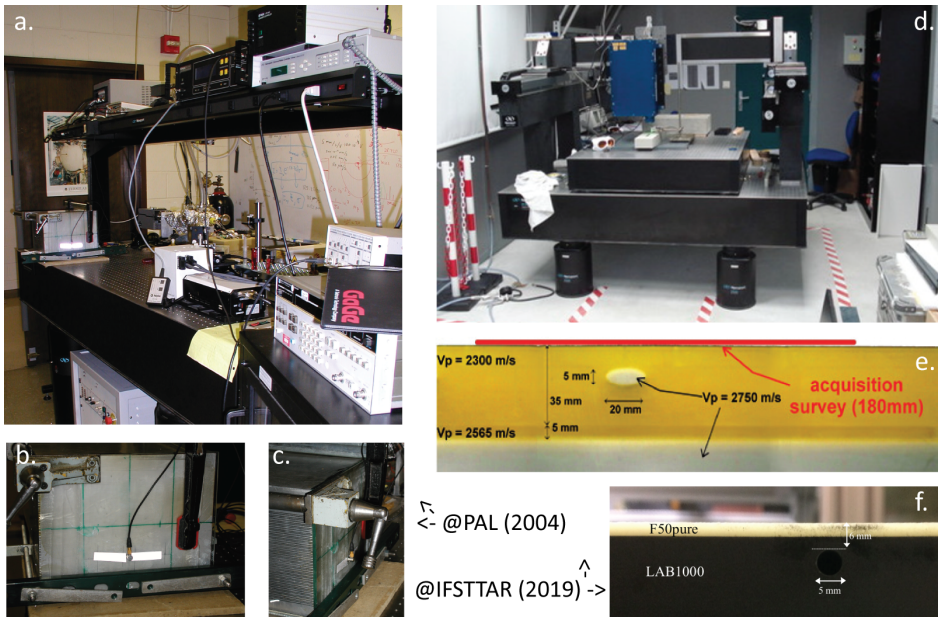

Figure 1.3: *The evolution of laser-Doppler small-scale physical modelling: (a) our first experimental set-up @PAL, Colorado School of Mines in 2004. I built it with the help of Kasper van Wijk and thanks to the advices of Xander Campman and John Scales; (b) front view of the PMMA glued on the aluminium block previously used by Campman et al. (2004, 2005), on which the reflective tape and the piezoelectric transducer are visible; (c) side view showing the Fibonacci pattern previously used by van Wijk et al. (2004); (d) global view of the MUSC measurement bench ('Mesure Ultrasonore Sans Contact' in French) @IFSTTAR nowadays; (e) developed by Bretaudeau et al. (2011, 2013) to record wave propagation in multi-layered, reduced-scale and highly controlled media; (f) a 2D cavity manufactured in a 2-layer model studied by Filippi (2019).*

address issues of surface-wave depth penetration, the presence of dipping layers, and the associated limitations and systematic errors propagating in conventional one-dimensional (1D) surface-wave inversion (Fig. 1.2). The layers of this study, tilted or not, were made of polymethylmethacrylate (PMMA) glued at the top of Scales and van Wijk (1999) aluminium block. Thermoplastics or melted epoxy resin-based materials can be assembled in order to mimic complex underground structures and offer various contrasts of mechanical properties (Bretaudeau et al., 2011). Dewangan et al. (2006) have used XX-paper-based phenolic material composed of thin layers of paper, in order to simulate a tilted transversely isotropic medium. An agar-agar gel has been used in an experimental set-up designed to study surface- and body-wave separation and identification through array processing (de Cacqueray et al., 2011). Similar experiments were performed to study wave separation algorithms and velocity variations monitoring problems (de Cacqueray et al., 2013). More recent studies take advantages of new laser set-ups able to record horizontal components (Valensi et al., 2015). In dedicated laboratories such as MUSC (Bretaudeau et al., 2011), the use of manufactured models helps studying more realistic structures (see Fig. 1.3d,e). The difficult understanding of waves interactions with 'real cavities' is for instance currently studied, with both laboratory models (see Fig. 1.3f) and multi-component field data by Filippi (2019).

1.1.2. Building 'less simple' models

In these laboratories, metal and thermoplastics are for instance frequently used because they are easily manufactured into various shapes and provide a wide range of mechanical parameters (Bretaudeau et al., 2011). In various contexts, from civil engineering to seismology, there however is an obvious need to study the propagation of seismic waves in more complex and realistic media. In the domain of geological analogue modelling, several authors managed to mimic seismic prospecting acquisition techniques on water saturated sandbox models (Sherlock, 1999; Sherlock and Evans, 2001; Buddensiek et al., 2009; Krawczyk et al., 2013). Buddensiek (2009) and Krawczyk et al. (2013) were for instance able to build multi-layered models, using sand and glass powders, perturbed by various structures such as channels or shear zones. These teams, along with others (Ekanem et al., 2013; Solymosi et al., 2018), however focus their studies on reflection seismic (frequently for offshore purposes) and have developed small scale models immersed in water tanks.

Granular materials such as natural sand, granular silica or glass beads offer great potential and flexibility in terms of physical models (PM) construction (more particularly regarding the choice of geometry and intrinsic parameters). Their use appears of great interest for the physical modelling of mechanical-wave propagation in several geophysical applications, more particularly when problematic of unconsolidated and/or porous materials have to be considered, for instance to target near-surface exploration and hydrogeological prospecting issues. Following these aims, we first addressed the ability of laser-based experiments in the characterisation of dry granular materials involved in geological analogue modelling (Bodet et al., 2010b), thanks to available data provided by Jacob et al. (2008). But before going any further, we had to explore the 'jamming transition'...

1.2. Mechanical waves in granular materials

1.2.1. Gravity-induced gradient and guided modes

In early laser-Doppler physical modelling experiments (Campman et al., 2004; van Wijk et al., 2004; van Wijk and Levshin, 2004; Campman et al., 2005; Bodet et al., 2005, 2009a), we did not intend to simulate perfectly scaled seismograms (e.g. in terms of acquisition geometry, frequency ranges, source size and radiation pattern) but only addressed theoretical and methodological aspects related to seismic data processing and inversion. One particularly interesting feature was the 3D characteristics of these 'laboratory simulations'. The PM were most of the time considered as elastic, homogeneous or multi-layered (assumptions easily verified when manufactured materials were used). Yet, if we want to build physical models using unconsolidated granular materials, the applicability of elasticity theory has to be considered to avoid misinterpretation of experimental data (Makse et al., 2004, 1999; Bachrach and Avseth, 2008; Tournat and Gusev, 2010).

The elastic properties of an unconsolidated granular packed structure under gravity can be described with the Hertz-Mindlin contact theory to model the intergrain forces (Mindlin, 1949; Walton, 1978). In the mechanically free surface vicinity of such medium, P- and S-wave propagation velocity ($V_{P,S}$) can be considered as power-law dependent on pressure (Gassmann, 1951), hence on depth (z) when bulk density (ρ) can be assumed constant. The velocity structure of such medium can be modelled as $V_{P,S} = \gamma_{P,S}(\rho g z)^{\alpha_{P,S}}$, where g is the gravity acceleration, $\gamma_{P,S}$ is a coefficient mainly depending on elastic properties of grains, porosity and coordination number of the packed structure, and where $\alpha_{P,S}$ is the power-law exponent predicted equal to 1/6 when considering a random close packing of uniform spheres. However, laboratory experiments show that within

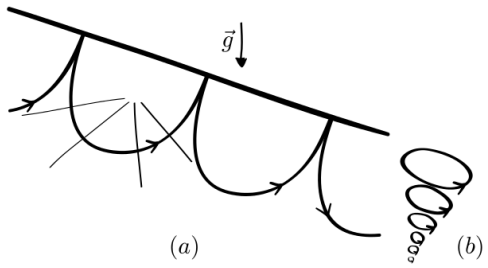

Figure 15. Principles of guided acoustic waves in granular media under gravity. (*a*) Representation of a guided mode in the geometrical acoustics approximation. As the speed of sound increases in depth, the wavefronts (thin lines) are deflected towards the free surface. Take care that the rays represent conventionally plane waves (thin lines): the vibration therefore takes place everywhere, not only in the vicinity of the rays. A guided mode corresponds to a phase matching between waves reflected several times at the free surface and brought to the surface by the gradient in the speed of sound. (*b*) Motion of grains in a guided mode of order 1.

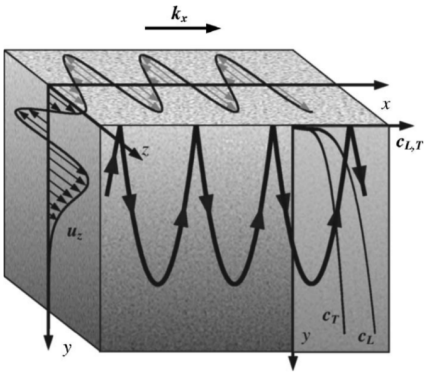

FIG. 1. Qualitative presentation of an unconsolidated granular material with gravity-caused depth (y) variations of elastic properties, shown with a gradient filling and as a power-law depth dependence of sound velocities c_L and c_T at the right. The thin arrows indicate the particle displacements for the SH modes both in the volume and at the surface. The path of a ray in GA approximation (thick lines with arrows) is also shown.

Figure 1.4: *Two conceptual presentations of guided modes in unconsolidated granular materials with gravity-induced depth gradients of elastic properties by Andreotti (2012) (left) and Aleshin et al. (2007) (right).*

real materials, several imperfections such as weak dispersion in grain sizes or sphericity can lead to strong contact disorders which may induce deviations of $\alpha_{P,S}$ from 1/6 (Schon, 1996; Makse et al., 1999; Zimmer et al., 2007a; Tournat and Gusev, 2010). As an example, Zimmer et al. (2007a) present a collection of experimental results (with associated references) from various types of granular assemblages (dry or saturated sands or glass beads) of seismic velocities values at static pressures varying from 0.1 kPa to 20 kPa. The presented data typically show power-law coefficients varying from 1/4 to 1/6 with increasing pressures. At slightly higher pressures (30 kPa to 200 kPa), experiments performed on confined 3D disordered glass bead samples showed $\alpha_P \approx 1/4$ as well (Jia et al., 1999). More recently, Jacob et al. (2008) and Bonneau et al. (2008) experimentally observed coefficients close to 1/3 at very low pressure, typically lower than 1 kPa, going down to less than 100 Pa (Tournat and Gusev, 2010).

In most experiments previously cited, seismic velocities were basically estimated using material samples confined at a given pressure into a cell bounded by a pair of transducers generating and receiving longitudinal and/or transverse motions. To estimate $\alpha_{P,S}$ at very low pressures, Jacob et al. (2008) tackled the problem through an alternative approach. Theoretically, the vertical gradient of the elastic properties in unconsolidated granular packed structure under gravity induces the upward bending of the rays, in the near surface of the medium (so called 'mirage effect' for instance described in Liu and Nagel (1992) and more recently illustrated by Tournat and Gusev (2010), see illustrations in Fig. 1.4). The combination of this gravity-induced rigidity gradient with a free surface enables the propagation of low velocity Guided Surface Acoustic Modes (GSAM). These GSAM, localised near the free surface, consist in shear horizontal waves (SH-), and in polarized in the vertical plane waves (P-SV). P-SV waves are commonly considered as a result of interactions between longitudinal (or P-) waves and shear vertical (SV-) waves in inhomogeneous medium, theoretically described for dry granular media by Gusev et al. (2006); Aleshin et al. (2007); Gusev and Tournat (2008) and Bonneau et al. (2007). The dispersion relations of GSAM

can be computed for a given set of the medium elastic parameters (ρ, $\gamma_{P,S}$ and $\alpha_{P,S}$) (Aleshin et al., 2007). Jacob et al. (2008) actually measured the GSAM dispersion at the free surface of an unconfined glass bead sample (excited by a mechanical source and probed thanks to a laser-Doppler vibrometer) and estimated $\gamma_{P,S}$ and $\alpha_{P,S}$ through an optimisation procedure.

As noted earlier, Bodet et al. (2010b) worked on the datasets provided by Jacob et al. (2008) to characterize dry granular materials involved in geological analogue modelling. They also addressed the efficiency and robustness of classical seismic prospecting techniques in the characterisation of near-surface continuous velocity gradients. But in order to be able to apply these techniques, they made an important approximation for their interpretation of the wavefield by considering it in the framework of elastic-wave propagation in stratified media instead of GSAM theory. They actually decomposed GSAM into typical near-surface seismic events of the vertical plane, namely P- and P-SV waves. Considering the P-wave train of weak dispersion at high frequencies, they picked first arrival times. They transformed the recorded wavefield into the frequency-wavenumber domain and extracted P-SV-wave dispersion curves. They finally inverted both dataset separately for 1D P- and S-wave velocity profiles with depth accounting for elastic-wave propagation in stratified media. Inferred VP and VS appeared to match estimation made by Jacob et al. (2008) in the framework of GSAM theory. Retrieved coefficients were close to 1/3, as theoretically anticipated. Bodet et al. (2014b) suggested to perform a thorough experimental and numerical study to verify these findings. These study is partly reproduced in the following.

1.2.2. Laser-Doppler probing

Physical model preparation

The granular material mainly used in Bodet et al. (2014b) consisted of 180-300 μm diameter glass beads sieved into a 1000×800×300 mm wooden box (Fig. 1.5). Compared to previous experiments (Jacob et al., 2008; Bodet et al., 2010b), the physical models to be constructed were chosen large enough for two main reasons: it was first important to limit wave reflections from the bottom and the edges of the box in order to maximize the size of the study window; secondly, the experimental set-up aimed at recording lines long enough to achieve greater investigation depths than in Jacob et al. (2008) and Bodet et al. (2010b). The length of the box was thus set to 1000 mm so as to enable the acquisition of at least 500 mm long record lines, at a reasonable distance from the edges ($>$ 250 mm). However, the height of the box remained too small to avoid the occurrence of bottom reflections in the study window, mostly because of practical limitations in terms of material quantities and model weight (assuming a bulk density of 1600 kg.m^{-3}, filling the box would approximately involve 380 kg of glass beads). The height of the models built for this study did not exceed 230 mm and involved, at the very most, 295 kg of glass beads.

The glass beads deposition process was designed to simultaneously ensure a good homogeneity of the medium compaction and to estimate its bulk density. Ideally, specific devices such as 'sand distributors' or 'sand hoppers' should be used to guarantee experimental reproducibility. These apparatus are for instance used to perform 'sand raining' or 'pluviation' in geological analogue modelling (Souloumiac et al., 2010, 2012; Maillot, 2013) or in geotechnical physical modelling (Murillo et al., 2009). But mainly because they are less cohesive than sand, glass beads are easily deposed in a homogeneous manner without this kind of automatic devices. The glass beads were thus here simply but thoroughly sprinkled by hand into the box (Fig. 1.5b.), by adopting the following protocol: glass beads were gently poured into a sieve (of 640 μm mesh size) following a sweeping motion over the box; once a given glass beads quantity was sieved (25 kg most of the time), the wooden box was gently shaken; if needed, a leveller was used to plane down the surface of

Figure 1.5: *Physical model construction and set-up for granular media: (a) we used calibrated glass beads (a lot!) or sands of various diameter sizes and distributions; (b) the material was poured or sieved, vibrated or not, depending on both its type and anticipated mechanical properties of the model (the process is detailed in the following section); (c) the global view of the set-up shows typical items for the acquisition (quite similar to those presented earlier...), except for the source which consists in a metal stick attached to a low-frequency shaker (a great variety of source, shakers, orientations, coupling etc had to be tested (Jacob et al., 2008; Dhemaied, 2011) before obtaining satisfying and reproducible results (Bodet et al., 2014b)). (d, e, f) detailed views of the amplifier used for the force source signal, the stick and scattered laser spot (another issue of the process to be discussed) and the oscilloscope stacking the acquisitions...*

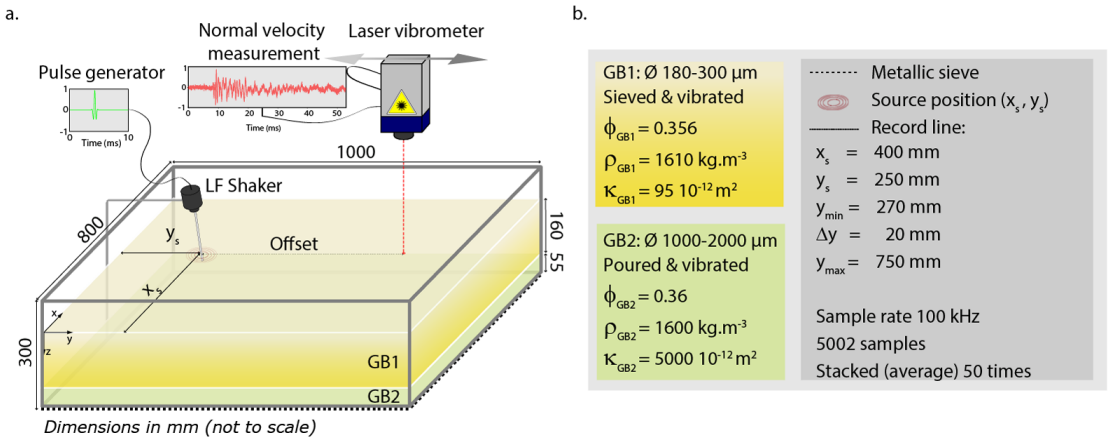

Figure 1.6: *(a) The physical model is prepared with a layer of 180-300 µm diameter glass beads (GB1) sieved into a 1000×800×300 mm box at the top of a layer of 1000-2000 µm diameter glass beads (GB2). The bulk densities (ρ_{GB1} and ρ_{GB2}) are estimated during the deposition process and on samples. Their values lead to porosities ϕ_{GB1} and ϕ_{GB2} close to the random close packing limit. Permeabilities in each layer (K_{GB1} and K_{GB2}) are measured on samples. A laser-Doppler vibrometer is used to record seismograms of particle vertical velocity at the surface of the physical model excited by a metal stick attached to a low-frequency shaker at position (x_s, y_s). Following a step by step procedure, the laser scans the surface and particle normal velocities are recorded at each offset along a linear section, the source remaining still. (b) Detailed legend providing properties of the medium and acquisition parameters. Modified after Bodet et al. (2014b).*

the medium; the thickness of the obtained glass beads layer was then measured to control its bulk density (according to the material provider, the density of glass beads was 2500 kg.m^{-3}). Each previously described step was repeated until the expected final thickness was reached. Several tests were preliminarily performed to optimize this deposition process in order to minimize the use of the flattening tool. By sieving and vibrating the glass beads this way, the obtained layer invariably presented a bulk density between 1600 and 1610 kg.m^{-3}. These estimations were consistent with laboratory measurements performed on small samples, that showed a bulk density of 1610 kg.m^{-3}. From the latter measurements, the porosity of the physical model was estimated as equal to 0.356. Such value appears close to the random close packing limit (Valverde and Castellanos, 2006). Similar results were recently obtained using a similar 'rainfall packing protocol' on smaller samples (Khidas and Jia, 2012).

Three different physical models were presented by Bodet et al. (2014b) in order to address the reproducibility of both the granular medium preparation and data acquisition. In this summarized presentation, only one is given as example (Fig. 1.6). The physical model consists of a 160 mm thick layer of 180-300 μm diameter glass beads (GB1 on Fig. 1.6a) sieved at the top of a 55 mm thick layer of 1000-2000 μm diameter GB (GB2 on Fig. 1.6a) (GB2 was designed to perform experiments involving pore pressure variations that will be presented in section 1.3.2). The bulk densities of layers GB1 and GB2 were ρ_{GB1}=1610 kg.m^{-3} and ρ_{GB2}=1600 kg.m^{-3}). They lead to porosities ϕ_{GB1}=0.356 and ϕ_{GB2}=0.36. The intrinsinc permeabilities in each layer (K_{GB1}=95 10^{-12} m^2 and K_{GB2}=5000 10^{-12} m^2) were measured on separate samples of similar porosities. These measured properties are summarized in Fig. 1.6b.

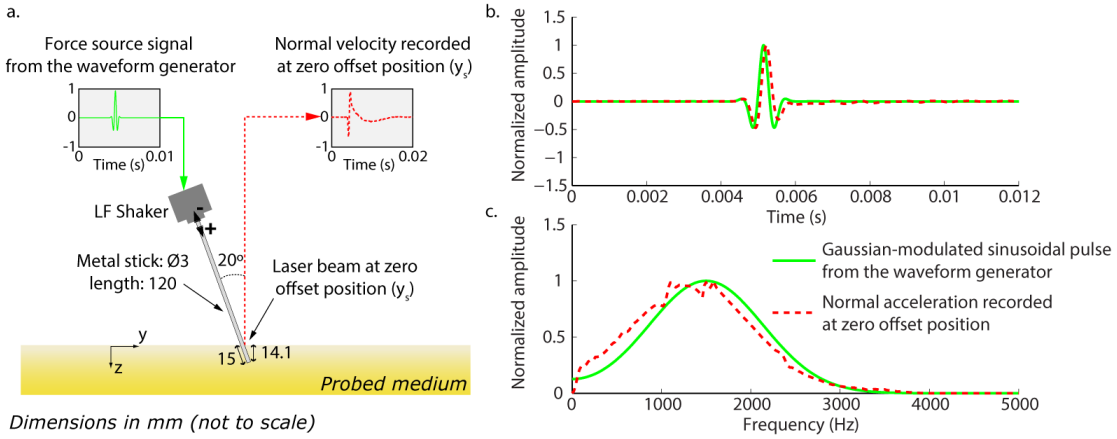

Figure 1.7: *Source set-up and specifications. (a) The force source signal (green line on the left inset) was sent from a waveform generator to a low-frequency (LF) shaker exciting a metal stick buried in the granular material. The laser beam was set at the zero offset position (y_s on Figure 1.6) to record the stick normal velocity (red dashed line on the right inset). (b) The force source signal (including a triggering delay) was a short pulse with its frequency spectrum centred on 1.5 kHz (green lines). Except for a slight shift toward low frequencies due to 'ringing of the stick', the signal recorded at zero offset position (red dashed lines), differentiated to acceleration here, fit the original force source signal (green lines). Modified after Bodet et al. (2014b).*

Experimental set-up and data acquisition

The experimental set-up presented on Figure 1.6a basically involved a mechanical source and a laser-Doppler vibrometer to mimic, at the laboratory scale, a typical field seismic acquisition. The medium was mechanically excited by a 3 mm diameter metallic stick attached to a low-frequency (LF) shaker driven by a waveform generator. The stick was buried in the granular material with an angle of 20° from the normal to the free surface (at position (x_s, y_s) on Fig. 1.6a). A detailed view of the source set-up is given on Fig. 1.7a. The force source signal was a Gaussian-modulated sinusoidal pulse with its frequency spectrum centered on 1.5 kHz (green lines on Fig. 1.7b). The source remaining still, the laser-Doppler vibrometer scanned the surface of the granular medium by constant steps (5, 10 or 20 mm, depending of the experiments). Up to 100 traces were recorded (using an oscilloscope) in linear single-channel walkway mode along the Oy direction (parallel to the long edges of the box, see Fig. 1.6b for details about the acquisition geometries). Each trace was stacked 50 times and the time sampling rate was 100 kHz over 5002 samples. For one source location, the wavefield was thus recorded as a 'seismogram' of normal component of particle velocity at the surface of the medium, as presented on Fig. 1.8a.

The recorded wavefield (Fig. 1.8a, 25 traces with 20 mm spacing) presents distinct and coherent events in the 0.25-2.5 kHz frequency range. The first event (P on Fig. 1.8a) occurs at high frequency with an apparent velocity of 160 m.s^{-1}. It is followed by a low frequency wave-train (P-SV on Fig. 1.8a), of 50 m.s^{-1} apparent velocity. The seismogram presents several strong reflections hyperbolae of high frequency (rP). At short offsets, the wavefield includes significant amplitudes related to the source ringing and, at long times, multiple reflections on the edges of the box. Multiple reflections and source ringing are considered as experimental artefacts and boundary effects that will not be taken into account in the following. In the framework of GSAM theory

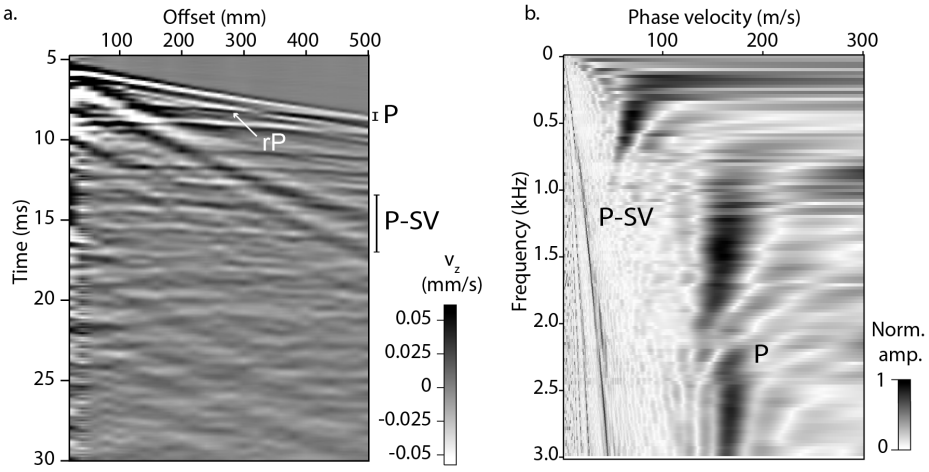

Figure 1.8: *(a) Seismogram of particle vertical velocity recorded at the surface of the physical model (25 traces with 20 mm spacing, see Figure 1.6a). Raw data, including the triggering delay, show that, despite strong amplitudes associated to source ringing and ghosts, the recorded wavefield presents coherent events identified as P- and P-SV wave trains. Strong bottom-reflected arrivals (rP) and possible multiples are clearly apparent. (b) The wavefield was transformed by a slant-stack to the frequency-phase-velocity domain. On these normalized dispersion images, the propagation modes previously identified are confirmed (maxima in black: one P-SV mode at low frequency and low velocity in the 0.25-1 kHz frequency band; and two P modes at higher frequencies and higher velocities in the 1.25-2.5 kHz frequency band). Modified after Bodet et al. (2014b).*

(Gusev et al., 2006; Aleshin et al., 2007; Jacob et al., 2008; Gusev and Tournat, 2008), the late and low velocity event (P-SV on Fig. 1.8a) corresponds to a 'slow mode' mainly controlled by the shear properties of the medium but which contains a compression contribution. Its amplitude is weak compared to the early event (P on Fig. 1.8a) which corresponds to 'fast modes' that can be assumed purely compressive. At highest frequencies, the first P arrivals are interpreted as direct rays bending upward. Their incidence being close to normal to the free surface, these longitudinal modes have a significant vertical component which dominates the recorded wavefield. The P and P-SV events identified in the seismogram respectively depend on compressive and shear properties of the medium and can be processed and interpreted to infer the 1D elastic structure of the physical model. The wavefield was then transformed into the frequency-phase velocity domain (by a slant-stack in common shot gathers after correction for geometrical spreading (McMechan and Yedlin, 1981; Mokhtar et al., 1988)). On the resulting normalized dispersion image presented on Fig. 1.8b, the maxima correspond the propagation modes previously identified on Fig. 1.8a (one P-SV mode at low frequency and low velocity in the 0.25-1 kHz frequency band; and two P modes at higher frequencies and higher velocities in the 1.25-2.5 kHz frequency band). These coherent events propagate with wavelengths varying from 50 to 250 mm in the 0.25-1 kHz frequency band of significant amplitudes. The shortest wavelengths are satisfactory compared to the glass beads diameter. But low frequency data will be interpreted with care in the following because longest wavelengths appear slightly greater than the thickness of the physical model.

1.2.3. Testing the elastic stratified medium approximation

Retrieving the elasticity of the material

The first arrival time was picked at each trace, providing the experimental traveltime versus offset curves presented on Figure 1.9a. The results clearly show a smooth non-linear increase of traveltime with offset, illustrating the gravity-induced velocity gradient with depth and suggesting no apparent lateral variations. The maxima observed on the dispersion image of Fig. 1.8b were as well extracted for the P-SV event as a phase velocity dispersion curve (Fig. 1.9b). As noted above, only one 'slow mode' is available and was first considered as the fundamental one.

According to wavelengths of the early event, ray theory should provide satisfying approximation at all distances and depths to simulate traveltime versus offset curves, assuming a vertically-heterogeneous layered P-wave velocity model, as previously suggested in Bachrach et al. (1998, 2000); Vriend et al. (2007) in the case of unconsolidated sands and as applied to similar glass beads in Bodet et al. (2009b, 2010b). The P-wave velocity model, defined by the coefficients γ_P and α_P and assuming the bulk density to be constant with depth, was then estimated thanks to a grid search [1]. It was performed using $5 \leq \gamma_P \leq 40$ with a step size of 0.5 and $0.05 \leq \alpha_P \leq 0.45$ using a step size of 0.005. Using such ranges, it covered a total number of 5571 (γ_P, α_P) models. A simplified presentation of the 'inversion results', showing the ridge of lowest misfit values and associated actual minima, is given on the inset of Fig. 1.9a. The global minima remain centred on α_P=0.3, as in previous observations (Jacob et al., 2008; Bodet et al., 2010b). The minimum misfit value (actually obtained for $\gamma_P = 21$ and $\alpha_P = 0.3$) is depicted along the ridge by a red plain circle and its corresponding P-wave velocity profile is shown on Fig. 1.9c (red line) within 5 % error (shaded area). The associated traveltime versus offset curve is compared to picked data on Fig. 1.9a within 5 % error.

Assuming a 1D layered model of elastic properties bounded by an infinite half-space, theoretical dispersion curves can be computed in a fast and straightforward manner (for instance using Thomson-Haskell matrix propagator technique (Thomson, 1950; Haskell, 1953) in the framework of Rayleigh-wave theory). 1D-layered velocity models can thus be estimated from dispersion data using various local or global optimisation techniques. P-wave velocity being of weak constraint on surface-wave dispersion, only S-wave velocity profiles were interpreted here. We used the neighbourhood algorithm implemented in Sambridge (1999); Wathelet et al. (2004) and Wathelet (2008) to perform a stochastic search of the parameter space [2], namely γ_S, α_S. To avoid forward computation instabilities, the parametrization of the model actually involved a stack of 10 sub-layers (following the power-law variation with depth), overlaying the half-space. The half-space depth, of great importance in the parametrization since it depends on poorly known depth investigation of the method, was fixed to 50 % of the maximum observed wavelength, *i.e.* 125 mm, as a safe approach recommended by Bodet et al. (2005, 2009a). The valid parameter ranges for the sampling of velocity models are 5 to 200 m.s^{-1} for VS (based on dispersion observations). As noted

1. Performed with the following misfit function: $M_P(\alpha_P, \gamma_P) = \sqrt{\sum_{i=1}^{N_t} \frac{[t_i^p - t_i^c(\alpha_P, \gamma_P)]^2}{N_t \sigma_i^{p2}}}$, where t_i^p and t_i^c were respectively picked and computed traveltimes at offset x_i. Nt was the number of traces and σ_i^p the error in traveltime (picking) at each offset.

2. Using the following misfit function: $M_S(\alpha_S, \gamma_S) = \sqrt{\sum_{i=1}^{N_f} \frac{[v_i^p - v_i^c(\alpha_S, \gamma_S)]^2}{N_f \sigma_i^{p2}}}$, with v_i^p and v_i^c being respectively picked and computed phase velocities at frequency f_i. N_f is the number of frequency samples associated to phase velocity measurements errors σ_i^p.

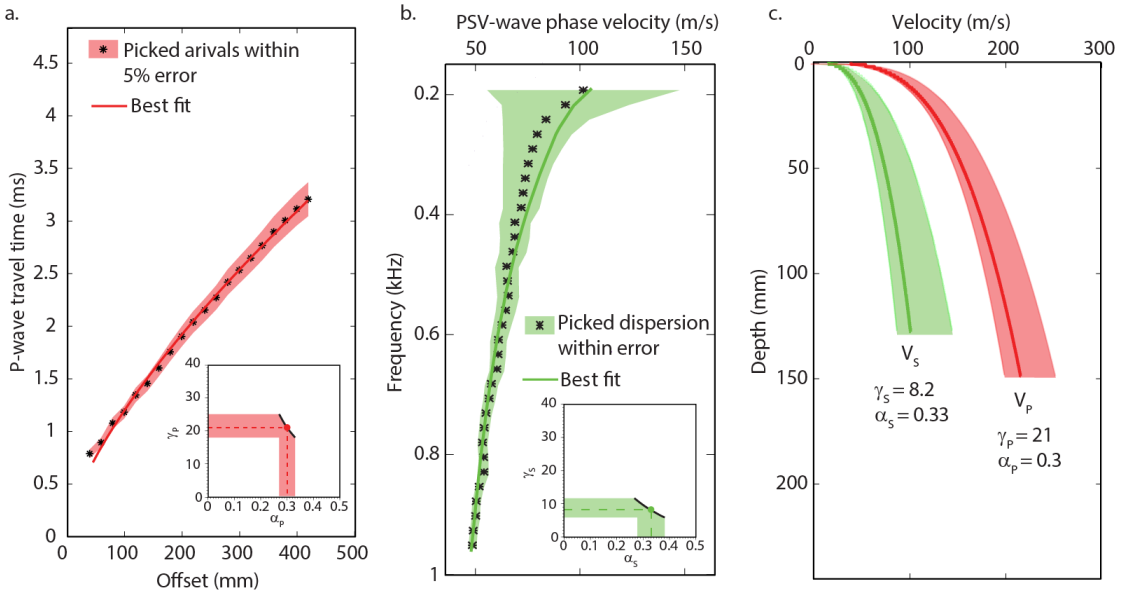

Figure 1.9: *(a) A grid-search inversion of first arrival times versus offset data (a, black stars whithin errors) was performed in the framework of ray theory to retrieve γ_P and α_P. The best fit (a, red line) is obtained for $\gamma_P = 21$ and $\alpha_P = 0.3$. The dispersion data (b, black stars whithin errors) were inverted in the framework of Rayleigh-wave theory thanks to a random search for α_S and γ_S. The best fit (a, green line) is obtained for $\gamma_S = 8.2$ and $\alpha_S = 0.33$. Corresponding VP and VS profiles with depth are given (c) within errors (shaded area) thoroughly estimated by Bodet et al. (2014b).*

above, only S-wave velocity profiles were interpreted but P-wave velocities in the top layer and in the half-space were generated and remained part of the actual parameter space. Density is set as uniform (1610 kg.m^{-3}). Dispersion data were inverted with 5 distinct and independent runs, generating a total of 25500 models. According to the minimum misfit value (green plain circle on the inset of Fig. 1.9b), the best fit to data occurs at $\gamma_S = 8.2$ and $\alpha_S = 0.33$. The associated dispersion curve is compared to picked data on Fig. 1.9b within 5 % error, and the corresponding S-wave velocity profile is shown on Fig. 1.9c (green lines within shade area).

An important number of (γ_P, α_P) and (γ_S, α_S) pairs exhibit low misfit values around both minima (as shown by the ridges on insets of Fig. 1.9a and b). These models fit to data within estimated errors as well, suggesting a significant uncertainty in the determination of the actual parameters of the power-law. These equivalences were thoroughly tested in Bodet et al. (2014b) and provided an attempt to evaluate the uncertainty on the estimated power-law coefficients.

Comparison to a numerical simulation

In this study, we interpreted the wavefield in the framework of elastic-wave propagation in stratified media instead of GSAM theory. This approximation appeared acceptable according to the very good agreement of retrieved parameters compared to results presented in previous studies (Jacob et al., 2008; Tournat and Gusev, 2010), with power-law coefficients confirmed to be close to 1/3 as such low confining stress. We then suggested to use the obtained elastic parameters as inputs of a 3D numerical model of the experiments in order to compare recorded data to a synthetic

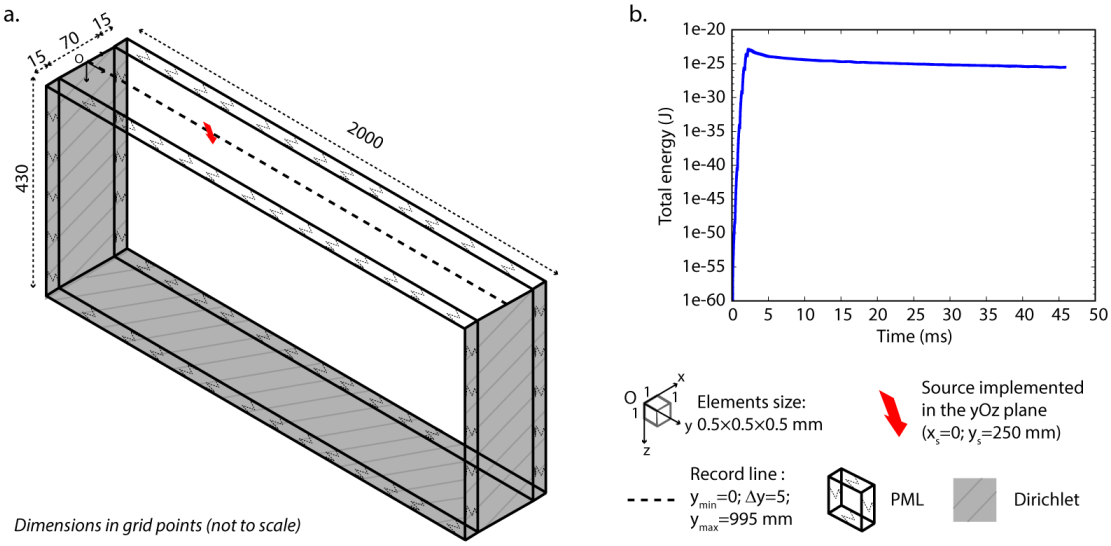

Figure 1.10: *(a) The numerical model developed by Roland Martin @GET (Univ. Toulouse) is discretized by elements of 0.5×0.5×0.5 mm for a mesh of 70×2000×430 (350×1000×215 mm). The mesh is extended in the Ox direction by PML layers in order to simulate only 'a slice' of the actual medium along the experimental line. The free surface is defined at the top of the computational domain and Dirichlet conditions are defined to simulate the edges and bottom of the box. The force source is implemented in the yOz plane with an angle of 20° from the normal to the free surface, to meet the experimental configuration (see Fig. 1.7). The receivers (dashed line) are spaced each 5 mm (10 grid points) at the free surface in order to collect a seismogram of the vertical component of particle velocity (see Fig. 1.12a). (b) Evolution of total energy over 115000 time steps. Modified after Bodet et al. (2014b).*

wavefield computed from an elastic finite difference formulation of the problem, and address the limits of such elastic approximation.

Despite the 1D character of the medium previously detailed, the implemented source imposed a 3D formulation to properly simulate the experiments. According to anticipated fine space and time discretisation required to simulate mechanical-wave propagation in the medium, modelling the entire box would have been of great computational cost. The lateral symmetry of the experimental set-up and the 1D structure of the medium made it possible to introduce absorbing conditions such as the perfectly matched layer (PML) conditions, in order to concentrate simulations in a thin slice of the model along the experimental record line. A detailed presentation of PML formulations used here is given in appendix B of Bodet et al. (2014b). The numerical simulations of this study involved the convolutional PML (CPML), as developed in 3D finite difference formulations for purely elastic, poroelastic or viscoelastic media (Komatitsch and Martin, 2007; Martin et al., 2008; Martin and Komatitsch, 2009).

The numerical model was discretized by elements of 0.5×0.5×0.5 mm for a mesh of 2000×430×70 (Fig. 1.11a). This leads to a model of 1 m in length by 0.215 m in depth and by 0.35 m in width. The mesh was extended by PML layers discretized over 15 points on each side of the box in the direction of the width (the effective width including the PML had a size of 0.5 m). The free surface was implemented at the top of the computational domain using the zero normal traction assump-

tion. Dirichlet conditions (zero velocities) were imposed on both sides in the length direction and at the bottom of the model. The simulated model was laterally homogeneous and its velocities followed the power-law trend with depth defined earlier, with the parameters estimated experimentally and summarized in Fig. 1.6. According to the discretisation, velocities consequently vary from values VP=31.7 m.s^{-1} and VS=12.9 m.s^{-1} close to the free surface up to VP=240.71 m.s^{-1} and VS=199.95 m.s^{-1} at the bottom (the bulk density being 1610 kg.m^{-3} as observed in the experiments). The time step Δt=0.4 μs corresponded to a stability Courant–Friedrichs–Lewy number of 0.3. The grid spacing corresponded to nearly 7 points discretisation per minimum wavelength, which was well taken into account by our fourth-order staggered finite difference spatial discretisation.

The source has been carefully implemented to match, as far as possible, the experimental conditions described in Fig. 1.7. The geometry of the buried part of the stick has been projected on the numerical mesh and we implemented the experimental force source signal. The source was thus located at 0.25 m from the left side of the box (see Fig. 1.10). The receivers were spaced each 5 mm (10 grid points) all along the length of the model, at the free surface. In order to be able to reduce the computational time, we ran the simulations over 100 Intel Xeon processors of the CALMIP computing centre located in Toulouse (France). The box was cut in slices along the highest dimension (Oy length direction) and information between processors was sent by using hybrid openMP/'send-receive' MPI communications. The wavefield was well absorbed without instabilities and good convergence of the solution was obtained even close to the base of the PML, as depicted on Fig. 1.10b which shows the evolution of total energy over long time period of 115000 time steps (50 ms).

Figure 1.11a shows the seismogram of the vertical component of particle velocity computed at the free surface of the numerical model along the record line presented on Fig. 1.10a. The black dashed lines delimit the space and time window used in the experimental study, in which first (P) and bottom reflected (rP) arrivals appear clearly. The P-SV wave train is present as well but is more dispersive and of higher amplitude than in the experimental data (see Fig. 1.8a). These differences in terms of amplitudes and dispersive character are confirmed on the normalized dispersion images (see Fig. 1.11b) on which higher order P-SV propagation modes are visible whereas the P mode hardly appear compared to the experimental data (see Fig. 1.8b). The first arrival (P mode) time of the numerical data was picked at each trace and compared to the theoretical and experimental traveltime versus offset curve (Fig. 1.12a). Computed arrival times fitted both experimental and theoretical results within less than 5 % error. The dispersion curves picked for the P-SV modes identified on the dispersion images of Fig. 1.11b clearly fit both experimental and theoretical dispersion (black stars and red lines respectively on Fig. 1.12b). The P mode picked on the numerical dispersion image appeared noisier due to its weak amplitude, but remained satisfactory compared to experimental data (black stars on Fig. 1.12b) and theoretical dispersion (red dashed lines on Fig. 1.12b) computed using Thomson-Haskell matrix propagator technique and including the complex-valued roots of the dispersion equation.

1.2.4. Take away message

In Bodet et al. (2014b), we made important approximations to estimate the elastic properties of the probed granular medium: instead of GSAM theory in a materiel of continuously varying properties, we considered the recorded wavefield in the framework of elastic-wave propagation in stratified media. We decomposed observed GSAM, depending on frequency and phase velocity ranges, into P- and P-SV waves as it is typically done for seismic applications. Picked first arrival

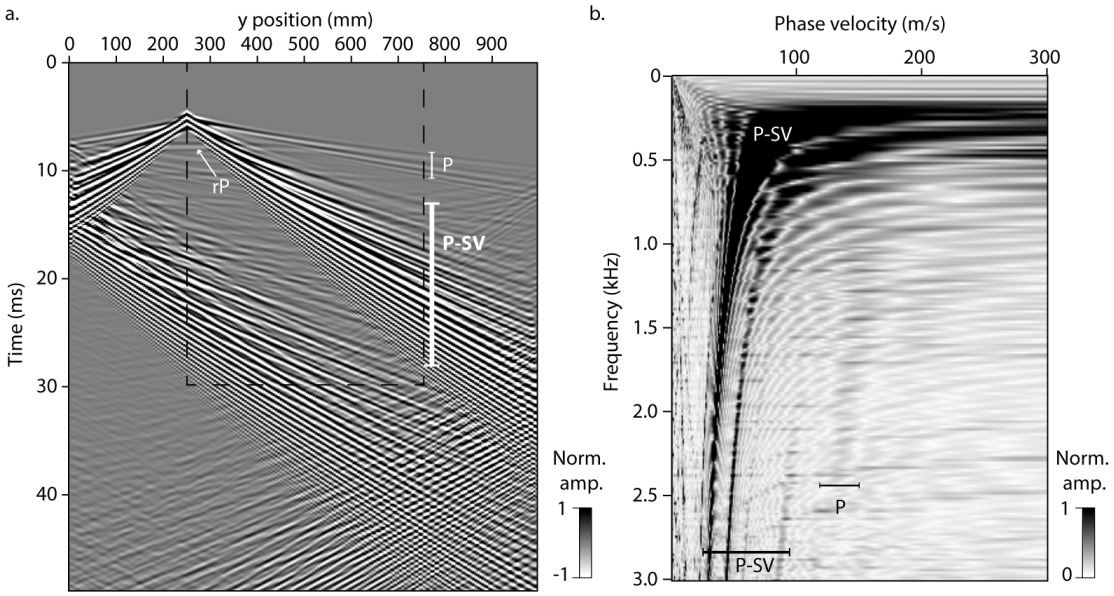

Figure 1.11: *(a) Seismogram of the vertical component of particle velocity computed at the free surface of the numerical model along the record line presented on Fig. 1.10a (the presented data the include the triggering delay). The black dashed lines delimit the space and time window used in the experimental study, in which first (P) and bottom reflected (rP) arrivals clearly appear. The P-SV wavetrain is present as well but is more dispersive and of higher amplitude than in the experimental data (see Figure 1.8a). These differences in terms of amplitudes and dispersive character are confirmed on the normalized dispersion images (maxima in black) (b) on which higher order P-SV propagation modes are visible whereas the guided P modes hardly appear compared to the experimental data (see Fig. 1.8b). Modified after Bodet et al. (2014b).*

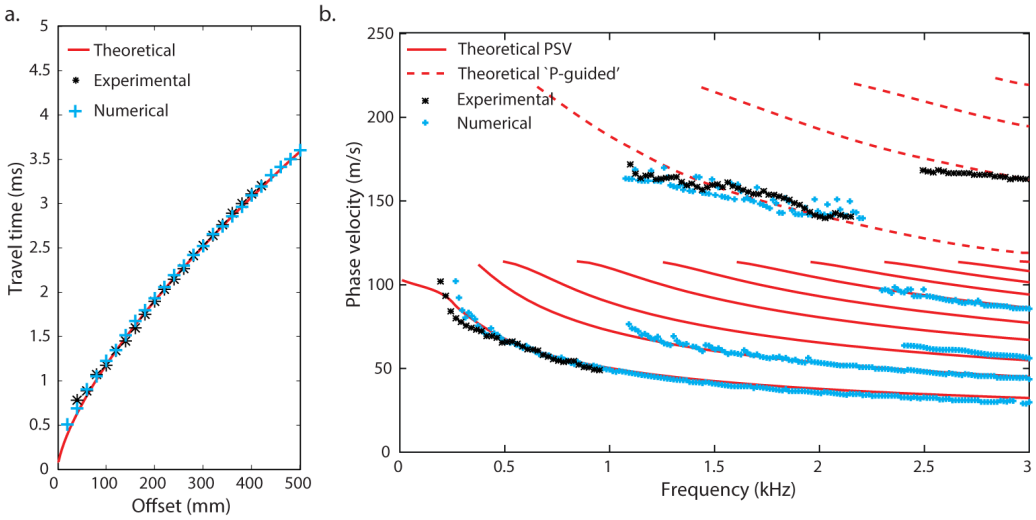

Figure 1.12: *(a) The first arrival (P mode) time of the numerical data is picked (blue markers) at each trace of the seismogram in Fig. 1.11a and compared to the theoretical (red line) and experimental (black stars) traveltime versus offset curves (the triggering delay are removed). (b) The dispersion curves picked for the P-SV modes identified on the dispersion image of Fig. 1.11b (blue markers) clearly fit both experimental (black stars) and theoretical dispersion curves (red line). The P mode, picked as well on the numerical dispersion image appears noisier due to its weak amplitude, but remains satisfactory compared to experimental and theoretical P mode dispersion(red dashed lines). Modified after Bodet et al. (2014b).*

times and P-SV dispersion data were inverted separately, for 1D Pressure- and Shear-wave layered velocity profiles following a power-law trend with depth, as suggested by theoretical models. Retrieved coefficients were close to 1/3, as it is theoretically anticipated at very low confining stress (typically lower than 1 kPa).

These power-law models were then used as input parameters of a 3D elastic finite difference simulation of the laboratory study. Thanks to the controlled character of such experiments, we were able to achieve a thorough implementation of the physical model geometry and of the source. The data extracted from the simulated wavefield fitted both theoretical and experimental values. Interestingly, the 'elastic simulation' also did perfectly reproduced the 'fast modes' dispersion that were observed in experimental data but not used in the inversion process. The approximations we made for the interpretation of the experiments were consequently valid as far as elastic properties of the medium and bounded frequencies domains were considered. However, the experimental and simulated wavefields presented dramatic discrepancies in terms of amplitudes. Consequently, we have to find a way to better implement numerically the coupling between the metallic stick and the glass beads to study potential effects of the source on the observed amplitudes. On the other hand, this issue has to be addressed experimentally by implementing alternative sources (such as piezoelectric transducers or high-power pulsed lasers). Eventually, the possible viscoelasticity of the medium and specific non-linear rheologies have to be considered as well (Martin et al., 2018), more particularly to explain the amplitude contrasts observed between P and P-SV modes.

1.3. Increasing degrees of complexity

Despite the limitations cited above, the laboratory process detailed by Bodet et al. (2014b) provides a validated experimental framework for the physical modelling of seismic-wave propagation in unconsolidated granular media at very low effective stress. Then, by using physical models of increasing degrees of complexity, the systematic benchmark of innovative seismic prospecting processing and inversion techniques should be successfully conducted. In addition, the porous character of granular materials makes it possible to build physical models of controlled pore overpressures (varying both in time and space). The experimental environment of this study can be easily adapted to inject various types of pore fluid into the physical models.

1.3.1. Pore overpressure

The experimental set-up was adapted to investigate the influence of pore overpressures [3] on recorded signals and associated changes in the rigidity gradients within the physical model (Fig. 1.13).

The physical model and basic set-up were the one presented in Fig. 1.6. As shown on Fig. 1.13 and 1.14a, the physical model was actually deposed at the top of a compressed air reservoir [4]. A metallic sieve (dashed lines on Fig. 1.14b) was glued on a perforated plate (Fig. 1.13b) at the

3. In Bodet et al. (2014b), we also used a Biot poroelastic 3D extension of the 2D CPML SEISMIC-CPML code developed in Martin et al. (2008). With this code we simulated the presence or absence of viscous damping by fluid-solid interface friction, but it appeared that the compressibility modulus of the frame was almost not changed by the presence of fluid because the bulk modulus of the air is much lower than the frame modulus, as detailed in Bodet et al. (2014b) (appendix C) and in Legland et al. (2012). The obtained seismograms were almost unchanged (very few phase delay or amplitudes changes) and so behaved the total energy (changes less than 1 %).

4. Most of the experimental design is based on the techniques the techniques developed by Mourgues and Cobbold (2003, 2006) to simulate fluid overpressures in sandbox modelling.

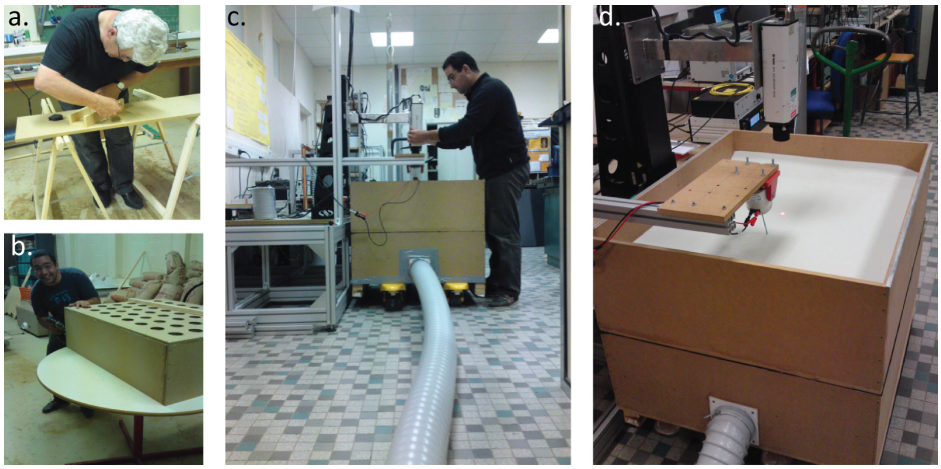

Figure 1.13: *(a) Jean-Claude Mathieu (Univ. Le Mans) et (b) Amine Dhemaied (PhD student at UPMC, 2007-2010) working on the experimental device designed developed by Régis Mourgues to generate a pore pressure gradient in the physical model. The set-up presented in Fig. 1.9a is actually deposed at the top of a compressed air reservoir, in which the air is kept at a given overpressure value (P_{base}) at the base of the thanks to an air blower (see the pipe on pictures c and d). A metallic sieve glued on a perforated plate (b) allows the air flowing from the reservoir into the granular material. The overpressure is controlled by a water manometer installed on one side of the box, at the base of the physical model and below the sieve.*

top of the reservoir (below the physical model). Thanks to an air blower, the air was kept at a given overpressure value P_{base} in the reservoir. P_{base} was measured thanks to a water manometer installed on one side of the box, at the base of the physical model, below the sieve. The sieve allowed the air flowing from the reservoir into the granular material. Assuming no lateral leakages, the air flow thus generated a vertical non-hydrostatic pore pressure gradient in the physical model, controlled by the overpressure in the reservoir. The 55 mm thick GB2 layer actually served creating a transition zone of intermediate permeability in order to ensure a homogeneous injection of the air into the upper layer. The experiments were performed with three different values of P_{base}: 0, 1000 and 2000 Pa. The estimated bulk densities and permeabilities of both layers made it possible to approximate a priori stress and pressure profiles with depth (z) in the physical model, as given on Fig. 1.14b. $\sigma(z) = \rho g z$ is the normal stress, Pp(z) is the pore pressure and $\sigma'(z) = \sigma(z) - Pp(z)$ the resulting effective normal stress (often written using the pore fluid overpressure ratio λ such as $\sigma'(z) = \rho g z(1-\lambda)$). Pore pressures were computed in each layer (considering the parameters of Fig. 1.6), thanks to Darcy's law which provides satisfactory results in such media, although air is compressible.

Seismograms of particle vertical velocity (25 traces with 20 mm spacing), presented on Fig. 1.15, were thus recorded for each reservoir overpressure. Despite strong amplitudes associated to source ringing and ghosts (Sr on Fig. 1.15), the recorded wavefield shows similar P- and P-SV wave trains at each reservoir overpressure. GB2 being approximately ten times larger in diameter than GB1, this bottom layer aimed serving as a diffusing zone (at least at high frequency) and at limiting the contribution of bottom reflections (bR on Fig. 1.15) and possible multiples (mR on Fig. 1.15). The data recorded at $P_{base} = 2000\ Pa$ (Fig. 1.15c) shows a deterioration of the signal to noise ratio probably due to the noise generated by the air blower. The wavefield recorded at each P_{base} value

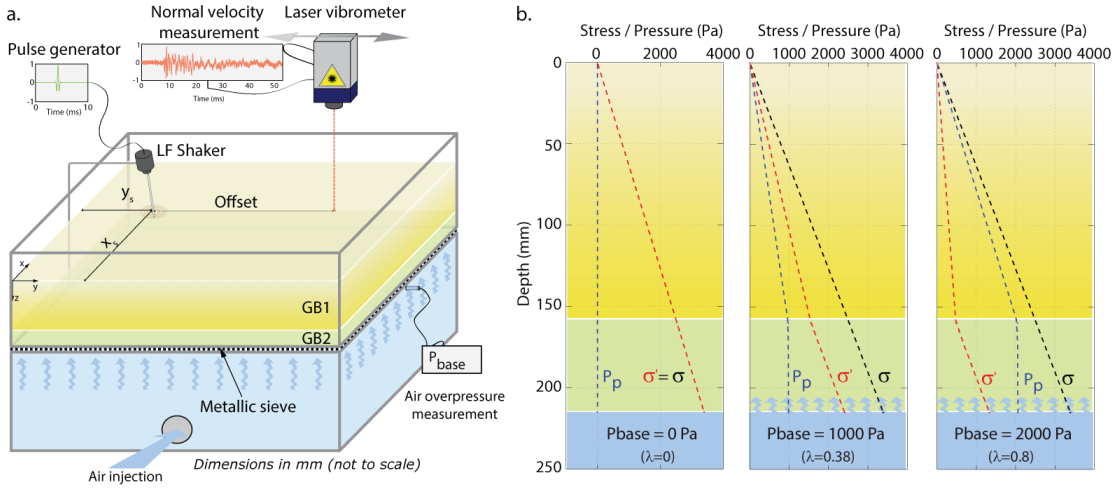

Figure 1.14: *(a) A laser-Doppler vibrometer was used to record seismograms of particle vertical velocity at the surface of the physical model excited by a mechanical source at position (x_s, y_s). (b) The experiments were performed with three different overpressure values P_{base} in the reservoir: 0, 1000 and 2000 Pa. The estimated bulk densities and permeabilities of both layer (Fig. 1.9b) made it possible to approximate a priori stress and pressure profiles in the physical model. σ is the normal stress, Pp is the pore pressure, λ the overpressure ratio and $\sigma'(z) = \sigma(z) - Pp(z) = \rho g z(1-\lambda)$ the resulting effective normal stress.*

was then transformed by a slant-stack to the frequency-phase-velocity domain (Fig. 1.16), in order to address its dispersive character. On these normalized dispersion images, the propagation modes previously identified on Fig. 1.15 are confirmed (P and P-SV, corresponding to maxima in black on Fig. 1.16).

As noted in the previous section the high frequency and early event (P on Fig. 1.15 and Fig. 1.16) corresponds to 'fast modes' (assumed purely compressive). The late and low velocity, low frequency event (P-SV on Fig. 1.15 and Fig. 1.16) corresponds to a 'slow mode', strongly dispersive and mainly controlled by the shear properties of the medium. Both P- and P-SV wave trains show a global decrease of wave propagation velocities confirmed on extracted data presented in Fig. 1.15d and 1.16. This evolution of apparent velocities with the overpressure in the reservoir is coherent with a decrease of differential pressure of the medium.

1.3.2. Pore fluids

In a more recent study, we focused on the application of seismic methods to the monitoring of water content variations in the vadose zone (more details in Chapter 3). Following the methodology proposed above, we performed laser-Doppler scans of a glass beads physical model presenting different water levels (Pasquet et al., 2016a). We successfully adapted the laboratory set-up (Fig. 1.17) in order to keep its size and weight to a reasonable practical level, while meeting experimental requirements in terms of impermeability and solidity. We built a glass aquarium with dimensions $800 \times 400 \times 300$ mm, including two 50-mm wide tanks installed lengthwise on both sides of the aquarium (Fig. 1.17). These two tanks were connected with the central part by two 15-mm high openings located at the tank bottom and covered with a metal sieve allowing for imbibing the granular medium from the bottom by gradually increasing the water level in the tanks. Glass

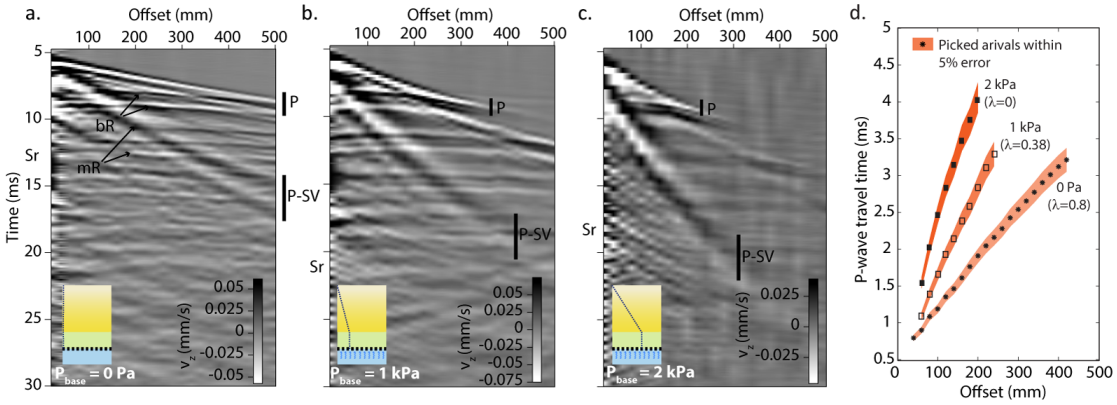

Figure 1.15: *Seismograms of particle vertical velocity (25 traces with 20 mm spacing), recorded with increasing reservoir overpressure: (a) 0 Pa, (b) 1000 Pa and (c) 2000 Pa. Raw data show that, despite strong amplitudes associated to source ringing and ghosts (Sr), the recorded wavefield presents coherent events identified as P- and P-SV wave trains. Strong bottom-reflected arrivals (bR) and possible multiples (mR) are clearly apparent. Recorded data with P_{base}=2000 Pa (c) present a deterioration of the signal to noise ratio probably due to the noise generated by air injection. (d) P-wave first arrivals show a global decrease of apparent propagation velocities with increasing P_{base}.*

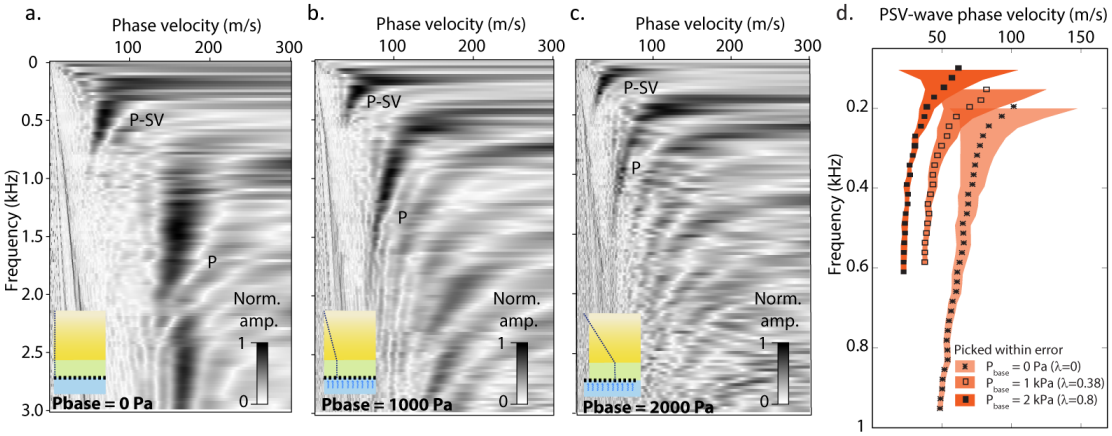

Figure 1.16: *The wavefield recorded at each P_{base} value (a) 0 Pa, (b) 1000 Pa and (c) 2000 Pa, was transformed by a slant-stack to the frequency-phase-velocity domain. On these normalized dispersion images (maxima in black), the propagation modes (P and P-SV) previously identified on Fig. 1.15 are confirmed. (d) P-SV wave dispersion show a global decrease of wave propagation velocities with increasing P_{base}.*

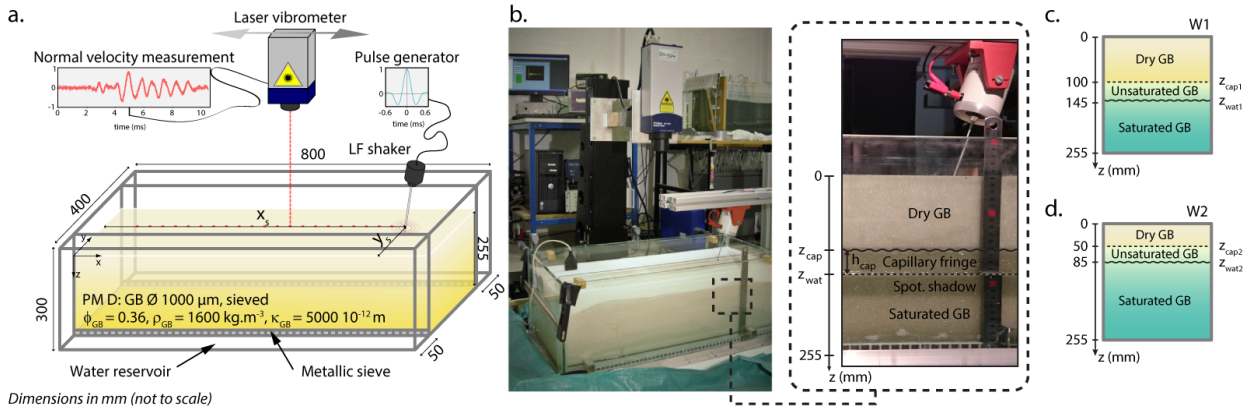

Figure 1.17: *The physical model was prepared with 1000 µm diameter glass beads sieved into the central part of a 800 × 400 × 300 mm aquarium designed by Régis Mourgues, so as to obtain a 800 × 300 × 255 mm model. The water level (z_{wat}) and the capillary fringe (z_{cap}) were ultimately increased stepwise by filling the side tanks. (a) A laser-Doppler vibrometer and positionning system provided by Vincent Tournat (Univ. Le Mans) were used to record seismograms of particle vertical velocity at the surface of the medium excited by a mechanical source at position (x_s = 655 mm; y_s = 150 mm). The surface of the medium was scanned with a constant step along a 500-mm long a linear section, the source remaining still. Similar scans were reproduced with (b) z_{wat1} = 145 mm and z_{cap1} = 100 mm (W1) and with (c) z_{wat2} = 85 mm and z_{cap2} = 50 mm (W2). (d) The set-up involved a TDR probe to monitor water content variations. We were unfortunately not able to invert recorded signals to saturation data. We used levels estimated through the glass walls, as show on the picture. Modified after Pasquet et al. (2016a).*

beads with a diameter of 1000 μm were used to build the physical model. Thanks to the low cohesiveness of glass beads and their well classified size, we were able to ensure an homogeneous deposition of the glass beads by simply pouring them into a sieve following a rotary movement sweeping all the aquarium (Bodet et al., 2014b). The model was composed of glass beads evenly distributed over a thickness of 255 mm. Based on the work of Bodet et al. (2014b), the density of glass beads could be approximated to 1600 kg/m^3. Similarly, Bodet et al. (2012) measured the hydraulic permeability values of glass beads with a similar granulometry (around 5000 10^{-12} m^2). The use of such glass beads thus ensured a homogeneous imbibition of the model from the bottom. For each acquisition, the water level was ultimately increased stepwise by filling the side tanks.

Using the same laser-Doppler vibrometer and source design (Fig. 1.17) as Bodet et al. (2014b), we recorded small-scale seismograms at the surface of the dry model (D, Fig. 1.18a) and with two distinct depths of capillary fringe (z_{cap}), estimated visually through the glass walls of the aquarium (W1 with z_{cap1} = 100 mm, Fig. 1.18b; W2 with z_{cap2} = 50 mm, Fig. 1.18c). Despite possible multiples due to ringing of the stick (Sr), each seismogram presents similar and coherent wavefields in which both P- and P-SV wave trains clearly appear. Bottom reflections (rP) are clearly identified as well on D and W1 models. Energetic events with very low frequencies and low apparent velocities (C) are also visible at different times, masking part of the signal contained in the P-SV wave train. These events are probably originating from the conversion of guided waves at the interface between the granular medium and the glass walls of the aquarium. Seismograms obtained with different water levels present a clear increase of the attenuation compared to the

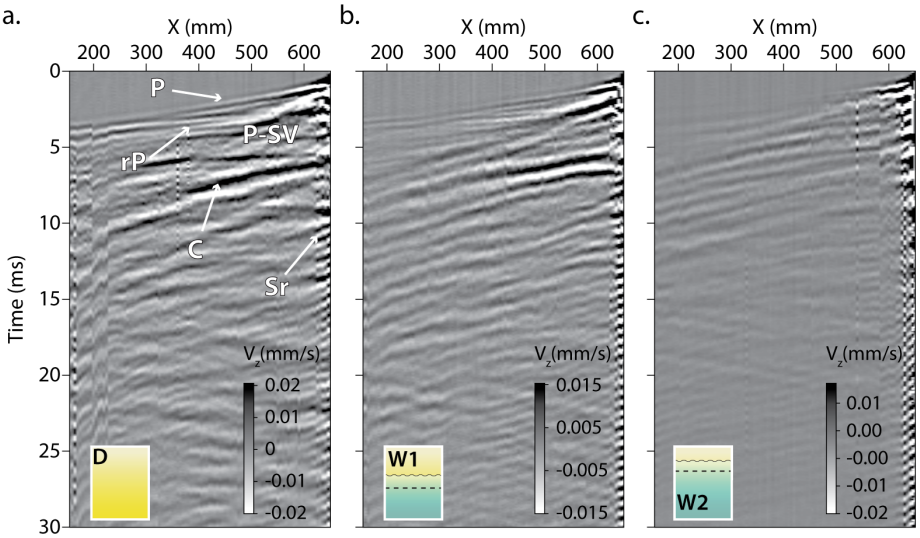

Figure 1.18: *Seismograms (vertical component of the particle velocity, V_z), recorded at the surface of the dry model D (a) and with increasing water levels W1 (b) and (c) W2. The recorded wavefield presents coherent events identified as P- and P-SV waves. Strong bottom reflections are visible (rP), along with low frequency energetic events (C) probably originating from the conversion of guided waves at the interface between the granular medium and the glass walls of the aquarium. Strong amplitudes associated to source ringing (Sr) are also present at short offset. The seismograms show slight changes in apparent velocities but important variations in amplitudes. Modified after Pasquet et al. (2016a).*

seismogram obtained with the dry model.

Despite the noise and multiple reflections on the data due to the reduced dimensions of the set-up, we were able to extract reliable P-wave traveltime (Fig. 1.19a) and P-SV dispersion data (Fig. 1.20a) for the dry and wet models. After validating traveltimes and phase velocities obtained for the dry granular medium with elastic 3D finite difference simulations (Martin and Komatitsch, 2009; Bodet et al., 2014b), we inverted these data to infer 1D VP and VS profiles following a power-law trend with depth, as suggested by theoretical models. Retrieved coefficients were close to 1/3, as it was previously observed by Jacob et al. (2008) and Bodet et al. (2010b, 2014b). In comparison, the data extracted from the wet models clearly showed the influence of increasing water level on the recorded wavefield. The results show a decrease of first arrival times for the partially saturated models W1 and W2 compared to the dry model D (Fig. 1.19a). The non-linear increase of first arrival times with the offset related to the velocity gradient in depth remains visible for W1, while W2 shows first arrival times divided along three segments with distinct slopes. P-SV dispersion curves (Fig. 1.20a) show a different behaviour: greater phase velocities for W2 compared to D, when the values remains almost unchanged for W1 (considering picking errors).

If the estimation of the elastic parameters of the dry medium could be achieved in a relative straightforward manner in the framework of elastic-wave propagation in stratified media, it remained hardly possible to invert the data obtained for partially saturated granular media in the absence of a comprehensive theoretical model. To overcome these drawbacks, Paolo Bergamo (Politecnico di Torino) proposed to study the differences of traveltimes and phase velocities observed

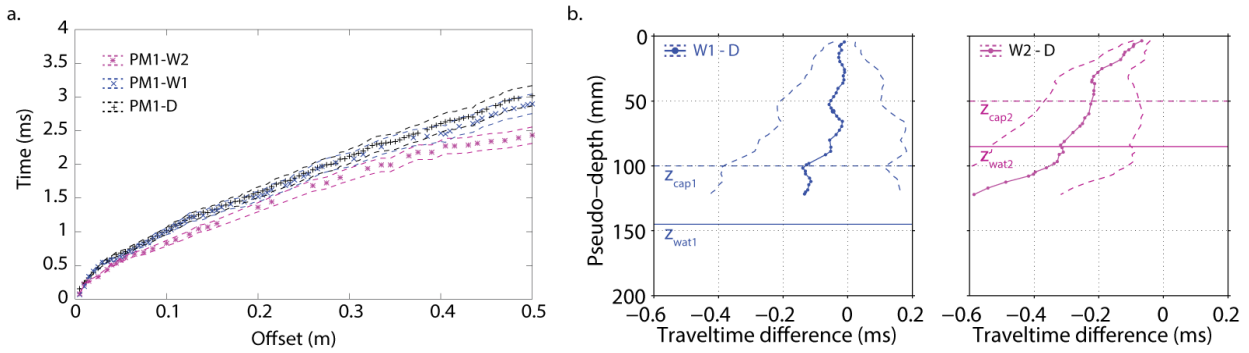

Figure 1.19: *(a) P-wave first arrival times picked for the dry model D (black), and the wet models W1 (cyan) and W2 (magenta) within a ±5 % error (solid line). (b) Differences between picked traveltimes of the dry and wet models. The corresponding water level z_{wat} and capillary fringe depth z_{cap} are represented for both models with solid and dashed lines, respectively. Modified after Pasquet et al. (2016a).*

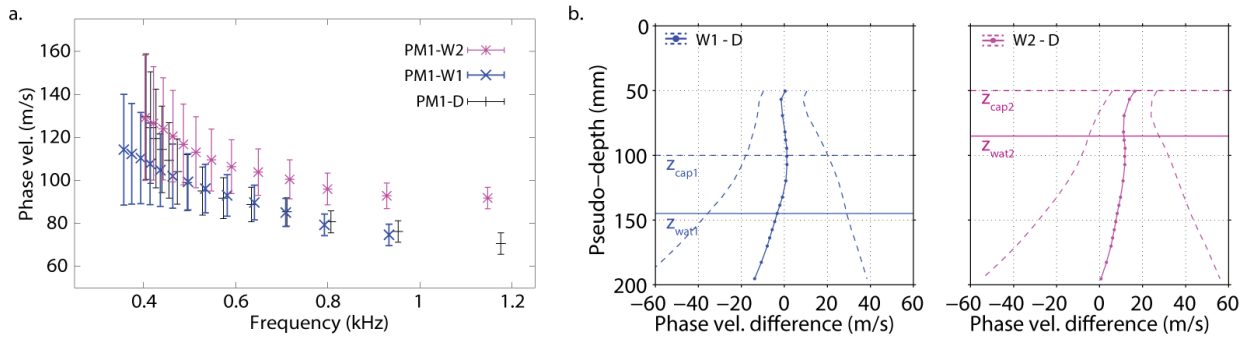

Figure 1.20: *(a) Dispersion curves of the fundamental P-SV propagation mode for the dry model D (black), and the wet models W1 (cyan) and W2 (magenta). (b) Differences between picked phase velocities of the dry and wet models.. The corresponding water level z_{wat} and capillary fringe depth z_{cap} are represented for both models with solid and dashed lines, respectively. Modified after Pasquet et al. (2016a).*

between the dry and wet models (Fig. 1.19b and Fig. 1.20b respectively). Time differences were evaluated locally with a moving window sliding along the offset axis, negative differences referring to shorter traveltimes in the corresponding wet model. Using the elastic parameters estimated in the dry model, we were able to convert offset values in terms of pseudo-depth by retrieving the maximum propagation depth of theoretical rays emerging at each picked trace. The same approach was also applied for dispersion data, using phase velocity versus frequency curves of the fundamental mode. Phase velocity differences were estimated using a moving window sliding along the frequency axis, negative differences referring to slower phase velocities in the corresponding wet model. Finally, frequencies were transformed into wavelengths, which were then converted in pseudo-depths.

The calculated time differences are presented along with the corresponding water and capillary fringe levels in Fig. 1.19b. For both water levels, they provide information for depth between 0 and 125 mm. Time differences calculated for W1 remain mostly under 0.05 ms above z_{cap1}, which corresponds roughly to the traveltime picking uncertainty. Below z_{cap1}, the differences are more pronounced but the limited investigation depth prevents from imaging the trend of the time difference curve at z_{wat1} and below. Comparatively, time differences calculated for W2 are significantly greater than the picking uncertainty, even at shallow depth. Yet the most striking feature is the clear correlation of the two inflection points of the time difference curve with z_{cap2} and z_{wat2}. For their part, phase velocity differences are represented along with the corresponding water and capillary fringe levels in Fig. 1.20b for W1 and W2. They provide deeper information, going from 50 to 200 mm in depth. For W1, phase velocity differences mainly range within the phase velocity picking uncertainty, and present a significant decrease below z_{wat1}. As for W2, the calculated phase velocity differences are significantly greater than the picking uncertainty and clearly present a good consistency between the two inflection points of the difference curve and z_{cap2} and z_{wat2} (though the transition appears smooth compared to P-wave first arrival time differences).

This simple tool provided satisfactory results which clearly correlate with the observed water level and depth of the capillary fringe. Such acquisition and processing methodology needs to be proposed and validated at the field scale for the time-lapse monitoring of soil water content variations, using laser-Doppler acoustic probing, or more typical seismic acquisition equipment (more details in Chapter 3). It is finally worth noting the important variations in amplitudes of recorded seismograms with water content, confirming such attribute (already studied in exploration seismic) of great interest in near surface applications.

1.3.3. Geometry

We also worked on the feasibility of building granular physical models with a more complex geometry, property contrasts and velocity gradients within layers (Bergamo et al., 2014). The creation of two granular media with different elastic behaviours was achieved by adopting different granulometries and deposition techniques. Once we had evidence of the possibility to create granular materials with different degrees of stiffness, we were able to construct a physical model with two layers whose reciprocal interface is characterized by a uniform slope in the central part of the model itself (Fig. 1.21a). Several small-scale seismic acquisitions were then performed on the free surface of the model (Fig. 1.21b), in order to get a dataset exhaustively depicting elastic wave propagation in the model.

The following stage of the process involved the extraction of surface wave dispersion curves from the recorded seismograms and their inversion. In particular, we applied an algorithm by Bergamo et al. (2012) based on a spatial windowing of the traces to get several local curves from the same

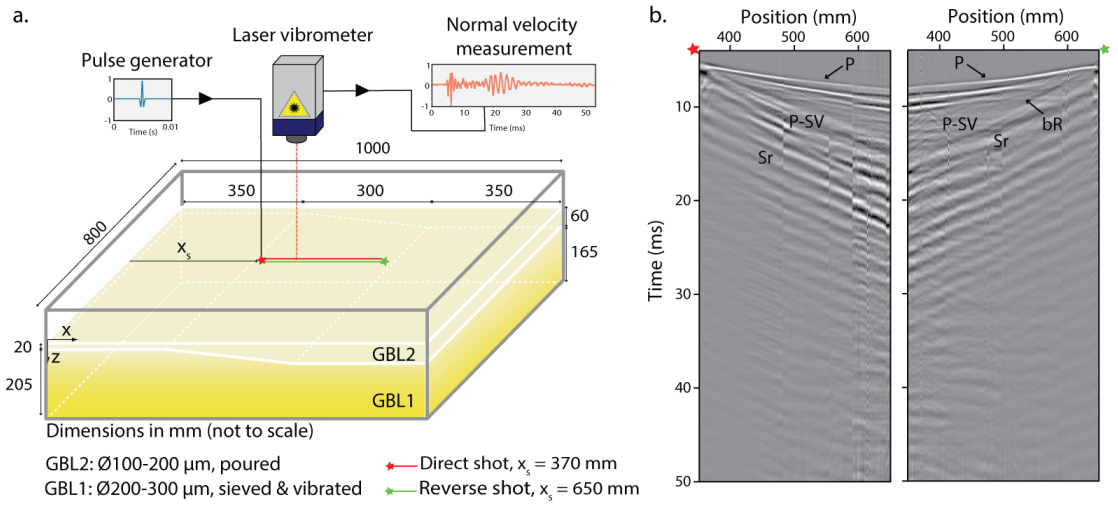

Figure 1.21: *(a) During Paolo Bergamo's PhD thesis, we were able to construct a physical model with two layers presenting distinct in-depth velocity gradients, separated by a sloping interface. (b) Recorded seismograms globally show that, despite strong amplitudes associated to the source ringing (Sr), the wavefields clearly present coherent events such as P- and P–SV wave trains. Along the Line 1 and the Line 5, it is possible to guess bottom-reflected arrivals (bR). Modified after Bergamo et al. (2014).*

seismogram (Fig. 1.22a). As far as the dispersion curves inversion is concerned, S-wave velocity was considered as power-law dependent on pressure. The unknowns to be retrieved were power-law parameters controlling the VS behaviour for each layer and the interface depth. Unknown parameters were not estimated by a single inversion process but by means of a step by step inversion procedure, isolating from time to time a parameter or a couple of parameters to be retrieved. Such procedure, although helped by the a priori knowledge of the model geometry, yielded accurate and meaningful results: the 2D structure of the analogue model was satisfactorily reconstructed (Fig. 1.22b), and the estimated values of the power-law parameters interestingly confirmed the results of previous theoretical and experimental studies (Aleshin et al., 2007; Gusev and Tournat, 2008; Jacob et al., 2008). By such correct and accurate results, we addressed the ability of the algorithm by Bergamo et al. (2012) in extracting a dense set of reliable local dispersion curves over the 2D portion of the models, so that we could thoroughly 'follow' the trend of lateral variations. This confirmed the efficient character of surface-wave methods when strong a priori information exists and the great importance of the parametrization (Wathelet, 2008). As anticipated by Bodet et al. (2009a) and Bodet et al. (2010b), the experimental set-up presented here should eventually provide an interesting tool for the imaging of dry analogue models in geology (Gressier et al., 2010; Mourgues et al., 2011, 2012).

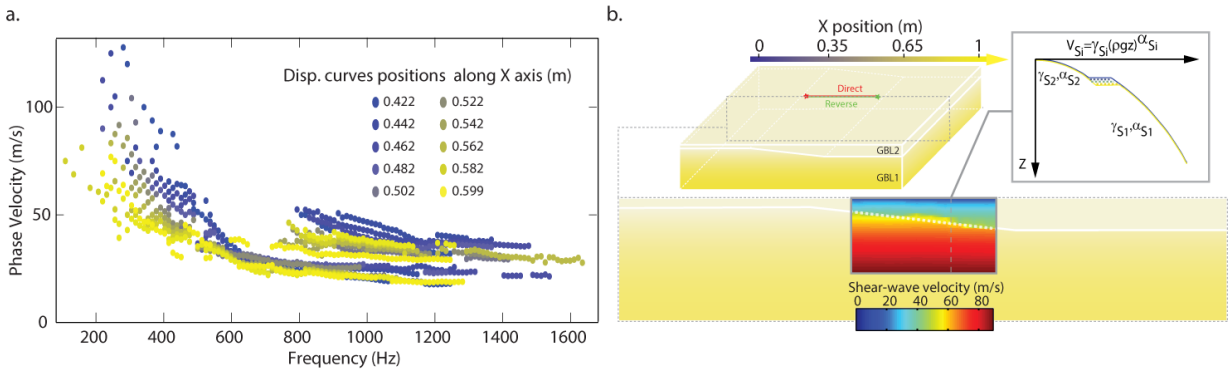

Figure 1.22: *(a) We addressed the efficiency of an innovative surface-wave processing technique developed to retrieve two-dimensional (2D) structures from a limited number of receivers, using a spatial windowing based on a set of Gaussian windows with different shape. (b) A step by step inversion procedure yielded accurate and meaningful results so that the 2D structure of the physical model was satisfactorily reconstructed, although strong a priori knowledge was required. The gravity-induced velocity gradients within each layer were accurately retrieved as well. Modified after Bergamo et al. (2014).*

1.4. Conclusions and perspectives

1.4.1. Elastic approximation and guided modes

By adapting the techniques suggested by Bodet et al. (2005, 2009a) and thanks to the inspiring experiments by Jacob et al. (2008) that we studied in Bodet et al. (2010b), we designed a mechanical source and used a laser-Doppler vibrometer to record small-scale seismic lines at the surface of multi-layered glass beads models (Bodet et al., 2014b). Yet, theoretical aspects of mechanical-wave propagation in such media had to be addressed first. When GSAM theory should prevail in unconsolidated granular packed structure under gravity (Tournat and Gusev, 2010), we only considered elastic-wave propagation in stratified media to interpret recorded data. Thanks to basic seismic processing and inversion methods, we were however able to correctly retrieve the gradients of pressure- and shear-wave velocities in our models. 3D finite difference simulations of the experiments offered, despite significant differences in terms of amplitudes, a supplementary validation of our approximations, as far as elastic properties of the medium were concerned. It highlighted kind of a paradox. A gravity induced velocity gradient in the vicinity of the free surface enables the propagation of GASM. If we consider the vertical component, the wavefield is then dominated with PSV guided waves. It means that in such structure, the usual paradigm with body waves (P) on one side and surface waves (pseudo-Rayleigh or PSV) on the other, simply breaks down. However, we showed that fast modes are mainly compressive and that their arrivals can be picked at high frequency to retrieve VP. In addition, the slowest modes dominate at lower frequencies, they are highly dispersive and we demonstrated that their dispersion can also be used to retrieve VS. This way, we finally characterized the medium exactly as if we had considered body and surface waves separately.

These results as well provided a better understanding of mechanical-wave propagation in granular materials at very low effective stress, 'outside the laboratory'. Vriend et al. (2105) for instance were able to better understand the 'behaviour' of booming sand dunes (Vriend et al., 2007). They later included the power-law we inferred in Bodet et al. (2014b) as a priori information in their forward models showing how sand dunes can act as a resonators and corrupt seismic signals (Arran et al., 2018). In near-surface or exploration seismic, the shallow layers can consist in unconsolidated material showing non-linear rigidity gradients with depth. These formations thus enable the propagation of guided modes that can be easily exploited thanks to their dominance in the seismic signal. Bergamo and Socco (2016) suggested a direct application of our studies (Bergamo et al., 2014; Bodet et al., 2014b) to simultaneously retrieve VP and VS power-law structure of loose dry sands from multi-modal dispersion inversion. They however choose a step-by-step inversion process which requires an assumption about the medium's Poisson ratio. An alternative would then be to consider the dispersion of the full wavefield to be inverted at once, for both VP and VS, as already suggested by Maraschini et al. (2010); Boiero et al. (2013). This approach should be more particularly interesting when body-wave investigation techniques (e.g. traveltime tomography) are limited in depth and in resolution because of: high attenuation of near-surface material; important surface topography; the presence of strong contrasts; 3D structures; low velocity layers etc, as it will be the case in Chapter 2).

1.4.2. Imaging lateral heterogeneities

In Bergamo et al. (2014), we took advantage of Bodet et al. (2014b) experimental set-up to simulate a seismic surface-wave survey over a laterally varying granular medium. We were able to construct a physical model with two layers presenting distinct in-depth velocity gradients,

separated by a dipping interface. We used this physical model to address the efficiency of an innovative surface-wave processing technique developed to retrieve 2D structures from a limited number of receivers, but not only. Our experimental set-up and processing tools showed their ability in imaging granular materials widely used for geological modelling purposes (Gressier et al., 2010; Mourgues et al., 2011, 2012). These results also encouraged us to implement stacking techniques on field data (Ezersky et al., 2013) to narrow down the lateral extent of our dispersion measurements and to perform 2D imaging of VS heterogeneities (Pasquet and Bodet, 2017). These aspects will be presented with more details in Chapter 3.

1.4.3. Influence of material properties

We then performed similar experiments in order to monitor granular media with varying pore pressures, in the context of geological analogue and seismic modelling studies (Bodet et al., 2012; Mourgues et al., 2011, 2012). A compressed air reservoir was used at the base of a model to generate a pore pressure gradient in the medium. Despite the noise generated by the air injection, recorded seismograms presented coherent and exploitable wavefields, showing the influence of decreasing differential pressure on the medium wave propagation velocities. We recently were able to implement non-linear rheologies in 3D (Martin et al., 2018), following previous studies by Dhemaied (2011); Dhemaied et al. (2011). We now intend to simulate Bodet et al. (2012) data by implementing the effect of pore overpressures combined with intrinsic attenuation, more particularly to later be able to address non-linear ultrasonic techniques for nondestructive evaluation, as suggested by Kim et al. (2016).

We finally adapted this experimental set-up to investigate the influence of varying water levels on seismic prospecting tools used in hydrogeophysics (Bodet et al., 2015; Pasquet et al., 2016a). The differences in traveltimes and phase velocities, observed between seismograms recorded on dry and wet models, showed patterns that matched the observed water levels and depths of the capillary fringe, thus offering attractive perspectives for studying water content variations in soils. These results for instance encouraged us to go for time-lapse seismic acquisitions on hydrosystems (Dangeard, 2019), as it will be shown in the following (Chapter 3). These aspects also interestingly showed how small-scale physical modelling of wave propagation can help choosing experimental or field acquisition strategy (Suzaki et al., 2017; Bergamo et al., 2016a,b).

1.4.4. Small-scale physical modelling : different approaches and applications

As pointed out by Blum and van Wijk (2010) and as cited earlier here, 'laboratory data has the real-life problems of noise, but has the advantage of doing controlled experiments [...]'. That is why, more than 15 years ago, following the example of Hayashi and Nishizawa (2001) and based on set-ups developed by Campman et al. (2004, 2005); van Wijk et al. (2004); van Wijk and Levshin (2004), we used laboratory physical modelling and laser-Doppler small-scale surveys to complement numerical studies and perform experimental benchmarks –and sometimes validations– of surface-wave modelling, processing and inversion techniques Bodet (2005). We believed that studying mechanical waves at the laboratory scale would bridge the gap between theoretical or numerical approaches and field-scale experiments (as it is difficult to simulate real-life noise and acquisition incidents and quite uncommon to have perfectly controlled field-scale test-sites at one's disposal).

Nowadays, small-scale physical modelling of seismic waves has been developed for a wide range of purposes and applications. Several teams see this approach mainly as a tool to perform 'experimental validations under controlled conditions' of their forward modelling or inversion methods,

but not only. Solymosi et al. (2018) for instance built an extremely complex topographic structure in a water tank to benchmark finite-difference and spectral-element simulations. Köhn et al. (2016) used ultrasonic measurements on PMMA to illustrate the potential of their two-dimensional Rayleigh waveform inversion. Devi et al. (2018) were able to record seismoelectric data in saturated glass beads models. Palermo et al. (2018) numerically investigated the interaction of GSAM with arrays of vertical oscillators. They actually integrally reproduced the design of our experimental set-up in order to validate their results (see Palermo et al. (2018) and supplementary materials).

As far as I am concerned, I believe the most interesting way to perform small-scale physical modelling of wave propagation in controlled laboratory experiments is to think it as versatile tools (Bodet et al., 2013, 2014a): to explore the effects of specific material properties or geometry on wave propagation (Mikesell et al., 2017); to better understand and adapt most recent advances in wavefield interpretation (Hejazi Nooghabi et al., 2017); or to suggest innovative methodological approaches Filippi (2019).

Chapter 2

Industrial application: tracking anomalies below railways

Reminder: this chapter mainly consists in the reproduction of internal reports (in French) to SNCF RESEAU who kindly authorised me to present them to this HDR committee. It is currently transposed to an article in preparation for submission. The text below corresponds to a direct translation of the chapter, my apologies if it sounds "Frenglish"!

Abstract

The renewal of railway embankments (RE) or the selection of appropriate maintenance actions require the characterisation of their mechanical properties. This is usually achieved with standardized geotechnical sounding and/or core drilling that remain local, destructive, expensive and of low efficiency/yields. Non-destructive evaluation techniques are suggested as alternative RE control tools for local diagnosis and monitoring, such as Electrical Resistivity Tomography (ERT). Microgravity surveys can as well be deployed to target cavities and/or decompressed areas in RE. Ground penetrating radar (GPR) is for instance used over long distances to delineate the shallower layers geometry and track down anomalous interface topographies. However, these methods do not provide quantitative information directly linked to standard mechanical moduli. In order to develop alternative approaches for the mechanical characterisation of RE, we studied a test site with identified maintenance issues, along the Northern Europe high-speed line (LGV-Nord). Bender Elements (BE) measurements of shear-wave velocity (VS) were performed on core samples collected at different locations along the line. The results showed a correlation between the phenomenon affecting the geometry of the tracks and the mechanical state of the RE, when conventional geotechnical soundings (e.g. field or laboratory tests) failed identifying significant anomalies. The VS obtained with BE tests showed that this parameter was a good indicator of soils 'quality' in RE. Surface-wave methods were thus identified as possible prospecting tools to estimate, in situ, the mechanical parameters of the RE layers, below railway tracks. In this context, we dimensioned and designed specific seismic acquisition setups to perform surface-wave profiling on RE. We carried out several tests along the LGV-Nord and defined a detailed processing and interpretation workflow, presented here as a tutorial example. Dispersion measurements systematically showed significant variations along the profiles, correlated with previously identified anomalies of different origins. The a priori knowledge about the RE LGV-Nord structure made it possible to invert dispersion measurements

for 1D vertical VS models evenly sampled along the tracks. The results showed a contrast of VS in the loess underlying the RE, between areas where the phenomenon was observed and those it was not. These results encouraged considering dispersion measurements as an appropriate tool of RE monitoring. The approach was successfully tested along older 'classical lines'. Ongoing projects aim at optimising this technique, developing its automatic implementation and suggesting semi-automatic processing and interpretation methods. An important goal is to eventually define usable links between seismic data and standard mechanical moduli conventionally required in RE monitoring. The RE being a very specific structure in terms of geometry and velocity contrasts, it also provides a great framework to the experimental study of guided seismic waves.

2.1. Introduction

2.1.1. Context and issues

Preserving and expanding rail transportation networks is a major challenge at both national and international levels. Design and maintenance of railway embankments (RE) requires the regular monitoring of their mechanical characteristics such as bearing capacity or cone penetration resistance for instance. However, having access to RE without perturbing the traffic is particularly difficult because of obvious operational and safety constraints. The main issue then (Saussine et al., 2017), is that the techniques classically used to study RE are mainly destructive, punctual, expensive and of low yields (geotechnical in situ tests, core-drillings). This is why there is a great need in the development and deployment of non-destructive 'on-the-fly' monitoring methods, allowing quick and efficient diagnoses of the RE state. Ground Penetrating Radar (GPR) is for example mounted on trains combined with high frequency levelling systems, for the fast and efficient investigation and imaging of RE shallow layers (detailed stratigraphy, water content etc e.g. Khakiev et al. (2014); Hugenschmidt et al. (2013)). This technique however suffers limitations in depth of investigation (DOI) in electrically conductive fine materials, such as clays which attenuate the signal and prevent access to underlying soils. In addition, GPR is perturbed by its high sensitivity to metallic elements, as well as to '3-dimensional' (3D) effects linked to the RE geometry and local civil engineering structures. In a similar manner, geophysical approaches of possible high yields, such as electromagnetic and capacitive electrical prospecting methods, are very difficult to apply along railways because of underground cables, electrical wiring systems and, of course, catenaries. Electrical Resistivity Tomography (ERT) however consists in a possible tool of great interest for the study of RE, as describe in details by (Gunn et al., 2018). Other techniques such as microgravimetry have been suggested by geophysicists to target cavities and/or decompressed areas (Fauchard and Pothérat, 2004; Talfumiere and Nebieridze, 2008; Nebieridze and Leroux, 2012). Yet they do not provide information about the RE mechanical properties in the standard framework of geotechnics.

In such context [1]:

— Is there a geophysical (non-destructive) method capable of mechanically characterizing RE and soils below the tracks?

— Will this method make it possible to differentiate the materials and soils these structures are built with? If so, at what resolutions (vertical and lateral)?

— Will this method allow to distinguish different states of the same material (water content, compaction/decompaction, etc)?

1. See details of the proposal in the appendix to the report by Bodet et al. (2014c).

— Will this method enable, in the long term, a sufficient yield for a decision aid ('to guide the choices in terms of design, monitoring and maintenance')?

2.1.2. The choice of surface-wave seismic surveys

Seismic prospecting methods

The mechanical parameters of soils shallow layers (compression and shear moduli) can be estimated in situ using seismic methods. They are based on the indirect characterization of seismic-wave propagation velocities from seismograms (records of the wavefield by means of a collection of sensors implanted at the surface and detecting the particle displacements generated by a seismic source; see e.g: Mari et al. (2004)). The refraction of body waves (compressional or pressure (P) and/or shear (S) waves), for instance, makes it possible to simply define near-surface geometry, as well as its compressional (VP) and/or shear (VS) velocities. Although considered fast to implement and relatively straightforward to process, these techniques suffer from several limitations (e.g.: Mari et al. (2004); Fauchard and Pothérat (2004)):

— the existence of civil engineering structures with a strong 3D character and/or offering important velocity contrasts, in the vicinity of the acquisition setup (at the surface as well as at depth), complicates the interpretation of seismograms (it becomes delicate to differentiate the various events of the wavefield which can either be due to the investigated layers at depth or to lateral '3D objects');

— refraction seismic implies the assumption of increasing velocities with depth. Lower velocity layers (LVL) will not be properly characterized and high velocity layers (HVL) will perturbed the investigation of deeper structures of interest;

— event detection is only easily possible with a good signal-to-noise ratio (sometimes impossible to obtain in urban and suburban conditions) and the study of S waves is all the more delicate, because they are more difficult to generate and identify on this type of records.

It appears that the above-mentioned limitations restrict the applicability of refraction seismic (and moreover reflection seismic, Mari et al. (2004); Fauchard and Pothérat (2004)) to the characterization of RE (presence of 3D structures, HVL, LVL, potentially significant background noise, etc).

Surface waves

From a theoretical point of view, the elastic strain generated by a mechanical dynamic source do not propagate in the Earth as body waves only. Actually, most of the energy propagates along the surface without penetrating deeply. If the mechanical properties of the medium are vertically heterogeneous (and more particularly its shear modulus), the propagation velocity of these guided waves (the 'surface waves', also named 'PSV' or 'Rayleigh' waves in the following) will depend on their propagation frequency. This property, called dispersion, makes it possible to retrieve, via an inversion procedure, the VS structure of the probed medium, below the acquisition setup. Active-source surface-wave dispersion measurements can be achieved using typical seismic shot gathers. The inferred VS models are 1D and measurements and interpretations are limited by several well-known theoretical and experimental constraints (O'Neill, 2003; O'Neill et al., 2003; Socco and Strobbia, 2004; Bodet et al., 2005, 2009a). However surface-wave methods, widely used in seismology since the 1950s, has known important theoretical and experimental developments for a wide range of near-surface applications since the 1980s (non-destructive evaluation, civil and geotechnical engineering, environmental geophysics, natural hazards, etc, see e.g. Socco et al. (2010)). The first applications of this technique were actually largely dedicated to the in situ

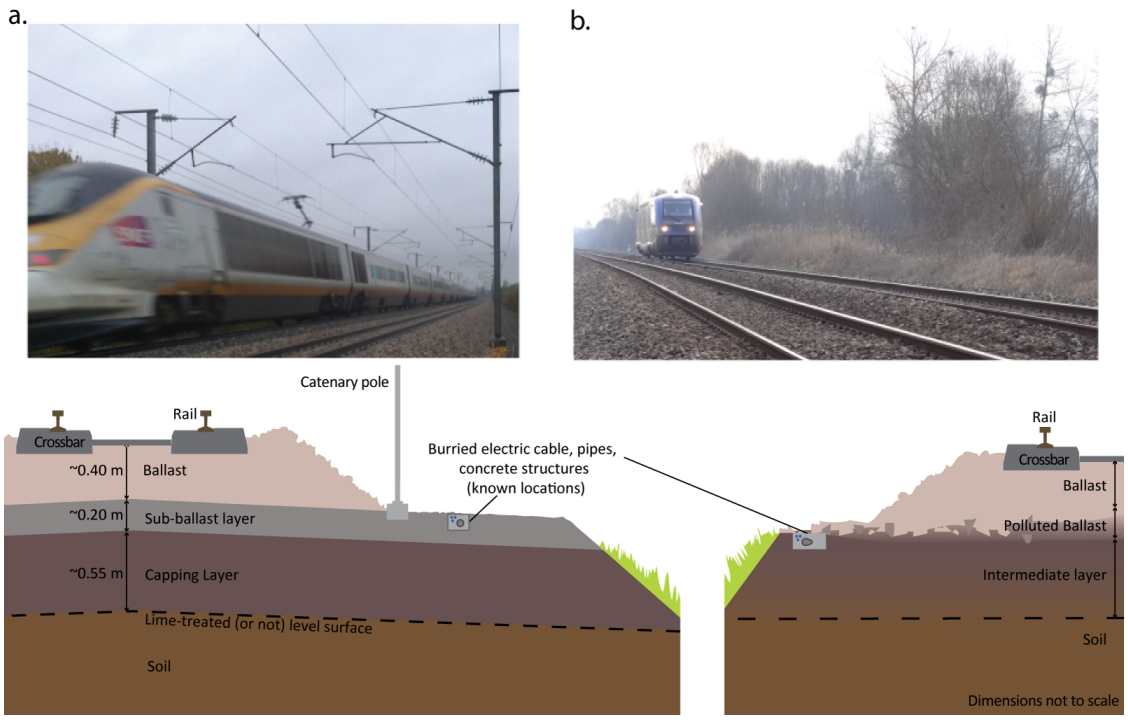

Figure 2.1: *Photographs (Bodet et al., 2014c) and diagrams (according to internal documents of the French Railroad Company (SNCF), orders of magnitude given as an indication) given as examples of the lines considered in this study : LGV-Nord (a) and conventional lines (b).*

characterization of soils and near-surface anthropic structures Heisey et al. (1982); Nazarian and Stokoe II (1984); Matthews et al. (1996); Hévin et al. (1998); Lai et al. (2002); Rydén et al. (2001, 2004)). The latest methodological advances show that 'surface-wave prospecting' can be deployed along linear sections or along a surface grid, in order to reconstruct a 2D or 3D model of near-surface VS distribution (Neducza, 2007; Boiero and Socco, 2010; Ezersky et al., 2013). A detailed presentation of the method, its acquisition, processing and inversion workflows is for instance given by (Pasquet and Bodet, 2017), along with a tutorial for most of the codes used in the following work. Further information and details can be found in the literature (see e.g.: O'Neill (2003); O'Neill et al. (2003); Socco and Strobbia (2004); Bodet et al. (2005); Socco et al. (2010); Pasquet (2014)).

Given the guided nature of surface waves, these events of the wavefield are less sensitive to the strong 3D character of the structures encountered in civil engineering applications (Karl et al., 2011). In addition, recent studies show a growing interest in the implementation of surface-wave prospecting in direct relation to geotechnical issues (Heitor et al., 2012) or in a railway context (Donohue et al., 2013, 2014; Hwang and Park, 2014; Jacqueline et al., 2014; Jacqueline, 2015; Jacqueline et al., 2017; Gunn et al., 2015; Bergamo et al., 2016a,b; Gunn et al., 2016; Sussmann Jr et al., 2017). These recent studies suggest to focus either on the ballast or on the RE and underlying soil. This project proposes a feasibility study of this approach as a means of in situ characterization of VS in the RE, whatever the type of contexts (high-speed lines on the left in Figure 2.1, or conventional lines, on the right in Figure 2.1) and whatever the type of issue encountered along the tracks.

VS of materials associated with RE

Dhemaied et al. (2014a) have experimentally shown [2] that VS is an acceptable criterion to differentiate materials within RE. This work was carried out on natural soils (likely to be used for RE) prepared and/or reconstituted in the laboratory to be characterized from a geotechnical point of view:

- with typical tests such as Atterberg limits, granulometry, proctor compaction tests, methylene blue values etc) on the one hand, and;
- with the 'Bender Element' technique (BE [3]). The impact of water content on the propagation velocities of mechanical waves in soils (e.g. Santamarina et al. (2005)) was also investigated in the laboratory using this technique (e.g. Santamarina et al. (2005)). e.g.: Cho and Santamarina (2001)) and/or using "acoustic" methods (e.g.: Fratta et al. (2005); George et al. (2009)), on the other hand, to estimate VS.

These tested soils were also specifically prepared to monitor the evolution of VS according to their water content (w). The results showed a systematic decrease of VS with w (at frequencies between 5 and 10 kHz). This work allowed to define, via the shear modulus obtained from the density and VS measurements, a 'characterization grid' sorting materials associated with RE by soil type and by moisture content (Dhemaied et al., 2014a,b).

A direct application of this work was proposed through the analysis of samples collected along a high-speed line (detailed in section 2.2) presenting a lack of stability identified during maintenance (Dhemaied et al., 2014a,c). The results of this application showed that among all the geotechnical tests performed (whether in situ or in the laboratory), only the mercury porosimetry (the microstructure) and the BE (the shear modulus) proved effective in identifying the defects observed on site. These studies thus support the idea of using surface waves as a tool for RE non-destructive evaluation.

2.1.3. Suggested approach

Since VS seems to be a sufficiently relevant parameter for the discrimination of soil types and their possible water content variations within RE, the estimation of VS by surface-wave dispersion measurement and inversion might be appropriate. This project therefore suggests a feasibility study of surface-wave prospecting for the systematic characterization of RE on representative sites presenting a lack of stability, defects and/or problematic levels of maintenance. However, given the environment and the geometry of the targeted structures, the experimental conditions limit the classical implementation of seismic methods (instrumental deployments are restricted both in space and time). The approach here therefore first aims at defining optimal setup configurations by adapting the usual experimental protocol to the scale of RE, while guaranteeing sufficient resolution for the measured velocities to be informative.

Seismic methods can be applied to very shallow targets (<10 m) using various types of sources, geophones and acquisition setups, depending on the objectives (e.g. Bachrach and Nur (1998);

2. Geotechnical study conducted from June 2012 to June 2014 as part of a École des Ponts ParisTech/SNCF postdoctoral contract.

3. The BE (Shirley and Hampton, 1978) are piezoceramic plates allowing the transmission and reception of a mechanical wave through a cylindrical sample to estimate its propagation velocity (VP or VS according to the transmission/reception mode). This technique is widely used for the estimation of small strain shear modulus in non-consolidated granular materials in general, and is the subject of active research for the study of soils in particular (e.g.: Lee and Santamarina (2005); O'Donovan et al. (2012)).

Baker et al. (1999); Abraham et al. (2004); Schmelzbach et al. (2005)), the key parameter being the measurement frequency range. In the past 10 years we have shown (Duranteau, 2010; Pasquet, 2014; Dangeard, 2019), in the same way as studies cited above (e.g. Schmelzbach et al. (2005)), that a classical near-surface seismic sources such as a 5 kg sledgehammer (or even smaller 1.25 kg hammers available) can generate a broadband signal at frequencies high enough to reach inframetric vertical resolutions, in media with propagation velocities lower than 250 m/s. In the case of RE, according to Dhemaied et al. (2014a) geotechnical results and test with BE, the velocities can be higher (up to 600 m/s). As a first step, care must be therefore taken to ensure that the frequencies are high enough to work at reasonable wavelengths. A dimensioning study (an extract of which is given in Figure 2.2) was carried out by semi-analytical modelling based on empirical RE models (the typical structures described by SNCF standards) with velocity ranges as observed in the laboratory by Dhemaied et al. (2014a), in order: (i) to check if the setup is sufficiently simple and quick to implement, adapted to both spatial and temporal constraints along railways (trackside occupancy limits, safety issues, etc); and (ii) to estimate signal resolutions to anticipate for real-life data acquisitions.

Once the setup dimensioned, it has been deployed on the site mentioned above, along the North European High-Speed Line (LGV-Nord) north of Hattencourt city. The detailed workflows and results of this feasibility study of high-resolution surface-wave prospecting for mechanical properties along RE are first presented in the following as a tutorial example. Once validated, the approach has been tested along classical lines, in much less constrained and structurally more heterogeneous contexts. Two examples are summarized here to feed the discussion: on site B along the Dijon/Is-sur-Tille line; and on site C along the Longeau/Boulogne line. Finally, this study will suggest perspectives for a more systematic implementation of the method and for a more quantitative exploitation of the results it provides.

2.2. Feasibility study along a high-speed line

2.2.1. LGV-Nord, Site A: context

An unusually frequent and local need for maintenance (in particular 'clogging operations') has affected track 2 (V2) along the LGV-Nord at site A (Figure 2.3). The origins of such an anomaly might have been, for example, linked to strong variations in the nature of underlying soils or to poor drainage. In order to precisely determine these origins, a geological and geotechnical survey (operated by the company GEOSOND; (Dhemaied et al., 2014a,c)) has been suggested. The lithological units observed along the tracks were as follows:

1. Quaternary embankments mainly from the RE construction and maintenance;
2. Loess characterized by beige silts more or less clayey, and;
3. Campanian chalk, whitish, poor in flint and possibly containing fine glaucous passages.

The RE has been built on 'natural' loess with the typical structure defined by the SNCF standards, as shown in Figure 2.4. The observed maintenance efforts were more pronounced along the V2 side. Figure 2.3 shows the areas where frequent maintenance was identified (in white dashed lines) as well as active anomalies observed in December 2013, during the geophysical survey described in the following (solid white lines on Figure 2.3).

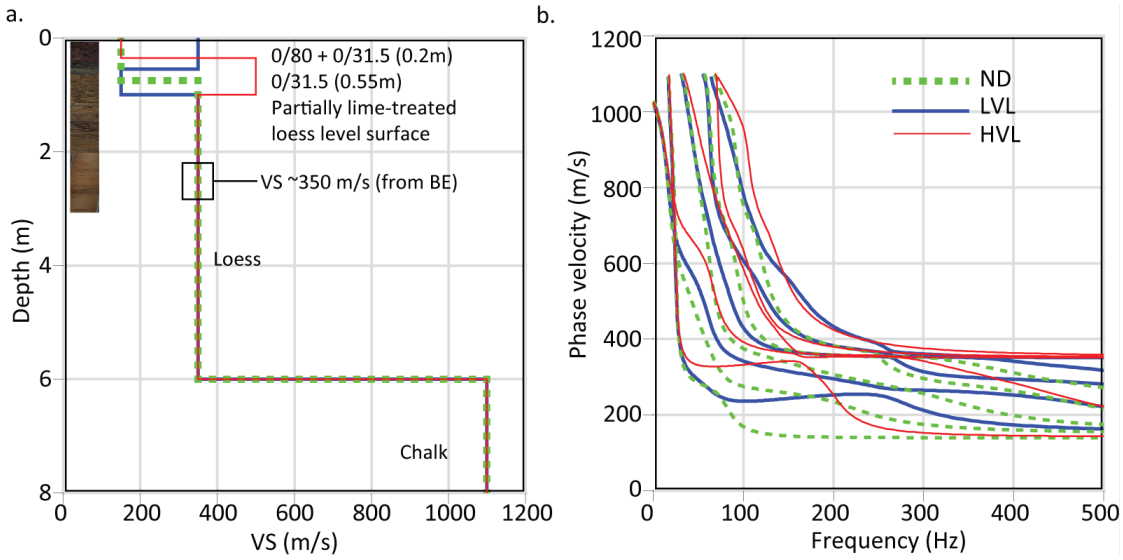

Figure 2.2: *Example result from the dimensioning study carried out by semi-analytical methods using geotechnical data to evaluate the frequency ranges and velocities to be anticipated in real conditions. Whatever the contrasts in expected velocities (a), the empirical models constructed from borehole data and typical ranges proposed by SNCF (ND: normally dispersive; LVL: Low Velocity Layer; HVL: High Velocity Layer), the simulated dispersion curves (b) show that the setup will have to be sufficiently long and with sufficiently short geophone spacings to obtain high-resolution dispersion images without being corrupted by spatial spectral aliasing, in particular to be able to separate the different propagation modes.*

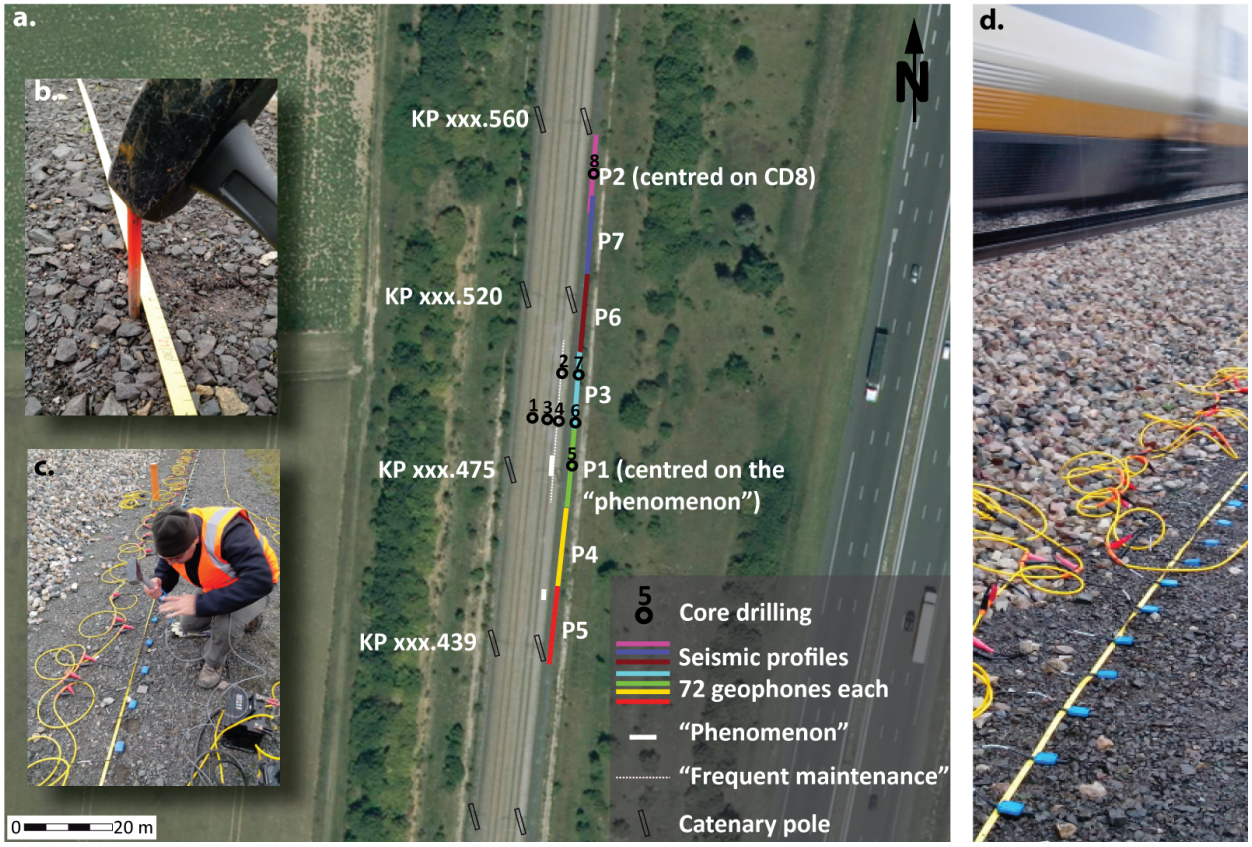

Figure 2.3: *(a) Schematic layout of the boreholes cores drillings (CD#) and seismic profiles (P1 to P8), the positions of which are given according to the referenced kilometre points (KP). Photographs (b, c and d) illustrating the installation of the setups along the trackside.*

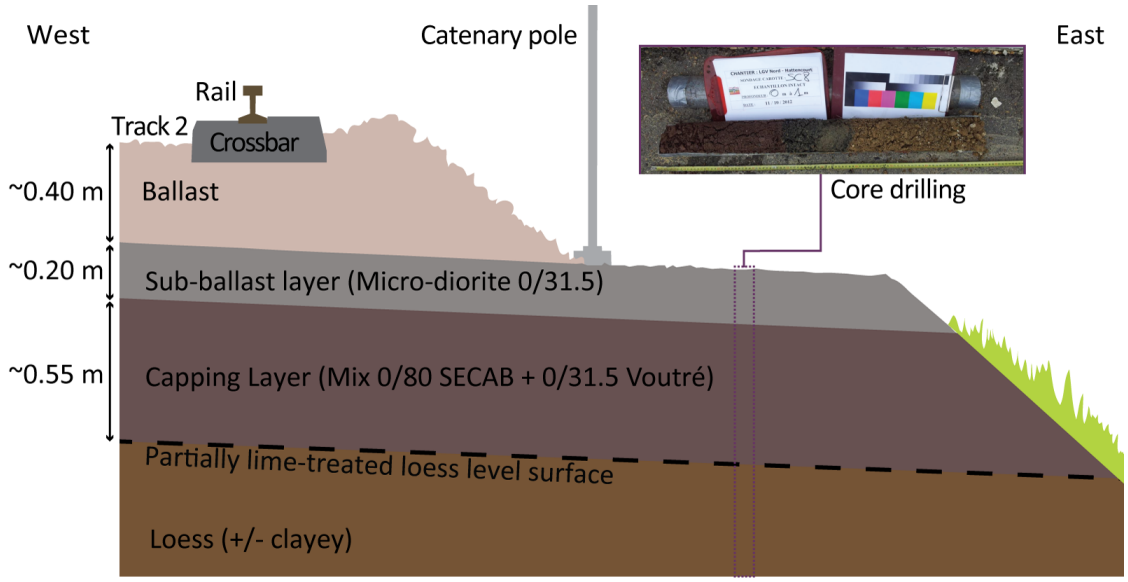

Figure 2.4: *Schematic section of the studied RE (typical structure defined by the SNCF norms). The details about layers materials are based on 'visual' monitoring data and interpretation of core samples collected by GEOSOND.*

2.2.2. Geotechnical tests

The geotechnical study performed by GEOSOND includeed 8 boreholes down to 3 and 12 m depths (black circles on Figure 2.3) as well as 5 dynamic cone penetrometer tests (DCP) 12 m deep (not presented here, see Dhemaied et al. (2014a,c); Heraibi (2019) for more details). These in situ tests were complemented by laboratory measurements such as Atterberg limits, granulometry, proctor compaction tests, methylene blue values, wet bulk density and water content estimations. The results (Dhemaied et al., 2014a,c) were coherent with the typical structure of RE, mainly involving vertical contrasts under the ballast, corresponding to: the sublayer and the capping layer, more compact (with a total thickness of 75-80 cm on average along the track) than the loess layer itself less compact than the chalk occurring between 6 and 7 m deep under the tracks. The results showed similar water contents and densities in the loess (respectively 20 % and between 1.6 and 1.7 Mg/m^3 between 1 and 3 m deep) whatever the locations of the drilling. The boreholes as well as the laboratory tests did not show significant variability of the RE structure along V2, nor from one trackside to another (see Dhemaied et al. (2014a,c)). This type of study therefore did not make it possible to identify the origins of the maintenance problem encountered along this line.

2.2.3. BE and porosimetry

To complement the classical geotechnical study summarized above, shear velocity measurements on samples that could be properly collected from the cores (cylindrical samples of 100 mm diameter and 50 mm height) were carried out using the BE technique at frequencies between 5 and 10 kHz. All samples were collected from the loess layer at one or several depths (depending on cores quality). The results, combined with water content and density measurements, are summarized in table 2.1. They show that the variation in VS (and consequently in shear modulus) xas partly correlated with the maintenance anomaly observed along V2. Additional tests (carbonate content) showed that

Table 2.1: *Measurements of density (ρ_d), water content (w) and orders of magnitude of velocities and shear moduli ($VS_{min-max}$ (m/s) and $G_{min-max}$ respectively) of the samples collected from boreholes at Site A. The depths correspond to core samples centers (modified from Dhemaied et al. (2014a,b)).*

Core Drilling (#)	Sample depth (m)	w (%)	ρ_d (Mg/m^3)	$VS_{min-max}$ (m/s)	$G_{min-max}$ (MPa)
CD1	1.6	20.6	1.65	120-134	28-35
CD1	2.3	15.7	1.73	125-137	30-36
CD1	2.6	15.7	1.73	596-687	675-897
CD2	2.6	19.8	1.60	165-183	52-64
CD3	1.6	18.1	1.71	152-172	44-56
CD5	1.5	20.1	1.67	312-366	185-255
CD6	1.1	20.9	1.70	153-173	44-57
CD8	2.3	19.3	1.57	296-378	166-271
CD8	2.9	15.4	1.65	357-390	242-289

this correlation was not related to the treatment of the loess. Finally, mercury porosimetry tests were carried out on these samples. The porosity spectra presented on Figure 2.5 (see Dhemaied et al. (2014a,c)) show a variability of the microstructure also partly consistent with the maintenance variations along V2.

2.2.4. Justification of the choice of seismic

The thorough laboratory geotechnical study by Dhemaied et al. (2014a) thus revealed that the origin of the maintenance problems would come from the loess present in the upper part of the earthworks at the base of the RE along the line. Classical measurements of water content, density, Atterberg limits etc, as well as in situ soundings such as DCP tests, did not show particular anomalies along the tracks. VS measurements by BE on samples however highlighted a variation in mechanical properties between the area where maintenance efforts were required and the area where they were not. As far as the water content did not change, the shear modulus proved to be a potential indicator of the loess layer 'quality' in terms of RE stability. The microporosimetry in the soil layer also confirmed a variation of its structure between the two areas. These results revealed a relationship between shear modulus degradation and the pore volume distribution of studied soils.

Such analyses unfortunately remain punctual, both in distance along the tracks and in depths at each sample collection location. The CD1 sample collected at 2.6 m depth for instance (see table 2.1 and Figure 2.5), was characterised by the highest shear modulus value while its porosity spectrum was spread out. The single sample collected and analysed for CD5 (see Table 2.1 and Figure 2.5) showed a high shear modulus value with a marked porosity maximum while it was located in the problematic area (see Figure 2.3). To avoid such ambiguities, regular sampling (along the tracks as well as at depth) would be necessary. Such studies are obviously not feasible in a systematic manner for the monitoring of RE along great distances (typically tens or hundreds of kilometres). In this context, systematic non-destructive in situ characterization of VS from seismic prospecting seems justified as an alternative monitoring tool.

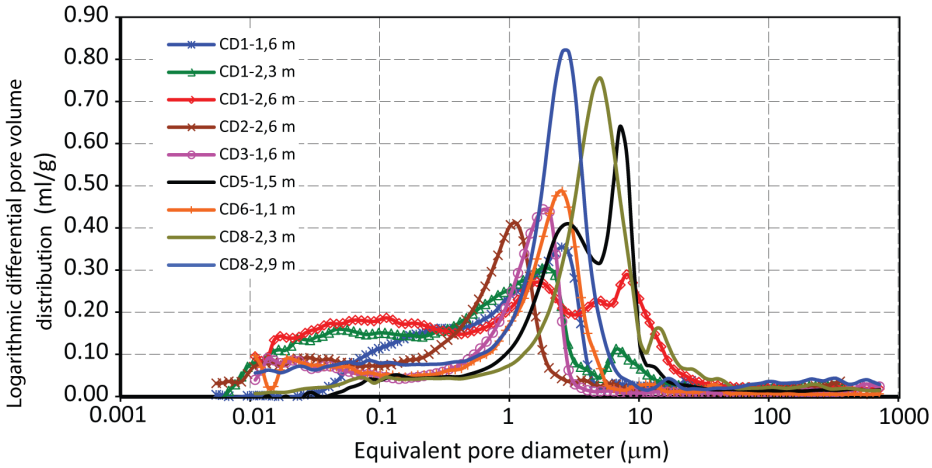

Figure 2.5: *Mercury porosimetry measurements carried out on samples collected from boreholes (see locations on Figure 2.3). The shear moduli estimated thanks to the BE tests on the samples are given for comparison (modified from Dhemaied et al. (2014a,c)).*

2.3. Surface-wave prospecting: implementation and dispersion measurements

2.3.1. Setup and measurement strategy

With dimension and acquisition parameters based both on the a priori well known structure of LGV-Nord embankment and on properties provided by the geotechnical results presented above, 7 seismic profiles of identical length were carried out along V2 (cf. Figure 2.3a). Each setup consisted in 72 vertical component geophones (14 Hz low cut-off frequency) 0.25 m spaced, to form a 17.75 m long profile. The setups were implanted along the trackside to guarantee a good geophone coupling with near-surface materials and to avoid the particular conditions of acquisition on ballast (Hwang and Park, 2014; Jacqueline et al., 2014). For each profile, seismic shots were performed with a sledgehammer on a metallic plate (see Figure 2.3c) every 24 geophones (between adjacent geophones) with first and last shot positions at half inter-geophone distance before and after the first and last geophone respectively. Each shot corresponded to the stack of 6 hammer/plate impacts to improve the signal-to-noise ratio. The recording length was 2 s with a sampling interval of 0.5 ms and a pre-triggering delay of -0.02 s. The profiles numbering (P1 to P7) corresponded to the implementation strategy decided during the survey:

— it was initially chosen to locate the first setup at the middle of the area presenting the worst maintenance efforts anomaly (P1 in Figure 2.3) and centred on CD5;
— then, another setup was located at the middle of an area that has never had maintenance problems (P2 in Figure 2.3) and centred on CD8;
— 5 other setups finally made it possible to complement the seismic line between these two profiles, with P5 slightly south of the high maintenance area where highly active anomalies were spotted during the survey.

The whole distance covered by these 7 profiles (see Figure 2.6) thus represented 120.9 m (which is less than 7×7.75 m because of an overlap between P7 and P2 due to the original choice of centring P1 on CD5 and P2 on CD8). The acquisition parameters and the relative positions of the profiles are shown in Figure 2.6.

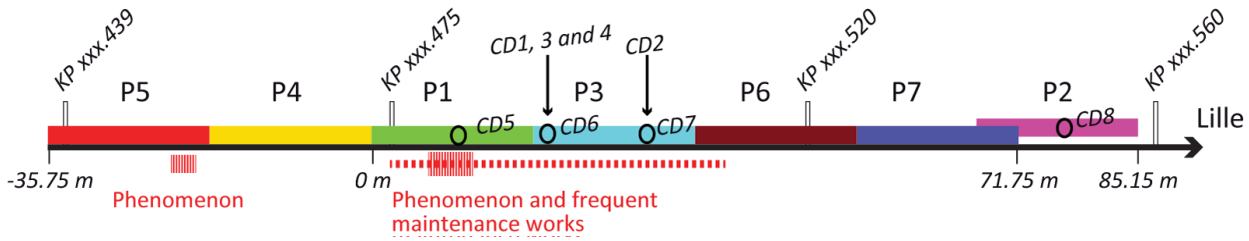

Figure 2.6: *Schematic layout plan of the seismic profiles (the positions of the catenary poles (KP# in km) and boreholes (CD#) are given as an indication).*

The first task carried out following this survey consisted in choosing the appropriate geophone window size for the surface-wave dispersion extraction from recorded sets of seismograms, in order to ensure the best compromise between expected vertical resolution and the need to limit the influence of lateral variations [4] on measurements as explained in details for instance in Pasquet and Bodet (2017). Surface-wave dispersion analysis is indeed limited by the classical trade-off between lateral resolution and investigation depth (Gabriels et al., 1987). On one hand, the inverse problem formulation imposes the investigated medium to be assumed 1D under the geophone spread. Additionally, the spread itself has to be short enough to achieve lateral resolution if profiling is performed. On the other hand, long geophone spreads are required in order to: obtain high resolution dispersion spectra; record wavelengths great enough to reach expected investigation depth; mitigate near-field effects; and discriminate modes at every available frequencies (e.g. O'Neill et al., 2003; O'Neill, 2003; Bodet et al., 2005, 2009a). In addition, as recommended by Bodet et al. (2005) and recalled by Steinel et al. (2014), direct and reverse shots on both side of a given spread (end-on and off-end) have to be considered to check the validity of the 1D assumption according to considered wavelengths.

2.3.2. Seismograms

For the survey presented here, the longest spreads consisted in 72 geophones. Considering such a length, only 2 shots were available and systematically compared for each profile. This work is illustrated here for P1 and P2 which will systematically serve as examples, since they are supposed to represent two very different states of the studied RE. Figures 2.7a and 2.7b present the 72 geophones seismograms obtained for P1 and P2 respectively. The seismic traces looks symmetrical as far as the guided waves are concerned, whether it is P1 or P2. The wavefield is very clearly disturbed by the catenary pole foundations at kilometre point (KK) xxx.475 for P1. The signal recorded along P2 is perturbed by 50 Hz noise probably because of the buried electrical networks and a possible contact of the geophone connectors with the wet ground after rain. Strong ambient noise generated by the highway in the east produced low frequency wave fronts on both P1 and P2. As shown on spectrograms of Figures 2.7a and 2.7b, the frequency content of the data is very satisfactory as far as dispersion analysis is concerned, with significant energy from 20 Hz to at least 250 Hz.

2.3.3. Dispersion

Each of the seismograms was then transposed, after correction for geometric attenuation, into the frequency-phase velocity domain. The result of such a wavefield transformation is called a

4. The term 'lateral variations' is sometimes used in seismic to mention variations encountered 'along' the profile.

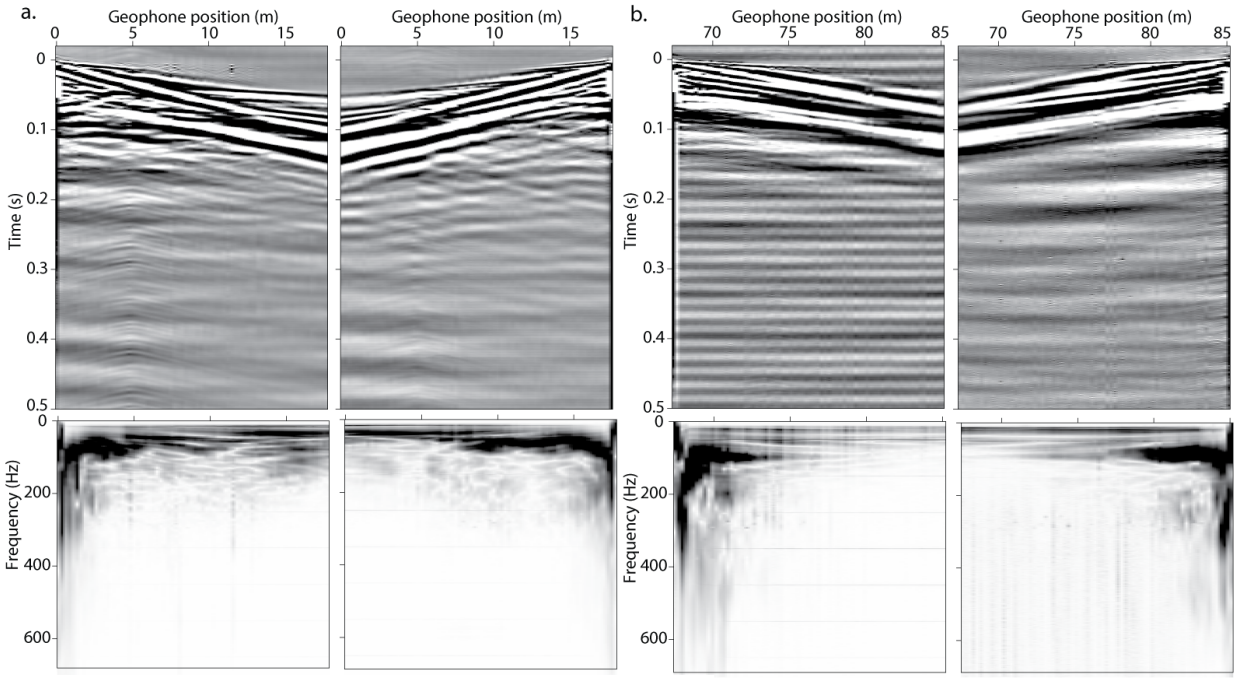

Figure 2.7: *(a) Normalized seismograms (top) and spectrograms (bottom) of the direct and reverse shots for P1 (the geophone positions are given in the local coordinate system shown in Figure 2.6). The seismic traces are perfectly symmetrical with respect to the guided wave train. The wavefield is very clearly perturbed by the pole foundations at kilometre point (KP) xxx.475. (b) The P2 shots show 50 Hz noise (probably due to the buried electrical networks and contact of the connectors with the wet ground after rain).*

'dispersion image' (see the tutorial of Mokhtar et al. (1988) for more details about the slant-stack in the frequency domain). The dispersion images obtained for each shot of profiles P1 and P2 are presented in Figures 2.8a,b and 2.8d,e respectively. The spectrograms are reproduced on these figures to show the frequency band in which the wavefield is sufficiently energetic to allow dispersion interpretation. Here again, whether it is P1 or P2, the direct and reverse shots produced very similar results. In this domain, the maxima (in black on Figures 2.8a, b, d and e) correspond to the dominant events of the wavefield: the PSV waves. It appears that a very large number of propagation modes are available in these images. But the difficulty of identifying their rank and the effective nature of the dispersion only made it possible to pick the first two modes (in red and white on Figures 2.8a, b, d and e). The maxima of the dispersion image resulting from the summation of the two shots are also given (Figure 2.8c for P1 and Figure 2.8f for P2) and compared with the individual picks on Figure 2.9. It clearly shows that the obtained dispersion curves are identical (taking the errors in dispersion measurements into account, according to the relationship introduced by O'Neill (2003) and essentially based on the resolution of the wavefield transformation). These results validated the hypothesis of weak lateral variations along the 72 geophones window (compared to involved wavelengths). They validated the stacking of dispersion images from direct an reverse shots, for both the improvement of the signal-to-noise ratio and the mitigation of near-offsets effects. Thanks to such stacking, it was also possible to preserve the highest frequency part of coherent wavefields present in the near-offsets traces (O'Neill, 2003; Bodet et al., 2005, 2009a). They also proved the weak influence on the dispersion analysis, of the noises identified on the seismograms as well as the repeatability of the measurement [5].

2.4. Variability of extracted dispersion along the line

2.4.1. Variability

As suggested by the seismograms presented previously, the results obtained for P1 and P2 (Figure 2.8) and the associated picked curves (Figure 2.9) show a very clear difference in terms of dispersion. These curves are superimposed on Figure 2.10a. While the first higher mode may be common to both profiles for a few points, the fundamental mode is clearly different from one area to another, with lower phase velocities in P1 than in P2. Since the fundamental mode is the one that reflects (very empirically) the properties of the medium, those measured in P1 and P2 suggest lower VS in the area affected by maintenance issues. The set of dispersion data obtained for the 7 profiles is finally presented on Figure 2.10b. The observed dispersion covers a range of wavelengths (0.3 to 18 m) considered as representative of the whole RE, including the upper part of the substrate [6]. The data show a partitioning of the dispersion that clearly corresponds to the observed differences in maintenance. This is a qualitative answer to the methodological questions posed by the project, at least as far as Site A is concerned. The following section provides a more quantitative interpretation of these measurements, attempting to estimate, from dispersion inversion, 1D VS models centred on each profile.

5. As mentioned earlier, this work was systematically repeated for each profile. Several window sizes were actually processed and it was finally found that the largest (the one offering the best spectral resolution) could be used.

6. Particular attention has been paid to the dispersion curves picking, e.g. by taking care to respect the limits related to the resolution of the wavefield transformation and near-offsets effects, as recommended by O'Neill et al. (2003); **?**); Bodet et al. (2005, 2009a) for instance.

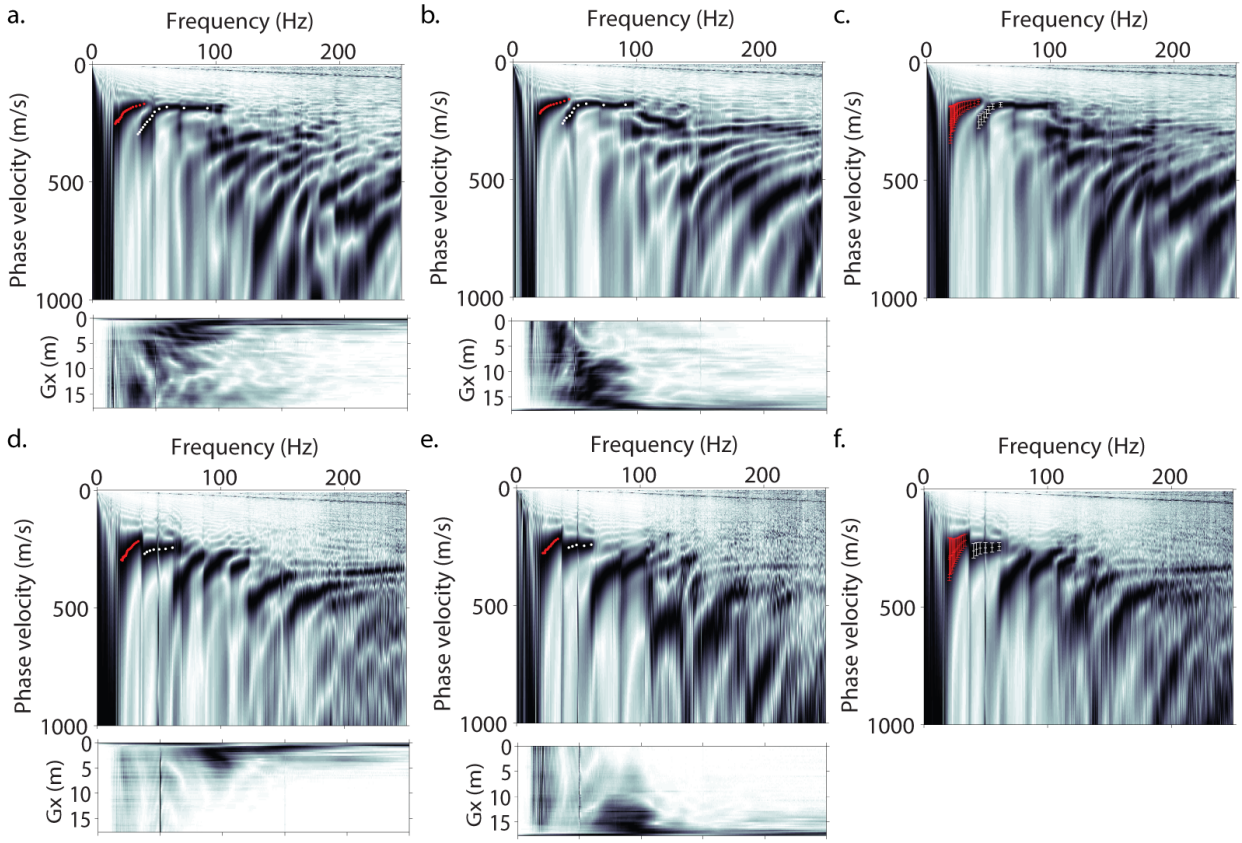

Figure 2.8: *Normalized dispersion images and spectrograms of the direct and reverse shots (a at b for P1, d and e for P2) and stacked images for each profile (c for P1 and f for P2). Among the large number of propagation modes appearing on these images, only the fundamental mode (in red) and the first higher mode (in white) have been picked (the errors in dispersion measurements are given empirically according to the relationship suggested by O'Neill (2003), essentially based on the resolution of the wavefield transformation).*

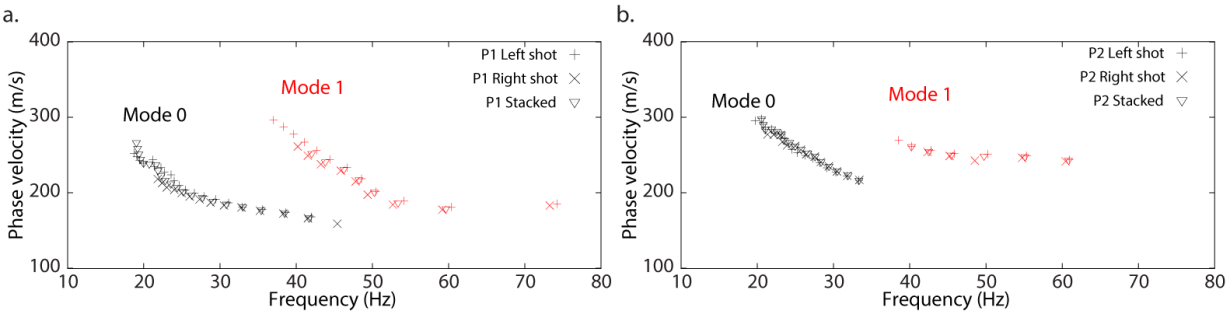

Figure 2.9: *Dispersion data plotted for each shot at P1 (a) and P2 (b) compared to those picked from stacked dispersion images. The fundamental mode (mode 0) is shown in black while the first higher mode (mode 1) is shown in red.*

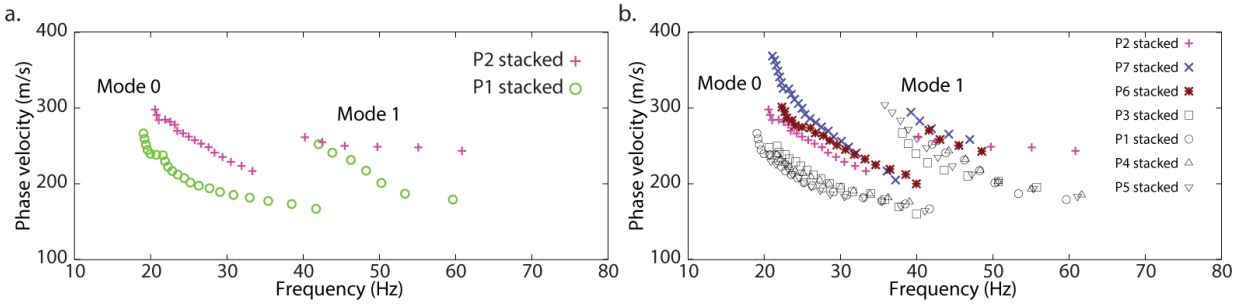

Figure 2.10: *(a) Comparison of the dispersion curves picked on the stacked images (see Figures 2.8c and f) for P1 (green) and P2 (purple). (b) Dispersion curves plotted for every profile.*

2.4.2. Interpretation of extracted dispersion: inversion for VS

The method used here for the 1D inversion of the dispersion is described through the example provided in the tutorial of Pasquet and Bodet (2017). The inversions were all performed with the *Neighbourhood Algorithm (NA)* developed by Sambridge (1999) and implemented by [7] for near-surface applications by Wathelet et al. (2004); Wathelet (2008). The NA is based on the partitioning of the parameter space into Voronoï cells [8] to randomly generate a large number of models within the parameter space defined, for a 1D representation of the medium, by a (fixed) number N of layers j (over a half-space) of varying thickness H_j, velocities VP_j and VS_j, and density ρ_j. For each generated model ($\mathbf{m}$), the difference between simulated dispersion (V_{cal_i}) and measured dispersion (V_{obs_i}) at each frequency sample (f_i) is given by: $misfit(\mathbf{m}) = \sqrt{\sum_{i=1}^{N_f} \frac{(V_{cal_i} - V_{obs_i})^2}{N_f {\sigma_i}^2}}$, N_f being the number of samples in frequency, and σ_i the phase velocity error associated with each sample.

This approach thus makes it possible to explore the parameter space to then select the set of models that 'produce' a simulated dispersion in agreement with the data according to the chosen *misfit*. Even if this technique tends to alleviate non-unicity issues sometimes encountered with the commercial tools available for surface-wave dispersion inversion, it remains strongly linked to the a priori of the user about the explored medium and the parametrization must be carried out with great care.

2.4.3. A priori info on RE and associated parametrization

The fact that the problem is addressed along a LGV provides very strong a priori info about the structure of the studied RE (see Figure 2.1). The number of layers and their thicknesses were well known (see Figure 2.4) and, in the case of site A, the approximate depth of the bedrock (the chalk) was given by geotechnical soundings. It was therefore suggested to try to fit the measured dispersion curves for each profile based on a mean a priori model of RE made up of 3 layers over a half-space, with parameters (velocity VS and thickness HS) free to evolve as follows:

— layer 0 (sub-layer) : $10 < VS0 < 750$ m/s and $0.1 < HVS0 < 1$ m;
— layer 1 (capping layer) : $10 < VS1 < 750$ m/s and $0.1 < HVS1 < 1$ m;

7. Open-Source Software 'Dinver', `www.geopsy.org`
8. This partitioning consists of dividing a n_p dimensional space into n_c cells (so-called Voronoï cells) so that each n_p model parameter is at the centre of a cell whose boundary in the n_p directions is halfway to the neighbour model in that direction.

— layer 2 (loess) : $10 < VS2 < 750$ m/s and $1 < HVS2 < 7$ m;
— layer 3 (chalk) : $10 < VS3 < 1500$ m/s; halph-space.

With such a parametrization [9] the algorithm benefited from the knowledge of LGV RE structures (number of layers in particular) but remained free to explore models very far from these a priori. The half-space was for example allowed to exist between 1.2 and 9 m depth. Its maximum depth corresponded to approximately 50 % of the maximum wavelength observed in the dispersion measured along the line, as well as half the size of the dispersion extraction window (as recommended by O'Neill et al. (2003); Bodet et al. (2005, 2009a)).

P1 and P2

For each profile, 100500 models have been generated within the parameter space described above. VP and ρ, of lower influences on dispersion, were also parameters of the models but were not considered here (see Pasquet and Bodet (2017) and basic references about the subject for more details). The results are presented for P1 and P2 on Figure 2.11. Each model is plotted with a colour depending on the distance (*misfit value*) between the data (black points and error bars) and the simulated dispersion. Despite the freedom offered by the parametrisation, the models corresponding to dispersion curves simulated within data error bars for both P1 and P2 involve two first layers shallower than 1 m on average, but do not present clear contrast for the chalk loess-interface (which is not surprising considering the size of the setup and the wavelengths involved [10]). Between these first 2 layers and the half-space, the 'best models' in terms of *misfit* values show a layer of constant VS of at least 4 m in thickness. A presentation of the misfit function in the thickness-velocity (HS2-VS2) domain given by Figure 2.13b, confirms the chalk depth is impossible to determine. On the other hand, this representation of the parameter space allows to quantify VS in the loess: e.g. approximately 190 m/s for P1 and 300 m/s for P2. The contrast obtained corresponds to the lateral variations observed along V2 and confirmed by the laboratory measurements with BEs.

Variability of VS along the line

The workflow described for P1 and P2 above has been reproduced for every profile, strictly keeping the same parametrization (no lateral constraints) and the same NA random model generation setup. The results obtained along V2 are thus synthesized on Figure 2.13a. Along these 7 profiles, the models systematically suggest two first layers a depth of less than 1 m, which is in very good agreement with the structure of the RE (sub-layer and capping layer theoretically presenting a total thickness of 0.75 m). The inversions also systematically show a layer at least 4 m thick and of constant VS, corresponding to the loess. In this layer, VS is variable along V2 as shown by the *misfit* maps (HVS2, VS2) presented on Figure 2.13b: from P5 to P3 (in the damaged zone) VS is close to 200 m/s whereas from P6 to P2 (in the healthy zone) VS is close to 300 m/s.

9. Many types of parametrizations have been tested by injecting more 'subjective' a priori info (fixed thicknesses, gradients in the loess, slight over-parametrization, etc). But a study focused entirely on the incorporation of higher modes and advanced data inversion is necessary for these results to be presented (Master's internship of R. Heraibi, SU).

10. Extraction of higher modes for a better description of the structure at depth is possible as shown in Figure 2.12.

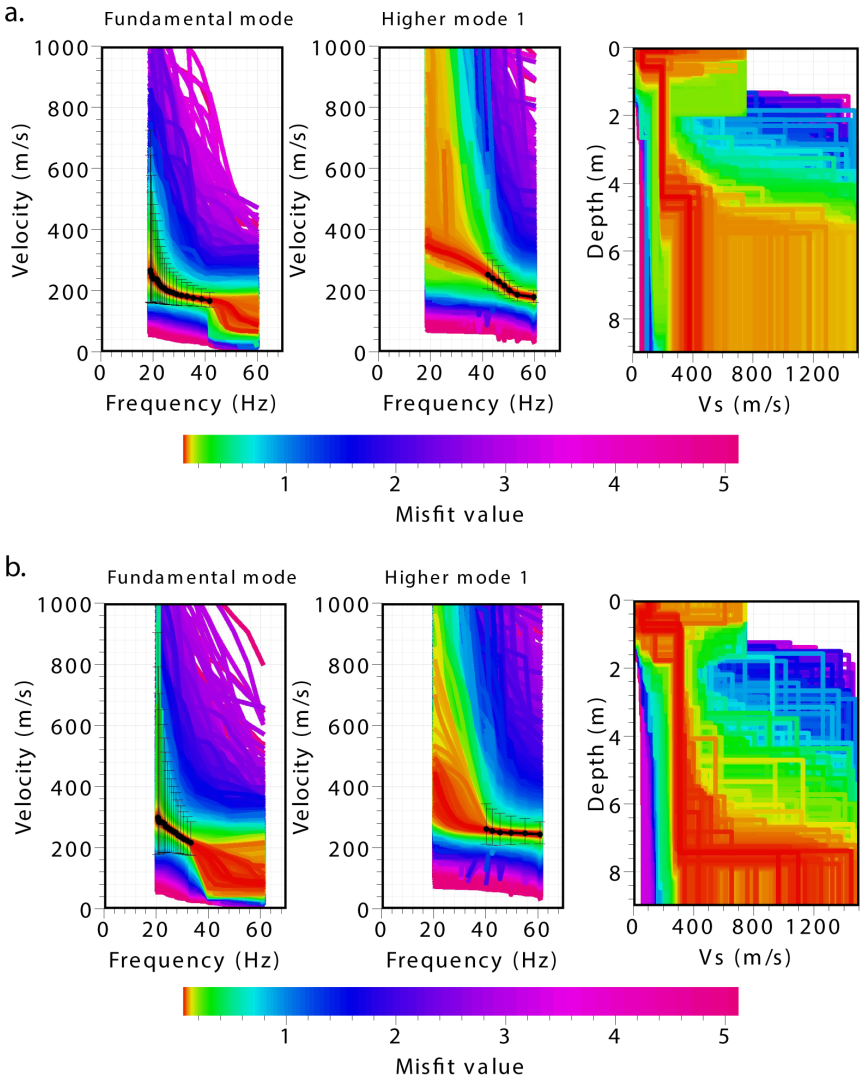

Figure 2.11: *Inversions of the dispersion curves for P1 (a) and P2 (b). Each model (right) is shown with a color depending on the misfit value between the data (black dots and error bars) and the simulated dispersion (each mode is shown separately). The 'best' models offer a possible interpretation of the first modes, but not of the other higher modes, as shown in Figure 2.12.*

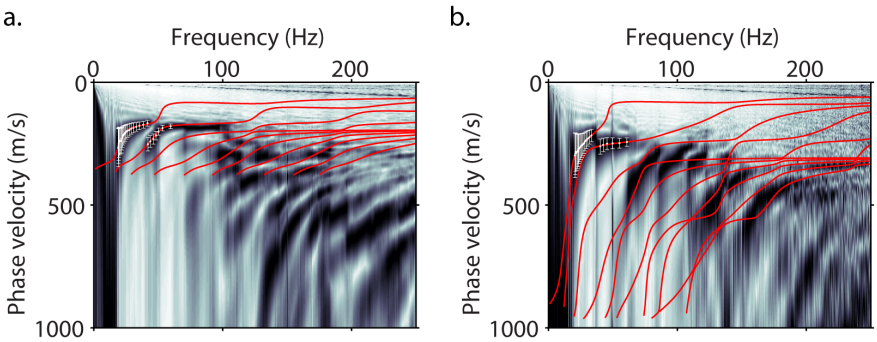

Figure 2.12: *Recalculation of the theoretical dispersion obtained from the 'best' models of Figure 2.11 for P1 (a) and P2 (b), suggesting a good interpretation of the first modes but the necessity of extracting higher modes for a better description of the medium at depth.*

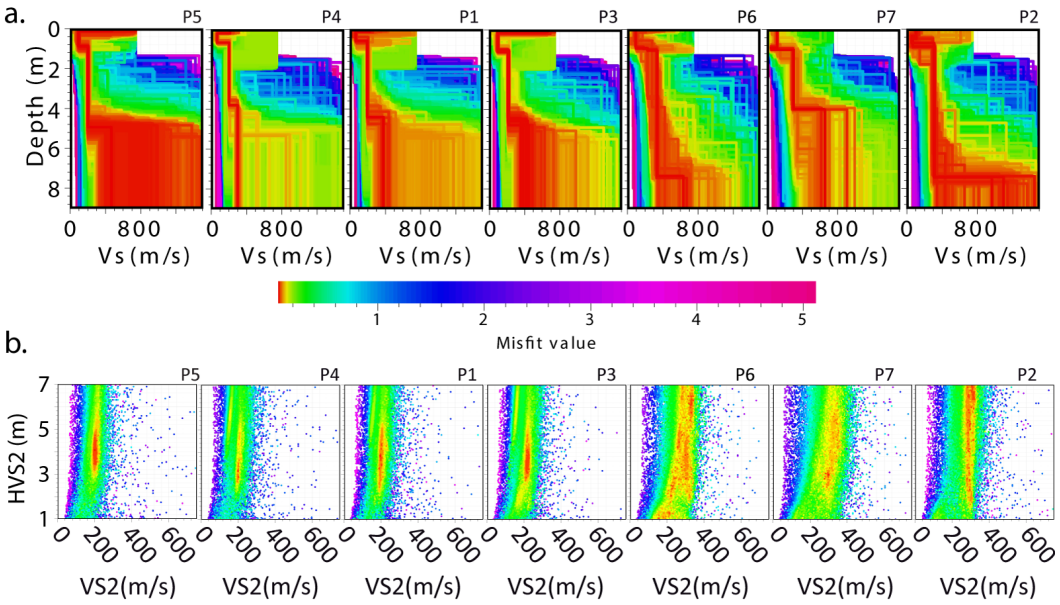

Figure 2.13: *(a) Set of inversions performed for the 7 profiles represented according to their relative positions along V2 (see Figure 2.6). Each model is represented with a colour depending on the deviation between the data and the simulated dispersion (misfit value). (b) Misfit maps for layer 2 (thickness (HVS2) versus velocity (VS2)) for the 7 profiles.*

2.5. Discussion, conclusions and perspectives

2.5.1. Proof of Concept

Dhemaied et al. (2014a) have shown, in particular with the use of BE on a wide range of soil samples, that VS was a good indicator of the 'quality' of materials in RE. Along the LGV-Nord (site A) Dhemaied et al. (2014a) showed that VS and microporosity were the only data able to identify the origin of maintenance anomalies, when classical geotechnical approaches (in situ or laboratory tests) failed. These results made it possible to propose this area of LGV-Nord as a test site for non-destructive and more efficient methods to monitor RE. The study presented here suggested surface-wave prospecting as a tool to estimate VS along these structures. It highlighted the advantage of this method linked to its robustness against ambient noise and compatibility with 3D structures (depending on involved wavelengths). A bibliographical study and dimensioning tests have enabled the development of a seismic setup adapted to the implementation of surface-wave prospecting along LGV-Nord. The systematic acquisition of direct and reverse shots allowed a reliable and repeatable dispersion measurement along the trackside. This approach, combined with dispersion stacking, offered sufficient spectral resolution to clearly identify several PSV-wave propagation modes. 7 profiles intercepting the area of unusual maintenance works produced very distinct dispersion measurements. They clearly showed a partitioning that corresponded to the observed RE stability issues, providing a qualitative answer to the methodological questions posed by the project.

The strong a priori knowledge about the RE structure available for this site then allowed an inversion of these dispersion measurements for 1D models of VS along the trackside. Despite the degrees of freedom offered by the parametrization for these inversions, the models systematically suggested the existence of two first layers at an average depth of less than 1 m (the sub-layer and the capping layer). The results also clearly presented a third layer of at least 4 m thick and constant VS. A presentation of misfit maps for these layers made it possible to quantify VS in the loess along the line (on average 190 m/s in the problematic zone and 300 m/s in the non-problematic zone). The identified contrast corresponded to the actual lateral variations observed along V2 and confirmed by BE measurements on samples. These results showed, in the case of such LGV site, that dispersion data and inversion could be considered as good criteria for the monitoring of RE.

2.5.2. Applicability to classical lines

The structure of conventional lines is much less constrained, in particular because of the variability of their construction methods (depending on the context and the period). Along these lines, the trackside and the embankments present strong 'natural' heterogeneities at the surface, as well as at depth. The experiment performed along LGV-Nord has therefore been reproduced along the conventional Dijon/Is-sur-Tille line (site B). Its RE consisted of a ballast layer and an intermediate layer directly lying on the natural soil, covering a marl-limestone transition (Figure 2.14). On this site, the measured signals were compromised by the very poor coupling of the geophones (due to a trackside layout polluted by the ballast, as well as to very strong surface heterogeneities, preventing the stacking of several shots). Only a meticulous and systematic study (Figure 2.15, cf. Bodet et al. (2017) for more details) of all the possible combinations for the extraction of the dispersion images allowed the RE anomaly to be detected (Wacquier, 2017).

A multi-method study was also carried out along the conventional Longueau/Boulogne line (site C) to better understand the origin of the disorders affecting the railway tracks built on peat soil (and to test the surface-wave approach complementarity with other geophysical and geotechnical

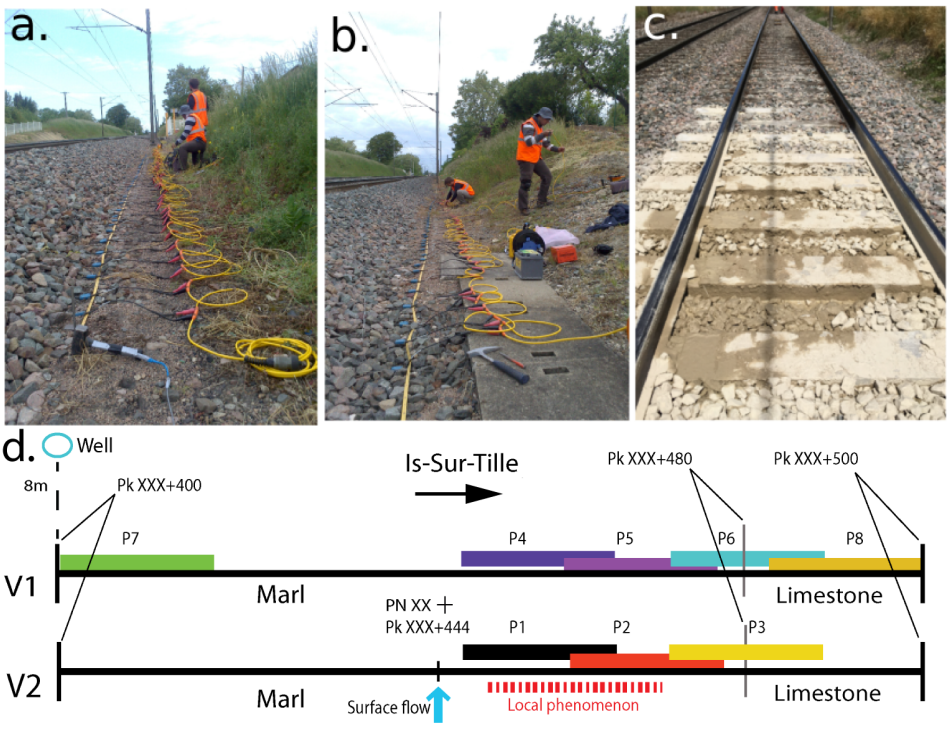

Figure 2.14: *Photographs of the acquisition setups on site B, showing (a) pollution of the runway by ballast, (b) lack of space for the setup implementation due to the presence of concrete structures for cables and (c) a perturbed levelling. (d) Diagram of the setup (not to scale) of the different seismic profiles. Each coloured band represents a seismic acquisition consisting of 72 geophones 0.25 m spaced, each involving 4 shots (1 shot every 24 geophones). The levelling issue is indicated with red dashed lines on V2 (KP : kilometric point; PN : level crossing). The transition between limestone and marl is located at KP XXX+480. The setups mainly targeted the fault zone (P1, P2, P3, P4, P5, P6, P8). A profile was also carried out in the 'healthy' zone, far away from the faults (P7) (modified according to Wacquier (2017)).*

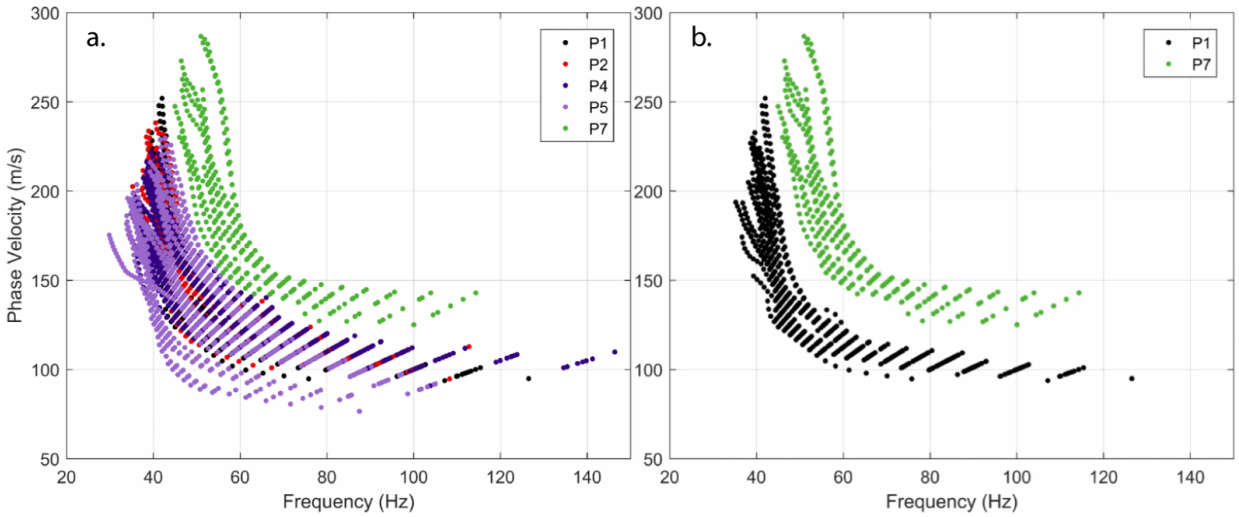

Figure 2.15: *(a) Set of PSV fundamental mode phase velocity-frequency picked data for direct or reverse shots of all profiles without stacking of the dispersion images. (b) Fundamental mode picked for direct or reverse shots of P1 and P7 only (still showing possible discrimination of the two zones in terms of phase velocities, modified from Wacquier (2017)).*

techniques). On this site, the observed tracks geometry anomalies seemed to result from a dynamic loading of the soil because of intermittent freight trains traffic (Boisson-Gaboriau et al., 2016). A surface-wave survey along the trackside (in the same way as for sites A and B) highlighted the most affected areas through an apparent decrease in estimated PSV phase velocities (Fig. 2.16, cf. Bodet et al. (2017) for more details). Dispersion data could not be inverted for quantitative results (the RE/peat contrast offering a so-called 'inversely dispersive' medium that is classically very difficult to quantitatively characterize at depth). The broad-band frequency content of measured signals nevertheless made it possible to determine the origin, at depth, of the anomalies (here attributed to the 'natural underlying soil') and to rule out the hypotheses of problems related to the bedrock or to the intermediate layer (Rhamania, 2015; Kyrkou, 2016; **?**).

2.5.3. Towards an operational framework

This work has led to the definition of a setup, an acquisition protocol and a processing method adapted to the in situ estimation mechanical properties variations in RE with surface waves:

- the approach has made it possible to detect and identify the origin of RE defects along the LGV-Nord, simply by the systematic extraction of the PSV waves fundamental mode;
- in the case of classical lines, despite strong heterogeneities at the surface and a delicate implantation of the geophones, it was also possible to locate problematic zones and to suggest their origin at depth (these two tasks however required a strong expertise in surface-wave processing);
- a quantification of these measurements (towards mechanical moduli) is possible in the framework of LGV-Nord, through inversion and confrontation with other geophysical and geotechnical data.

While these results are very encouraging with regard to the applicability of the approach developed during these projects, they remain to be validated in different contexts and above all to be

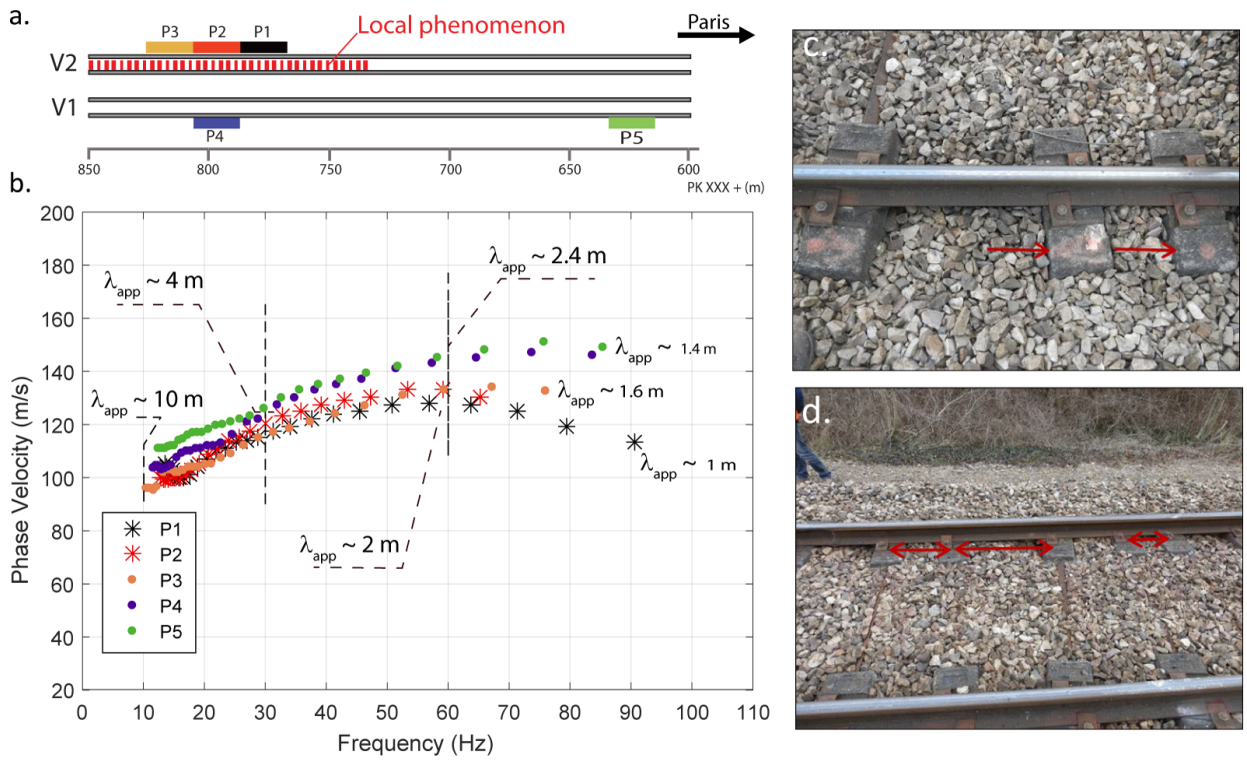

Figure 2.16: *(a) Implementation of the seismic profiles on site C (following the same configuration and strategy as for sites A and B). P1, P2 and P3 were located on the area with anomalies. P4 and P5 on areas with no defects. (b) The dispersion curves extracted at the centre of each setup (stacked direct and reverse shots) are represented and compared qualitatively. The dispersion curves from V2 (which presented anomalies), show lower velocities than the curves from the profiles of V1 (which was not affected). The simple transposition of data in the wavelength domain made it possible to estimate the pseudo-depth of investigation. (c, d) Anomalies observed on V2 (modified from Rhamania (2015); Kyrkou (2016); Wacquier (2017)).*

optimized. Several issues have to be addressed, such as:

1. the development of an operational and versatile methodology (e.g. adaptable to the variety of RE 'heritage' and the diversity of pathologies to be monitored);
2. the creation of a prospecting tool with a sufficient yield for decision-making support and to guide choices in terms of design, monitoring and maintenance.

It will therefore be necessary to carry on these developments:

— to optimize the setups in order to improve their resolutions (both vertical and lateral);
— to develop faster implementation techniques (not requiring geophones to be implanted and/or equipped with automatic sources);
— to adapt the processing techniques and tools to the railway environment on the one hand, and to the optimizations mentioned above;
— to suggest systematic techniques in order to quantify the uncertainties associated with observations by types/measurement contexts;
— to combine the acquisitions (GPR, DCP, seismic, etc) to increase their complementarity during processing, cross-check the data during interpretation with the use of deep learning approaches;
— to propose possible couplings between geophysical and geotechnical observables to tend towards a quantification of results in terms of mechanical moduli (SNCF standards).

Chapter 3

Environmental application: tracking water in hydrosystems

3.1. Introduction

As recently stated in Vadose Zone Journal's Research Highlights [1], 'water in the unsaturated vadose zone has an important function for many aspects of life. It is particularly important for plants' growth and serves as a buffer for movement of pollutants from the land surface to the aquifers. The amount of water present in the vadose zone also determines the partitioning of rainfall at the land surface into infiltration and runoff'. This water content and related physical properties of the soils are characterized by strong spatial and temporal variations mostly driven by weather and human activities. To understand this variability and its link to the stream-aquifer continuum, scientists seek to measure and monitor the soil water content at different scales using a large variety of techniques. Over regional to continental scales, remote sensing using microwave sensors are typically used to quantify soil moisture in the shallow surface layer (0-5 cm), using a combination of aircraft and satellite platforms. At local scale (basin, catchment), however, the monitoring of the Critical Zone (CZ) and associated hydrosystems mainly rely on local information, both in space and time, for instance provided by piezometric data, log analyses or water sampling and direct measurements with sensors in streams.

The understanding of underground water content, flows and associated transports is consequently an extremely complex task. The heterogeneity of the CZ itself is almost impossible to image (Binley et al., 2010). The processes it involves occur through a great variety of scales making it delicate to choose the suitable hydrological properties to study them (it is even more difficult to measure or estimate targeted parameters). In order to mitigate these limitations, hydrologists and hydrogeologists turned to geophysical methods over the past two decades (e.g. Rubin et al. (1999); Hubbard and Linde (2011)). The combined use of multi-scale probing and imaging techniques along with the integration of hydrological, hydrogeological and geochemical data is now classically suggested for the observation and study of the stream-aquifer continuum and of the CZ more generally (e.g. Parsekian et al. (2015); Binley et al. (2015). This approach, often referred to as 'hydrogeophysics', is predominated by electrical and electromagnetic methods due to their obvious links with physical parameters related to water content. Probing techniques with theory

1. https://dl.sciencesocieties.org/story/2016/sep/tue/small-scale-seismic-monitoring-of-varying-water-levels-in-granular-media-0

relying on mechanical properties of the Earth however emerged, such as geodetic methods which track surface deformation induced by underground pressure variations and are often combined with satellite and/or ground gravimetric measurement (e.g. Longuevergne et al. (2009); Schuite et al. (2015)).

As for mechanical properties-dependent geophysical methods, seismic prospecting techniques are commonly used at different scales in hydrogeophysics. Yet, seismic imaging remains mainly confined to the characterisation of geological structures then used to constrain hydrological models (Bradford and Sawyer, 2002; Pride, 2005). The seismic signal is by definition related to mechanical properties that partly depend on porosity, saturation and permeability. The behaviour of shear (S) and pressure (P) waves in the presence of fluid is partially decoupled. Then, the ratio of their propagation velocities (VP and VS), or the Poisson's ratio, classically permit imaging fluids in rocks. This strategy, well known in various applications in Earth sciences, remains however underused in near-surface geophysics, hence hydrogeophysics!

3.2. Proof of concept

The idea was then (back in 2009) quite simple: if estimating water content can be achieved thanks to combined measurements of VP and VS, let us go to our hydrogeologists' favourite sites and perform P- and SH-wave refraction tomography, as suggested by Turesson (2007); Grelle and Guadagno (2009). We could even try the use of surface-wave profiling techniques, as tested by Cameron and Knapp (2009), to estimate both VP and VS from only one acquisition. We asked to our favourite hydrogeologists if they could provide us with a well controlled and monitored hydrosystem, on which we could preform our seismic experiments. But such a site does not really exist: 'you always have uncertainties about the heterogeneities of the medium (not to say partial ignorance of its actual geometry and properties)' they would answer. So we decided to go to the beach, as already suggested by Bachrach and Nur (1998); Bachrach et al. (1998, 2000) and West and Menke (2000) [2].

On this beach in Merlimont (Pas-de Calais, France) we used a 72-channel seismic recorder with 14 Hz vertical and horizontal component geophones. A 0.5 m receiver spacing was used to obtain a 11.5 m long profile (Fig. 3.1c). We were using a metallic plate hit vertically by a 1 kg hammer as a 'P-wave source' (Fig. 3.1a). We tried to generate transverse motion in the sand with a manual source consisting in a heavy metal frame hit laterally by a 5 kg sledgehammer (Fig. 3.1a). A detailed presentation of the experiments with several sources, profile lengths, orientations et acquisition workflows, were tested by Duranteau (2010). Two seismograms are showed as examples on Fig. 3.2. On the vertical component geophones (Fig. 3.2a), the wavefield clearly shows nicely dispersive high amplitudes, low frequency and low velocity wave-trains, right after direct and refracted P-wave arrivals (picked in red). On the transverse component geophones (Fig. 3.2b), the low frequency, low apparent velocity and high amplitude part of the wavefield seems less 'continuously dispersive' along the profile, suggesting attenuation/scattering effects. First arrivals (picked in green on Fig. 3.2b) show a rather smooth non-linear increase with source-receiver distance. Picked arrivals were separately inverted for VP and VS vertical (1D) velocity structure, in the framework of elastic wave propagation in stratified media (Fig. 3.2c). It was not possible, given

2. Actually, West and Menke (2000) already had proven at that time that using seismic methods to track near-surface water was worth a try. We wanted to do it by ourselves and spend time on the beach, so we went to the Pas-de-Calais... during winter!

Figure 3.1: *Mimicking Bachrach and Nur (1998); Bachrach et al. (1998) and West and Menke (2000) experiments in Merlimont (Pas-de Calais, France). (a) Fayçal Rejiba hitting the sand as vertically as possible to provide seismograms for P-wave refraction. (b) Christian Camerlynck standing on our S-source to increase its coupling with the ground while Amine Dhemaied is getting ready to hit it as horizontally as possible to provide seismograms for SH-wave refraction. (c) Global view of the 3-component set-up dimensioned by Mickael Duranteau during his Master internship in 2010 (Duranteau, 2010).*

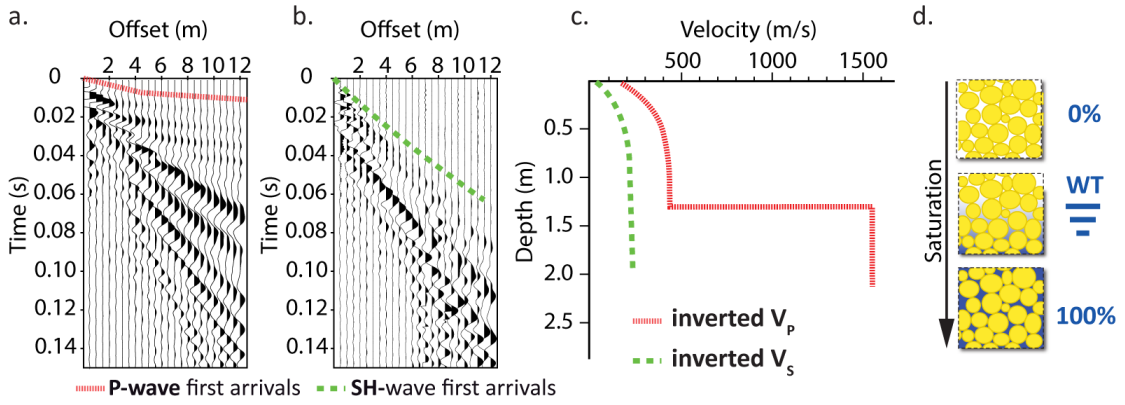

Figure 3.2: *(a) Seismogram of particle vertical velocity on which first arrivals correspond to direct and refracted P waves. (b) Seismogram of particle transverse velocity on which first arrivals correspond to direct upward bending SH waves. (c) Interpreted VP and VS vertical (1D) velocity structure, only considering a simplified binary dry-saturated model (d) (Duranteau, 2010).*

the spatial resolution of our set-up compared to the shallow water table, to take fine degrees of saturation into account (Fig. 3.2d). We nevertheless obtained a satisfying 'binary' estimation of the saturation profile thanks to the interpretation of both VP and VS.

This experiment illustrated the proof of concept as it has been previously proposed by West and Menke (2000) for instance: in the absence of strong prior information about the probe medium, estimating VS helps confirming if a contrast in VP is due to water or not. It is however clearly trickier than it seems. In soils and rocks, the important spatial variability of subsurface materials 'dry properties' is frequently of greater influence on seismic-wave velocities than the variation of water content itself. Based on this consideration, an alternative way to track down water distribution is to assume that it usually changes in time. The example on Fig. 3.3 clearly shows how water content variations strongly influence the seismic signal. Yet, even in such apparently simple media, the effects of fluid on both phases and amplitudes of the wavefield remain complex (Domenico, 1977; Géli et al., 1987; Brunet, 2006; Brunet et al., 2008; Sidler et al., 2010). When the water content increases in unconsolidated granular packed structures such as sands, the effective stress (e.g. Terzaghi, 1936; Bishop, 1959; Fredlund et al., 1978) no longer solely depends on gravity, but also on pore pressure and capillary action (Bear, 1972; Cho and Santamarina, 2001; Lu and Likos, 2004; Santamarina et al., 2005). Moreover, though studies have shown that VP decreases slightly to 99 % saturation and increases drastically beyond (Bachrach and Nur, 1998), others suggest that very small changes of saturation (e.g. related to air humidity variations) may increase the cohesiveness of the granular medium (and therefore VP) by creating 'liquid bridges' between the grains (Bocquet et al., 1998). Similarly, if the increase in the density of the equivalent medium in the presence of water can lead to a small decrease in VS, capillary forces observed at low saturation values are likely to have the opposite effect. One can easily anticipate that these features will be even more complex in soils, weathered layers and near-surface rocks formations which basically consist in non-linear transition(s) from unconsolidated materials to hard-rocks (without mentioning strong heterogeneities in porosity and permeability within similar lithological units, or the influence of fracturing at multiple scale, or the anisotropy etc).

Based on this simple experiment in Merlimont and on existing attempts in the literature cited

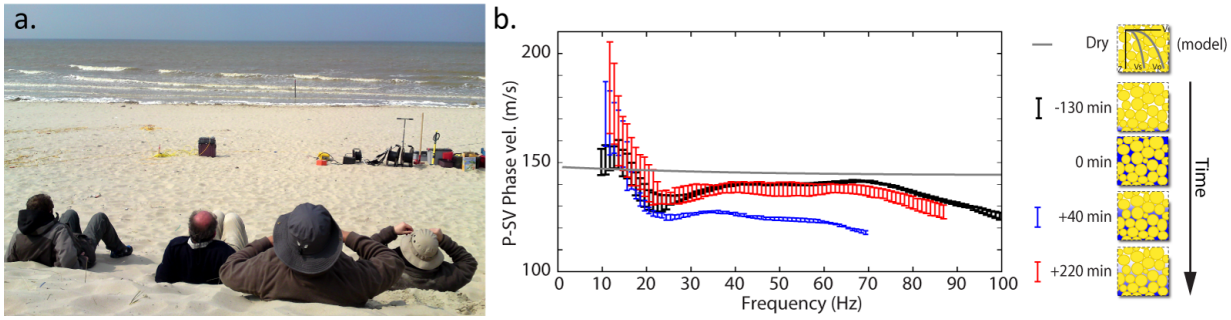

Figure 3.3: *(a) The Merlimont experiment crew waiting for the tide to rise and to submerge the seismic line in order to observe time-lapse variations of the wavefield. Following the example of West and Menke (2000), we were able to pick the fundamental mode of PSV waves at 3 distinct states. Modified after Duranteau (2010).*

above (e.g. Bachrach and Nur, 1998; Bachrach et al., 1998; West and Menke, 2000; Turesson, 2007; Grelle and Guadagno, 2009; Cameron and Knapp, 2009), we decided to adopt the following strategy:

- The targets of interest for the hydrogeologists are basically heterogeneous: we need to describe this heterogeneity with seismic methods but not only (geotechnics and non-seismic geophysics will be mandatory);
- VP/VS is obviously mandatory to have an idea of water content: we need to optimize existing techniques to retrieve these parameters (SH-wave tomography, surface-wave profiling);
- In the subsurface, spatial variations of 'dry properties' are frequently of greater influence on seismic-wave velocities than the variation of water content itself: we need time-lapse observations;
- The effect of fluid on the seismic wavefield remains complex and depends on the intrinsic properties of probe materials: we need rock physics models adapted to our near-surface targets.

In the following, we will show how we developed a workflow to systematically retrieve both VP and VS along the same profile with one acquisition, thanks to refraction tomography and surface-wave profiling. We then illustrate how we systematically tested these methods on well controlled hydrogeological sites in order to suggest an operational process for the study of hydrosystems' heterogeneities and water content spatial variations. A time-lapse approach has been developed as well, in order to capture temporal variations of water storage and to provide constraints to point continuous observations. We eventually show how our ongoing studies aim at extending the hydrodynamic modelling domains and providing adapted boundary conditions.

3.3. A simple methodology for the Critical Zone

`'In near-surface seismics, we shoot first and think later...', quoting S. P. (2014)`

3.3.1. Getting rid of the S-source (but still being able to image VS contrasts)

For near-surface studies, VP is typically retrieved with P-wave refraction tomography using a flat plate and hammer source with vertical component geophones (Schuster and Quintus-Bosz,

Figure 3.4: *(a) Christian and I carrying the S-source. (b,c) Top and bottom view of the frame. As noticed in the Merlimont experiment, this source is efficient only if one stands on the frame to increase its coupling with the ground while a second operator is trying to hit it as horizontally as possible, which is quite unsafe. Modified after Pasquet (2014).*

1993; Bauer et al., 2003, 2010; Uhlemann et al., 2016). The use of this method is widespread as it is easily implemented with a one-dimensional (1D) to three-dimensional (3D) coverage, quick to set up and relatively inexpensive. When applied for the estimation of VS, seismic refraction however requires a supplementary acquisition using specific sources strenuous to handle (Sheriff and Geldart, 1995; Jongmans and Demanet, 1993; Haines, 2007), as shown on Fig. 3.1b and Fig. 3.4. In addition, horizontal component geophones have to be levelled with care, which is often difficult on the field. As an alternative, surface-wave seismic methods are commonly suggested to infer the 1D VS structure of the Earth and subsurface materials (e.g. Gabriels et al., 1987; Jongmans and Demanet, 1993; Jongmans et al., 1996; Bitri et al., 1998; Park et al., 1999; Foti, 2000; Rix et al., 2001; O'Neill et al., 2003; Forbriger, 2003a; Bodet et al., 2005; Socco et al., 2010; Bergamo and Socco, 2016). In the early 2000's, surface-wave methods have rapidly grown in popularity among near surface practitioners with their access to multichannel equipment and the development of dedicated techniques and associated softwares. Among those techniques, the Multichannel Analysis of Surface Waves (Miller et al., 1999; Park et al., 1999; Xia et al., 1999) suggested 2D profiling by repeating identical single-shot seismic acquisitions along a profile, then extracting dispersion curves from each of these acquisitions. When targeting 2D shallow structures with strong lateral variability, this method is however limited by the classical trade-off between lateral resolution and investigation depth (Gabriels et al., 1987). On one hand, the inverse problem formulation imposes the investigated medium to be assumed 1-D under the spread. Additionally, the spread itself has to be short enough to achieve lateral resolution if profiling is performed (Fig. 3.5). On the other hand, long spreads are required to record wavelengths great enough to increase investigation depth and to mitigate near-field effects (e.g. O'Neill et al., 2003; O'Neill, 2003; Bodet et al., 2005, 2009a).

Several techniques have been developed to overcome these limitations. For example, O'Neill et al. (2003); O'Neill (2003) proposed a more comprehensive strategy providing local dispersion images along a profile using overlapping roll-along set-ups or several sources interspersed between the geophones. The procedure consists in computing dispersion images from identical subsets of the seismic set-up illuminated by different shots, then stacking the dispersion images obtained

for each subset to increase the signal-to-noise ratio and enhance the identification of surface-wave propagation modes. In the meantime, Hayashi and Suzuki (2004) developed an approach based on the analysis of common midpoints cross-correlations (CMPCC). With this technique, cross-correlations are initially calculated for each shot between all pairs of traces. Then, those having identical common midpoints (CMP) are combined and sorted by the distance between each pair of traces, resulting in a shot gather from which a local dispersion image associated with the CMP position can be extracted. Those two main approaches have subsequently been adapted and applied to numerous geophysical problems. For instance, Bohlen et al. (2004) used a gaussian moving window to extract the dispersion of Scholte waves from marine seismic data, while Grandjean and Bitri (2006) combined the stacking tools proposed by O'Neill et al. (2003) to the cross-correlation technique developed by Hayashi and Suzuki (2004) in order to increase the signal-to-noise ratio of local CMPCC dispersion images. Soon after, Neducza (2007) suggested a generalization of the stacking and windowing techniques described by O'Neill et al. (2003), introducing systematic parameters controlling the extraction of dispersion images along a seismic profile. We for instance successfully used a similar approach to tracks low velocity anomalies due to sink-holes along the Dead-sea shorelines (Fig. 3.6), where lateral contrasts were so strong that the only way to extract valid dispersion data was to narrow down, as much as possible, the processing window along the line (Bodet et al., 2010a; Ezersky et al., 2013). Boiero and Socco (2011) and Bergamo et al. (2012) published an improvement of these approaches using a series of Gaussian moving windows to extract local dispersion images from a single seismic set-up with a limited number of sources located on either side of the spread, following on the work of Socco et al. (2009) and Boiero and Socco (2010). A similar windowing technique was also used by Ikeda et al. (2013) to improve the lateral resolution of the CMPCC method.

Our workflow

Though numerous techniques have been proposed to process and invert surface-wave data over the last 15 years, only a few of them have been made available to the practitioners' community, especially when it comes to 2D profiling. In order to address this shortcoming, we presented in Pasquet and Bodet (2017) a free and open-source MATLAB-based software package that performs Surface-Wave dispersion Inversion and Profiling (SWIP [3]). Seismic data are handled with Seismic Unix, while the inversion is performed using the open-source software package Geopsy [4]. SWIP is mainly designed to retrieve 1D to 2D variations of VS from typical near-surface seismic data collected along linear profiles with various acquisition geometries (e.g. off-end shots, successive roll-along). It is particularly adapted (but not limited) to process datasets that were originally designed to estimate VP from P-wave refraction tomography and thus extract supplementary VS information. Each step of the designed workflow comes as follow (Pasquet and Bodet, 2017):

1. We implemented windowing techniques adapted from O'Neill et al. (2003) and Neducza (2007) to narrow down the lateral extent of dispersion measurements and realistically consider a 1D medium below each extraction spread, thus achieving the required lateral resolution for 2D profiling;
2. Seismic data are then transformed in the the frequency-phase velocity domain where phase velocities can clearly be identified. For this step, we implemented a slant stack in the frequency domain, as described by Russel (1987) and Mokhtar et al. (1988);

3. `https://github.com/SWIPdev/SWIP/releases`
4. `http://www.geopsy.org/`

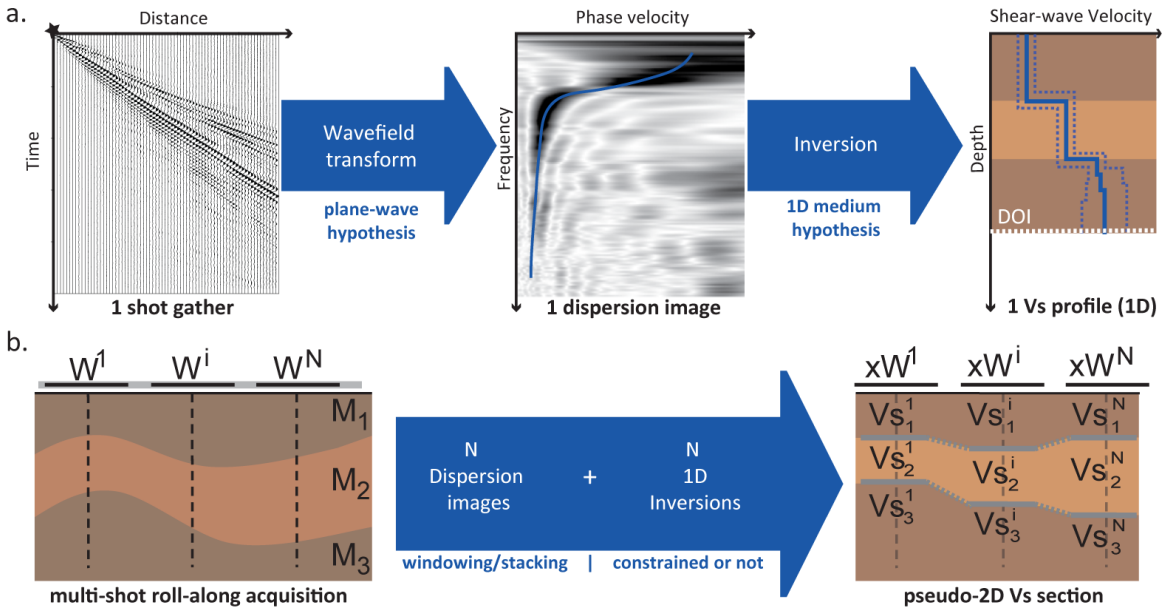

Figure 3.5: *Surface-wave profiling and associated limits (Bodet, 2005; Bodet et al., 2005). (a) Typical seismic shot gathers are transformed to the frequency-wavenumber (or frequency-slowness) domain, in which surface-wave propagation modes can be picked as dispersion curves. They are then inverted for 1D VS profiles with depth (the maximum depth of investigation (DOI) being mainly controlled by the spread length and the maximum recordable wavelength.). (b) When the method is implemented along linear sections with overlapping shot gathers (multifold acquisitions), it is possible to extract the dispersion in a more 'local' manner and to limit near-offset effects (Bodet et al., 2009a). Roll-along stacking of dispersion images basically involves an offset window (W) that moves along the records to extract local wavefields with common midpoints. The main controlling parameters are the minimum and maximum apertures of the moving window associated with a minimum and maximum offset constraint on the dispersion image computation. The stacking is achieved by summing the spectra of windowed data. Once each local dispersion curves is picked and inverted, each 1D profile is represented at its corresponding spreads midpoint, so as to obtain a pseudo-2D VS section of the probed medium.*

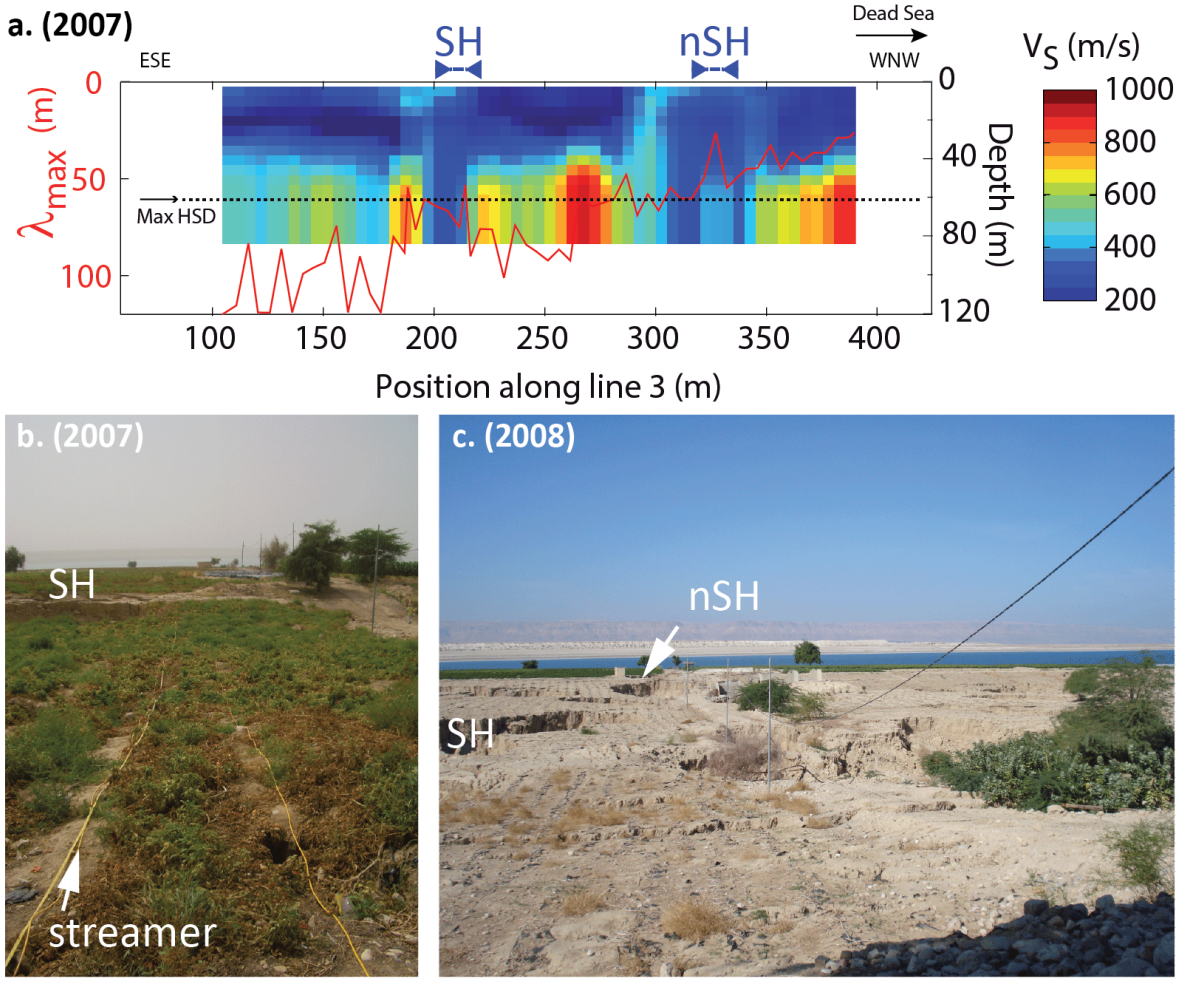

Figure 3.6: *(a) Pseudo-2D VS section of a seismic line intersecting an existing sinkhole area (b, SH) and a zone of intensive sinkhole development (c, nSH) during the 4 years following the acquisition (in 2007, during Amine Dhemaied's Master internship at UPMC) (Bodet et al., 2010a; Ezersky et al., 2013). This final pseudo-2D VS section (modified after Ezersky et al. (2013)) only represents merged (hence smooth) averages of all possible solutions at each position where dispersion data were extracted. By definition the final models interpreted from such data fitting process only consist in a possible estimation of the true VS structures. However, the outputs provided by the inversions can be used to address specific questions such as the depth or location of specific interfaces, the existence of velocity anomalies or the occurrence of strong lateral variations. It was the case here: we focused on shallow decompaction due to possible underlying cavities and shallow lateral hererogeneities due to sinkholes. We never claimed being able to image any associated salt layer at depth, as Polom et al. (2018) would pretend we did, note citing the appropriate reference by the way...*

3. To compensate the loss of spectral resolution caused by windowing the data (Gabriels et al., 1987), we implemented stacking techniques, also adapted from O'Neill et al. (2003) and Neducza (2007), to enhance signal-to-noise ratio, limit near-field effects, and give access to larger wavelengths necessary for increasing investigation depth (Russel, 1987; Forbriger, 2003a,b; O'Neill et al., 2003; Bodet et al., 2005, 2009a; O'Neill and Matsuoka, 2005; Zywicki and Rix, 2005);
4. Dispersion curves are extracted for each window with phase velocity uncertainty taking into account resolution limitations at low-frequency, following the algorithm described by O'Neill et al. (2003); O'Neill (2003); Bodet (2005);
5. These curves are then inverted for each window position using the neighbourhood algorithm (Sambridge, 1999; Wathelet et al., 2004; Wathelet, 2008) with different possible parametrizations (e.g. user-defined, refraction-based etc);
6. Models matching the observed data within the data uncertainty range (Endrun et al., 2008) are selected to build various output models and to estimate the investigation depth through their standard deviation or from empirical criteria (Bodet, 2005);
7. 1D VS models obtained for each extraction window are ultimately merged into a pseudo-2D section of VS.

The package offers to plot pseudo-sections of picked dispersion data (phase-velocity as a function of position along the line and frequency or wavelength). Such representation, adapted from electrical resistivity tomography codes, is very convenient to perform a quality control of picked dispersion and to check the coherence in mode identification, as well as the apparent lateral variations in the data. Once the inversion process achieved at each position, calculated phase velocities and residuals can be plotted as pseudo-sections as well, to review the inversion fit along the acquisition line and check for possible misinterpretations. The coherence of the 1D VS models eventually extracted can also be verified by superimposing theoretical dispersion curves on dispersion images. This particular representation helps pointing out possible modes misidentification and check if originally discarded higher modes could have been picked and inverted.

3.3.2. Validating the use of surface-wave on hydrosystems

Means we still needed the S-source for a while...

1D test on a continuous hydrosystem

Pasquet et al. (2015a) carried out seismic measurements in a site characterized by a tabular aquifer system, well-delineated thanks to Electrical Resistivity Tomography (ERT), log and piezometer data (Mouhri et al., 2013), as shown on Fig. 3.7. A simultaneous P- and surface-wave survey was achieved with a single acquisition set-up, followed by a SH-wave acquisition along the same line (Fig. 3.8a). A simple refraction interpretation (with direct and reverse shots, see Pasquet (2014); Pasquet et al. (2015a) for details) of P- and SH-wave first arrivals provided quasi-1D VP and VS models in conformity with the stratigraphy (Fig. 3.8b). VS models obtained through surface-wave dispersion inversion are matching those obtained with SH-wave refraction interpretation, except for a thin low velocity layer in surface, which has only been identified in surface-wave dispersion inversion results.

While VS remains constant in partially and fully saturated loess, VP exhibits a strong increase at a depth consistent with the observed water table level. Furthermore, VP values observed in

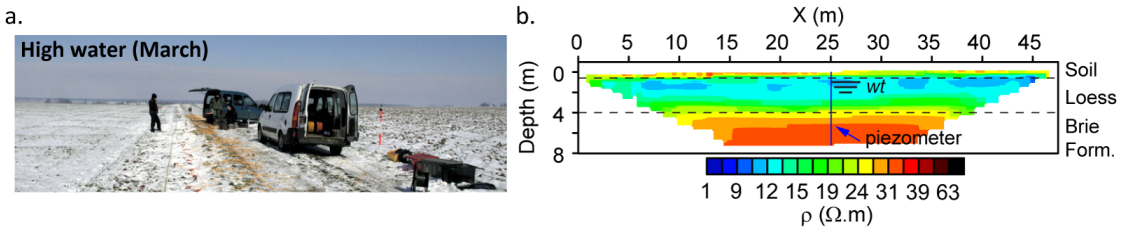

Figure 3.7: *(a) Our experimental set-up on the plateau at Orgeval experimental basin (in the framework Sylvain Pasquet's PhD thesis at UPMC, 2011-2014). It was centred on a piezometer in order to measure the water level during the acquisitions. (b) An ERT section helped confirming the 1D character of the shallow part of the hydrosystem at this location.*

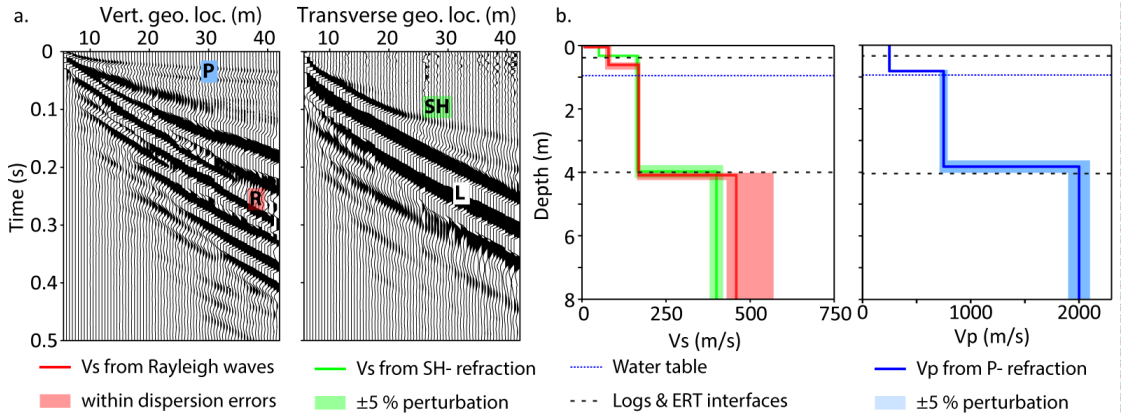

Figure 3.8: *(a) Seismograms of direct shots recorded with vertical and horizontal component geophones on wich P, Rayleigh (R), SH and Love (L) waves are visible. (b) Comparison of 1D VS models obtained from SH-wave refraction interpretation (in green) and surface-wave dispersion inversion (in red). The error bars of models retrieved from refraction analysis were estimated by introducing a perturbation of ±5 % on the central model parameters. As for error bars of the VS model retrieved from surface-wave dispersion inversion, they correspond to the envelope of accepted models fitting within dispersion data uncertainties. Modified after Pasquet (2014).*

the saturated loess remain lower (around 800 m/s) than the expected values in fully saturated sediments (usually around 1500-1600 m/s). It is however quite hard to find in the literature a range of typical VP values that should be expected in various partially and fully saturated sediments. Most of the existing studies present VP values in saturated sands, where the relationship between VP and water saturation is described by many authors (e.g. Bachrach et al., 2000; Foti et al., 2002; Prasad, 2002; Zimmer et al., 2007a,b). With more complex mixtures (e.g. containing a significant proportion of clays), the behaviour of VP with the saturation becomes more complicated (Fratta et al., 2005). VP values around 800 m/s have already been observed in saturated loess by Danneels et al. (2008) when studying unstable slopes. In such low permeability materials, full saturation can be hard to reach (due to an irreducible fraction of air in the pores), thus limiting the maximum VP velocity (Lu and Sabatier, 2009; Lorenzo et al., 2013). As anticipated, the study of VP alone remains insufficient to lead back to hydrological information.

VP/VS ratio were then computed (Fig. 3.9a) with VS models retrieved from SH-wave refraction

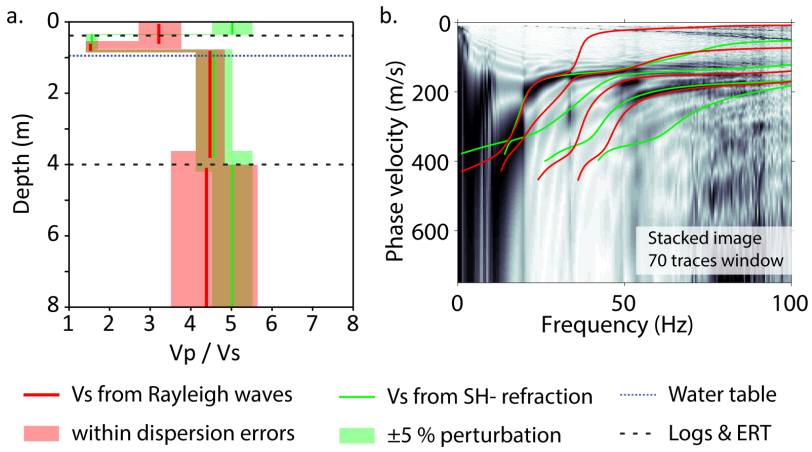

Figure 3.9: *VP/VS were computed with VS models retrieved from SH-wave refraction interpretation (in green) and surface-wave dispersion inversion (in red). In any case, VP/VS were retrieved from P-wave refraction interpretation (b) Dispersion curves calculated from both surface-wave dispersion inversion (in red) and refraction interpretation (in green) models are superimposed on the stacked dispersion image. Modified after Pasquet (2014); Pasquet et al. (2015a).*

interpretation (in green) and surface-wave dispersion inversion (in red). VP/VS ratio around 3 to 4 are estimated in the soil layer (Poisson's ratio ranges between 0.45 and 0.48). These values are typical of saturated soils (Uyanık, 2011), and may be explained by the presence of a melting snow cover on the site during the acquisition. Directly below the soil, the loess layer is characterized down to 0.75-0.85-m deep by VP/VS ratio values of 1.5 and Poisson's ratio values of 0.1. These values are unusually low, even for non-saturated sediments, and might be explained by the presence of a frozen layer. At this depth, consistent with the water table level (0.9 m), VP/VS and Poisson's ratio values increase to 4.5 and 0.47-0.48, respectively. This kind of contrast in a single lithological unit is typical of a transition between partially saturated (low VP/VS and Poisson's ratios) and fully saturated sediments (high VP/VS and Poisson's ratios). VP/VS and Poisson's ratios remain constant in the deepest part of loess and in the Brie limestone layer, reinforcing the assumption of a continuously saturated aquifer.

As a final quality control of inversion results, forward modelling was performed using the 1D VS average models obtained from both surface-wave dispersion inversion and SH-wave refraction interpretation. While models obtained from both methods are remarkably similar, the theoretical dispersion curves computed from surface-wave dispersion inversion results (in red, Fig. 3.9b) provide the best fit with the coherent maxima observed on measured dispersion images. The theoretical modes are consistent with the picked dispersion curves, and are well-separated from each other while they looked like a unique and strong mode at first glance. Interestingly, theoretical dispersion curves calculated from refraction models (in green, Fig. 3.9a) are clearly following this 'effective dispersion' which remains representative of the stratigraphy since models from both methods are in good agreement. There is however no evidence of water table level detection, though several authors noticed a significant VS velocity decrease in the saturated zone (O'Neill and Matsuoka, 2005; Heitor et al., 2012).

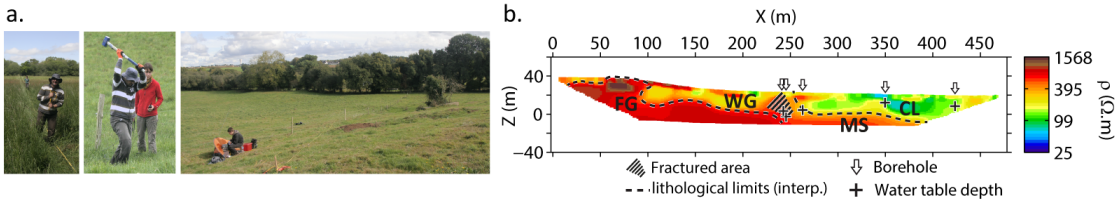

Figure 3.10: *(a) Amine Dhemaied deploying a seismic spread and hitting the ground along a more than 450 m long West-East profile on the Ploemeur hydrological observatory (south of Brittany, France) on which Sylvain Pasquet (right picture) tested the combined use of P-wave first arrival times tomography and surface-wave dispersion inversion and profiling (along with a systematic comparison with SH-wave first arrival times tomography). (b) Electrical resistivity values (ρ) interpreted from ERT carried out along the line. Four main structures are delineated: fresh granite (FG), weathered granite (WG), clays (CL) and micaschists (MS). The hashed area in corresponds to a possible evidence of the contact zone. Positions of the nearest monitoring wells are projected along the line and represented with white arrows, pointing downwards to the corresponding piezometric head level (black crosses). Modified after Pasquet (2014).*

2D test on a fractured hydrosystem

Valois (2011) tested the use of surface-wave profiling techniques as we developed it in Bodet et al. (2010a) to retrieve pseudo-2D VS section along his P-wave refraction tomography profiles on karsts. This preliminary study was encouraging but still had to be confirmed with a thorough experiment to evaluate the possible effects of several issues: refraction tomography and surface-wave profiling rely on different types of waves (body-spherical versus guided-cylindrical); they involve distinct characteristics of the wavefield (reflected/refracted wavefronts versus dispersive/modal propagation); they require different assumptions about the medium (2D 'smooth' models from initial gradients with depth versus 'blocky' juxtaposition of 1D vertical structures with few layers). The two methods provide results that are thus actually difficult to compare because of different resolutions and investigation depths. In traveltime tomography, the medium is described as a function of the 'ray coverage', which is strongly related to the spacing between sensors and sources and usually increases in high-velocity zones. In surface-wave methods the spectral resolution and maximum measurable wavelength are mainly controlled by the frequency band of the source and the length of sensors arrays used for dispersion extraction.

The methodology has thus also been tested (Pasquet et al., 2015b) in a fractured aquifer environment with strong discontinuities and lateral variations in lithology, at the surface and at depth, in the Plœmeur hydrological observatory (south of Brittany, France). This site is located along a contact between granite and micaschists, marked by a subvertical fault zone emerging as a fractured area, as shown by ERT results on Fig. 3.10b. A simultaneous P- and surface-wave survey has been achieved using a single acquisition set-up, and supplemented with a SH-wave acquisition along the same line in order to compare VS results obtained from SH-wave refraction tomography and surface-wave profiling. P- and SH-wave first arrivals observed along the line were used to perform first arrival times tomography and retrieve 2D V_P^{tomo} and 2D V_S^{tomo} models. Evenly spaced dispersion data were extracted along the line from P-wave shot gathers using windowing and stacking techniques. Successive 1D inversions of these dispersion data were achieved, using fixed VP values extracted from the V_P^{tomo} model and no lateral constraints between two adjacent

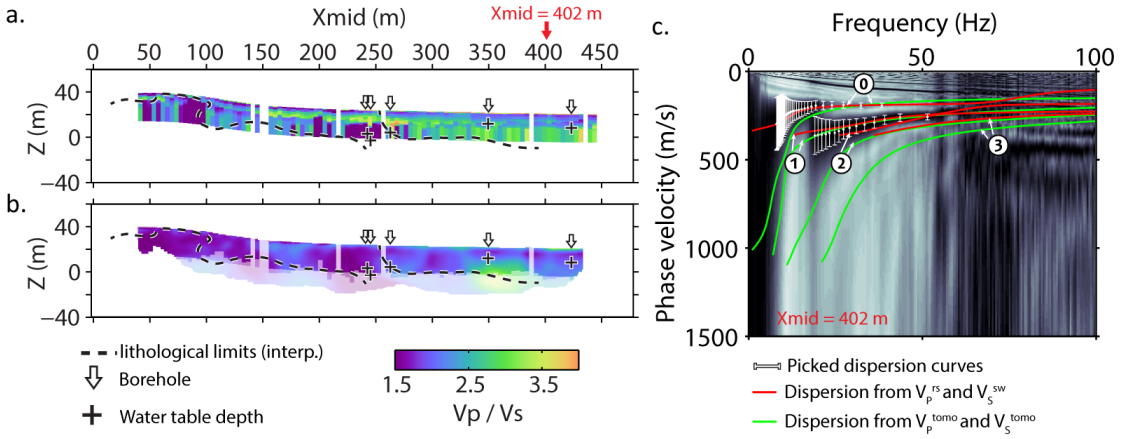

Figure 3.11: *(a) Pseudo-2D VP/VS section constructed with V_S^{sw} obtained from surface-wave profiling and V_P^{rs} obtained from P-wave tomography and resampled in depth according to the VS layering. (b) VP/VS section computed from V_P^{tomo} and V_S^{tomo} models obtained from P- and SH-wave tomography. The shaded area in b correspond to the extent of the VP/VS pseudo-2D section in a. Both sections are overlaid with limits interpreted from ERT results. Positions of the nearest monitoring wells are projected along the line as in Fig. 3.10b. (b) As an example post-inversion quality control, the fundamental (0), first (1), second (2) and third (3) higher modes of theoretical dispersion curves calculated from V_S^{sw} and V_P^{rs} (in red) and from V_S^{tomo} and V_P^{tomo} (in green) are superimposed on the stacked dispersion image obtained at $Xmid = 402$ m. Modified after Pasquet (2014); Pasquet et al. (2015b).*

1D inversions (see Pasquet and Bodet (2017) for more details). The resulting 1D V_S^{sw} models were then assembled to create a pseudo-2D V_S^{sw} section, characterized by strong velocity uncertainties in the deepest layers.

Despite obvious discrepancies between V_S^{tomo} and V_S^{sw} models as well as possible incompatibilities in terms of resolutions, investigation depth, lateral sensitivity and posterior uncertainties, Pasquet et al. (2015b) however computed VP/VS sections from both V_S^{sw} and V_S^{tomo}, as presented on Fig. 3.11a. The two sections interestingly present similar features, but the section obtained from V_S^{sw} shows a higher lateral resolution which is consistent with the ERT section. The VP/VS ratios obtained in the clays and micashists show a strong contrast consistent with the observed water table level (black crosses on Fig. 3.11a). Even if they are quite different, both models decently fit surface-wave dispersion along the line, as show on an example given at $Xmid = 402$ m on Fig. 3.11b.

The anticipated incompatibilities remain, more particularly between V_P^{rs} and V_S^{sw}, which can lead to anomalous VP/VS values. In addition, the inverse problem formulations and solving approaches of P-wave refraction tomography and surface-wave profiling are radically different. The resolutions (and available tools to benchmark it) of each VP and VS models are hardly compatible. The a posteriori uncertainties and the means to extract them consist in a serious issue as well. Joint inversion approaches combining PSV- and P-guided waves dispersion data along with P-wave refraction traveltimes could be developed, in the continuation of Maraschini et al. (2010), Piatti et al. (2013) and Boiero et al. (2013) works. Issues related to the model discretisation would however remain. Recent developments in Full Waveform Inversion (FWI, e.g. Virieux et al. (2017))

including surface waves, and their applications to near-surface targets (e.g. Athanasopoulos and Bohlen, 2017b,a; Groos et al., 2017) should be preferred.

3.4. Developing time-lapse applications on hydrosystems

3.4.1. Why ?

As pointed in the introduction of this chapter, the understanding of a hydrosystem mainly relies on sparse information that are usually not sufficient to fully describe its complexity and variability in space and time. Fortunately, hydrogeophysics provide appropriate tools to image spatial heterogeneities in the vadose zone (Hubbard and Linde, 2011; Binley et al., 2015). A time-lapse approach of these methods enables the monitoring of geophysical signals and properties linked to water content (Jougnot et al., 2015; Lumley et al., 2015; Singha et al., 2015; Uhlemann et al., 2017). In such context, electrical and electromagnetic techniques have been widely developed and have shown their efficiency. However, they can be ineffective in very electrically conductive (e.g. ground penetrating radar (GPR) over loess or clays) or resistive environments (e.g. ERT and electromagnetic induction over massive or fractured rocks – see e.g. discussions in Hubbard and Linde (2011)). To overcome these limitations, seismic methods have been recently suggested as a complement to describe the complexity of the vadose zone (as shown supra). As for their time-lapse development, a wide range of applications and target scales can be found in the literature where authors track changes of seismic signal and mechanical properties associated with climatic variabilities (Bergamo et al., 2016a,b; Ikeda et al., 2017), water level changes (Lu, 2014), permafrost thaw (Ajo-Franklin et al., 2017) or deep fluid storage (Arts et al., 2004; Chadwick et al., 2010). In the meantime, passive seismics have also been developed and recently proved to be efficient in the continuous auscultation of subsurface layers at the 0.01 % level (Lecocq et al., 2017; Fores et al., 2018). As for active seismic methods, Lu (2014) and Bergamo et al. (2016a,b) more specifically observed temporal changes in P-wave first arrival times or surface-wave dispersion due to varying hydrological conditions. We presented earlier in this manuscript a similar approach to track water level changes at the laboratory scale (Pasquet et al., 2016a). Point-by-point data differences showed inflection points at specific transition zones corresponding to the water and capillary fringe levels. This literature and experimental results encouraged us in developing tools to study soil water content variations in time, on the field.

Valois (2011), Pasquet (2014); Pasquet et al. (2015a,b) addressed the possibility to simultaneously retrieve VP and VS models from a single seismic acquisition with vertical component geophones only. Even if it enables the detection of the water table, this kind of inversion yet uses a discrete number of layers that cannot properly describe the continuous variations of the subsurface hydrological properties, as anticipated in our laboratory experiments (Pasquet et al., 2016a). The approach remains moreover limited by the important differences between the theories and methodologies involved in each techniques. Incompatibilities and discrepancies, more particularly in terms of resolution, as well as the difficult control of posterior uncertainties, limit the possible interpretation of estimated VP/VS to very well constrained studies only (e.g. with strong a priori information from logs, geotechnics, hydrogeology and alternatives geophysical characterisations). In the following, we show how such conditions highly improve this approach and enable its time-lapse implementation to study the dynamic of targeted processes. To achieve such goals, it was important to first perform a thorough analysis defining the content of valuable information carried by the seismic data of interest. As a first step, it was thus critical to estimate errors associated with the data picking processes.

3.4.2. Estimating measurements errors before any time-lapse interpretation

`'You become a true geophysicist only once you've manually picked thousands of seismograms...', quoting J.-L. M. (2019)`

Manual picking errors

Traditionally, both P-wave traveltimes and surface-wave dispersion data are manually extracted from the recorded wavefields by human operators. Di Stefano et al. (2006) for instance compared picking errors produced by a human operator and by an automated picking algorithm. Their results confirmed that manual picking makes it possible to identify complex events when the signal-to-noise ratio is too low or irregular for an automatic process to be efficient. The problem is that extracted data can vary from one operator to another because of the subjective nature of manual picking (Jiao and Moon, 2000; Saragiotis et al., 2002). The same analyst's picks may also differ because of physiological and psychological factors such as tiredness and boredom (Saragiotis et al., 2002). Eventually, field conditions (e.g. variability in near-surface structures, source type and depth, geophone coupling and signal-to-noise ratio) are also obvious sources of variability within time-lapse measurements (O'Neill, 2003; Sabbione and Velis, 2010; Senkaya and Karsli, 2014). This variability has to be estimated when strict reproducibility cannot be ensured, as it is in controlled experiments (Bergamo et al., 2016a,b). Because of the aforementioned reasons, picking errors are difficult to estimate in a systematic manner though they are crucial for the inversion processes and need to be carefully considered.

To tackle this issue, Bauer et al. (2010) performed repeated picking of P-wave first arrivals so as to estimate data uncertainty and improve tomographic inversions. O'Neill (2003) showed that surface-wave dispersion curve errors can be empirically estimated with a combination of Gaussian and Lorentzian distributions at high and low frequencies, respectively, thus significantly helping to constrain the DOI and provide safe bounds to a posteriori models. Dangeard et al. (2016b,a, 2018); Dangeard (2019) very recently developed and described in details a processing workflow to estimate these picking errors, for both P and surface waves, in order to provide practitioners with means to discriminate significant spatial and temporal variations in the data from measurements uncertainties (including background noise). An example of application on the Orgeval experimental basin is given in the following, in which time-lapse active seismic measurements will be used to constrain hydrogeological modelling at the stream-aquifer interface.

Seismic lines were deployed from February to August 2017 with a 2-month step, along a profile perpendicular to the Avennelles river, at the outlet the basin (Fig. 3.12). For each acquisition, the equipment, the geometry and acquisition parameters remained similar. In order to ensure optimal positioning of the line over time, a permanent marking system has been used. On each bank, a 96-channel seismic recorder with 14 Hz vertical component geophones was used with a 0.25 m spacing leading to 23.75 m long profiles. The source consisted in a metal plate hit vertically with a 1.250 kg hammer. At each position along the lines, we recorded and stacked 6 seismograms in the time-domain to increase signal-to-noise ratio. The sampling rate was 0.5 ms and the recording length was 2 s (with a pre-triggering delay of -0.02 s) to include the full surface-wave trains, coda and background noise. The seismic dataset eventually consisted in a total number of 97 seismograms per bank at each time step (776). P waves can be easily identified and their associated first arrival times were manually picked (e.g. two seismograms given as examples on Fig. 3.13a and b). As for surface-wave data, a good trade-off between lateral resolution, homogeneity (with comparison of direct and reverse shots) and investigation depth was found with an 11.75-m wide stacking window (48 geophones) for eight reverse and direct shots (Dangeard et al., 2017b). At

Figure 3.12: *Marine Dangeard (PhD thesis at UPMC/SU, 2015-2018), Solenne Schneider (Master internship, 2017), Agnès Rivière and collaborators, performing repeated seismic acquisitions through the Avennelles river, at the outlet the Orgeval experimental basin in February, April, June and August 2017. The set-up was centred on a high-frequency tracking system called LOMOS (LOcal MOnitoring Station), implanted in the stream to track changes in hydrological parameters. Two seismic profiles were deployed on both sides of the river (see a and b). (c) Each consisted in 96 geophones 0.25 m spaced. The source was a metal plate hit by a 1.250 kg hammer to obtain high frequencies (as recommended by Bodet et al. (2014c)). Modified after Dangeard et al. (2017b); Dangeard (2019).*

each window location along the line, the dispersion curves were manually extracted (e.g. Fig. 3.13c and d), rejecting wavelengths greater than 12 m, as recommended by Bodet et al (2009). The first window is centred at (theoretical locations: see Dangeard et al. (2017b) for positing uncertainty estimations) 5.875 m and the last one is at 17.875 m for the left bank and centered at 36.125 m and 48.125 m on the right bank, providing a total number of 98 window positions along each bank, at each time step (t).

Time-lapse variations versus picking errors

As mentioned earlier, in order to compare this dataset with hydrological observations, discriminate time-lapse variations from noise or measurement errors and invert it for both VP and VS models at each time step, the picking errors must be estimated following the workflow and the recommendations by Dangeard et al. (2018). 5 shot positions (for arrival times) and window centers (for surface wave dispersion curves) are selected and manually picked 15 times in a random order for each time step from February to August 2017. When 15 point values per position are available, the standard deviation is calculated for each offset and each frequency. These values are then plotted as a function of their population in order to determine the 99th quantile corresponding to the picking error for the time step. The overall uncertainty about the difference between the data of two time steps is then defined as the sum of the errors calculated at each (more details available in Dangeard et al. (2018); Dangeard (2019).

Point-by-point data absolute differences were then calculated for both P-wave arrival times (Figure 3.14) and surface wave dispersion curves (Figure 3.15) between each time step (as suggested by Bergamo et al. (2016a,b); Dangeard et al. (2018)). Positive differences are given in blue while negative ones are in orange. Data variations considered insignificant, i.e. included in the errors previously estimated, are shown in gray. As for traveltimes (Fig. 3.14), differences are negative between April and February. Between June and April, the differences are positive. Between August and June arrival time variations are mainly positive. On the right bank (Fig. 3.14b,d and f), systematic differences appear for geophones and shots located between 35 and 40 m, possibly

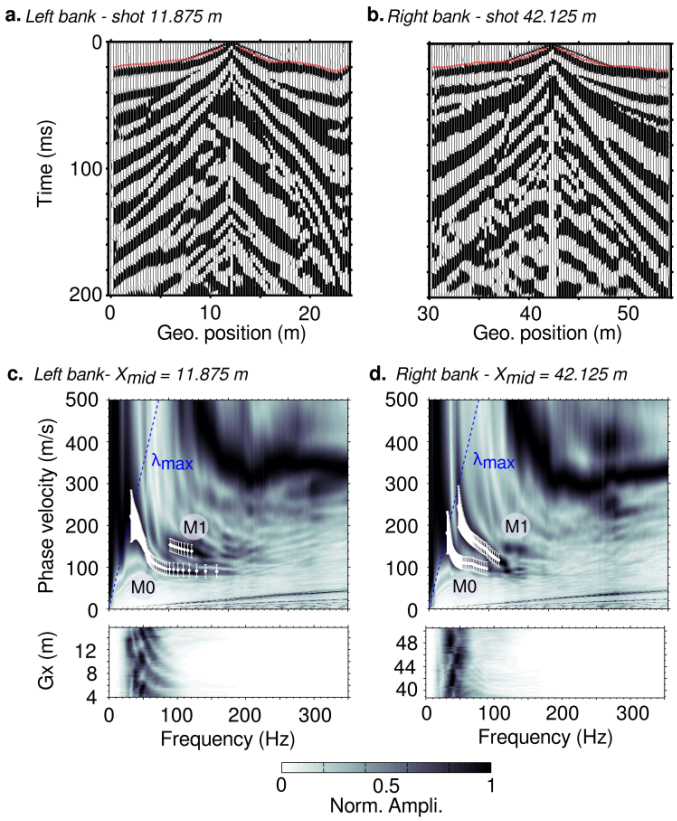

Figure 3.13: *Examples of seismograms recorded on both sides of the river (a and b) in February 2017, with corresponding (d and c) dispersion images (top) and spectrograms (bottom). The red dots on seismograms correspond to first arrivals and the white dots with errorbars on dispersion images to the fundamental mode (M0) and the first higher modes (M1), manually picked. Modified after Dangeard et al. (2017b); Dangeard (2019).*

explained by a poor coupling at this location. Phase velocity changes (Figure 3.15) are mainly positive between April and February and between June and April on both banks. Between August and June, differences in phase velocities are negative. Interestingly, phase velocity differences show opposite behaviours at high frequencies (on the left bank mainly).

Such temporal variations and their proof of significance thanks to Dangeard et al. (2018) workflow, make it possible to qualitatively determine changes in water content of the subsurface. As noted in previous sections, VP can decrease with saturation in partially saturated unconsolidated media. This is related to the increase in density (in the pores, water replaces the air). Then, from a threshold value $>$ 90-95% (depending on the medium) it increases substantially until the complete saturation is reached (the medium is harder to compress, see Bachrach and Nur (1998) for more details). As the first arrival times picked at each trace of the seismograms are dependent on VP, the apparent velocities they describe tend to have similar behaviours (even if this has to be considered with care since it depends on the media along the wave-path, from each source to each geophone). S waves, for their part, are very sensitive to small changes in water saturation when it is close to 0%: VS tends to increase due to the creation of capillary bridges between grains increasing their resistance to shear stress. Then, when air is replaced by water in the porous medium, VS tends to decrease (due to an increase in density, according to Cho and Santamarina (2001)). As the surface waves observed on seismograms of vertical particle velocities are strongly dependent on VS, their phase velocities tend to be similarly influenced (even if this has to be considered with care as well, since it depends on the media along the wave-path, below the stacking window and since surface waves include a compressive component).

Then, by using these empirical and qualitative relationships between wave (apparent) velocities and water saturation, we can describe the hydrogeological state of the near-surface at each period of seismic acquisition (Fig. 3.16a,b). Changes in seismic data indicate that in February water saturation is higher (Fig. 3.16c,d). This is consistent with a high piezometric level (Fig. 3.16b) and the apparent surface water saturation observed on the field. In April and June, the global saturation seems similar despite distinct piezometric levels and a completely dry ground surface (at the beginning of acquisitions in June). This can be explained by several rain events of intensity up to 6.3 mm/h during the acquisition in June 2017 (Fig. 3.16a). Finally, in August 2017, the watershed was flooded. The overall water content and the piezometric levels are higher than in June but lower than in February 2017.

The approach developed by Dangeard et al. (2018); Dangeard (2019) actually helps defining the spatio-temporal dynamic of the aquifer along the profile. However, this information cannot be integrated directly into the hydrogeological models. In the following, we estimate VP and VS by thoroughly inverting the seismic data and calculating the Poisson's ratio in order to finally depict an interpreted depth of the saturated zone.

3.4.3. Time-lapse models to constrain hydrodynamic modelling

A priori information (mandatory)

These inversions and their interpretations in terms of water-table depth appear to be possible at each time step thanks to the controlled quality of the data and their significant variations with time (considering estimated uncertainties) which obviously carries hydrological information. Yet, to enable time-lapse quantitative interpretation of such inversions, a priori information about the medium structure and heterogeneity is mandatory. In February 2017, we used a multi-channel resistivimeter with a 72 (left bank) and 96 (right bank) 0.25 m spaced electrodes in Wenner-Schlumberger array configuration, in order to provide a detailed electrical resistivity image of

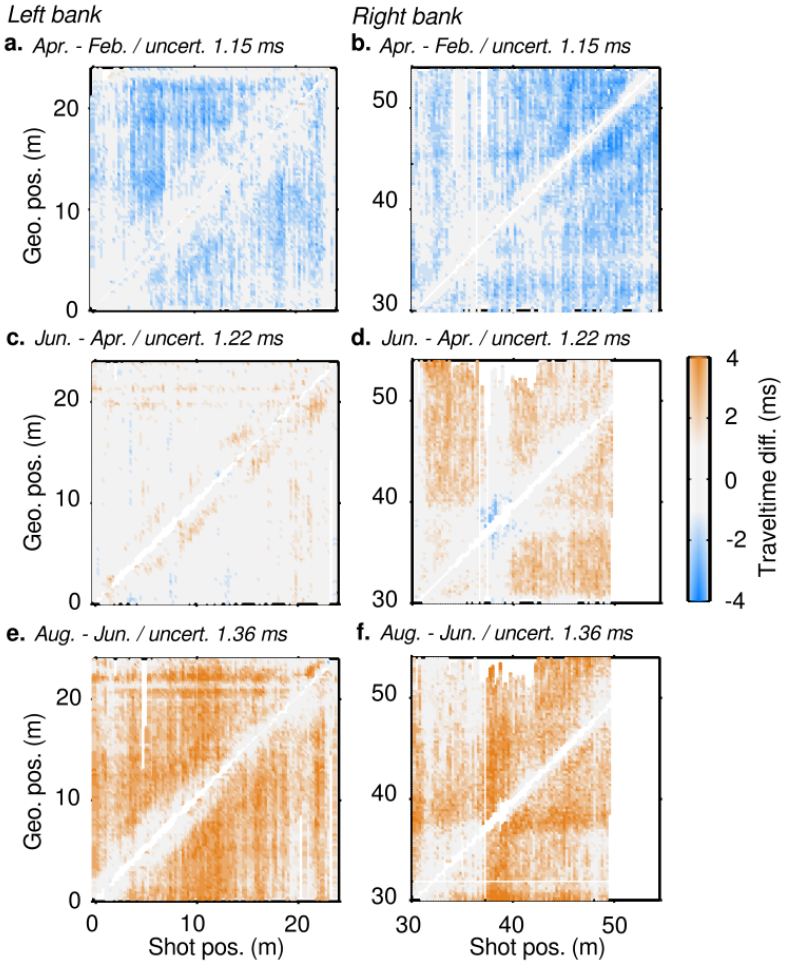

Figure 3.14: *Absolute differences calculated between the picked arrival times of April and February (a, b), June and April (c, d) and August and June (e, f) 2017. The differences are represented according to the positions of shots and geophones. The color scale takes the statistically estimated picking uncertainty (in gray) into account (the blanks area at the end of the lines on c and d correspond to an interruption of the experiment in June because of a thunderstorm. Modified after Dangeard et al. (2017b); Dangeard (2019).*

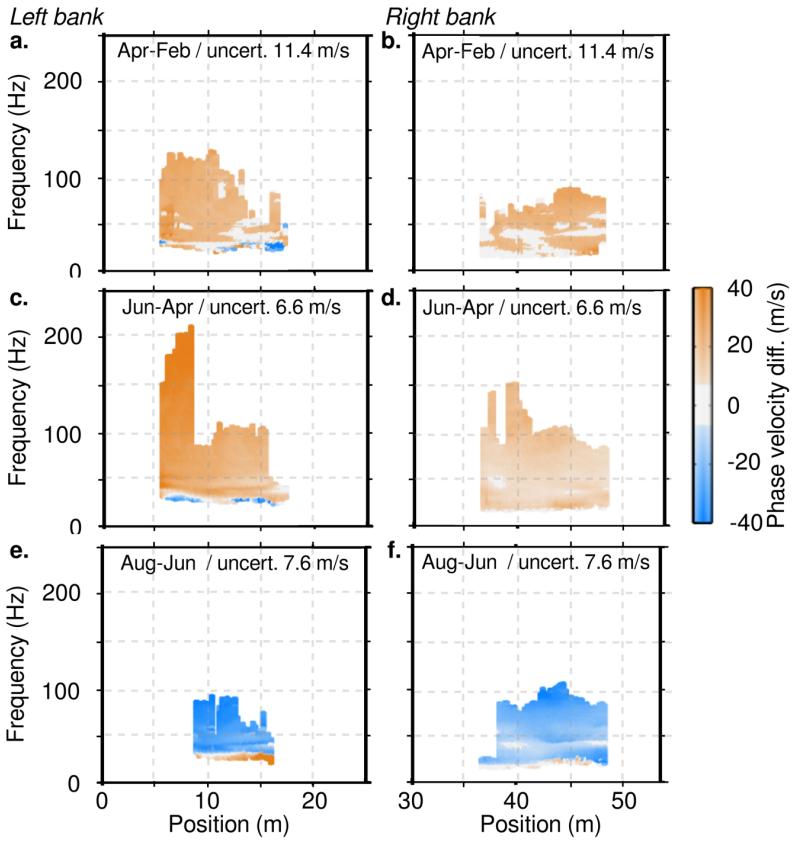

Figure 3.15: *Absolute differences calculated between surface-wave dispersion curves of April-February (a, b), June and April (c, d), and August and June (e, f) 2017. The differences are plotted as a function of the window position and the frequency. The color scale takes the statistically estimated picking uncertainty study (in gray) into account. Modified after Dangeard et al. (2017b); Dangeard (2019).*

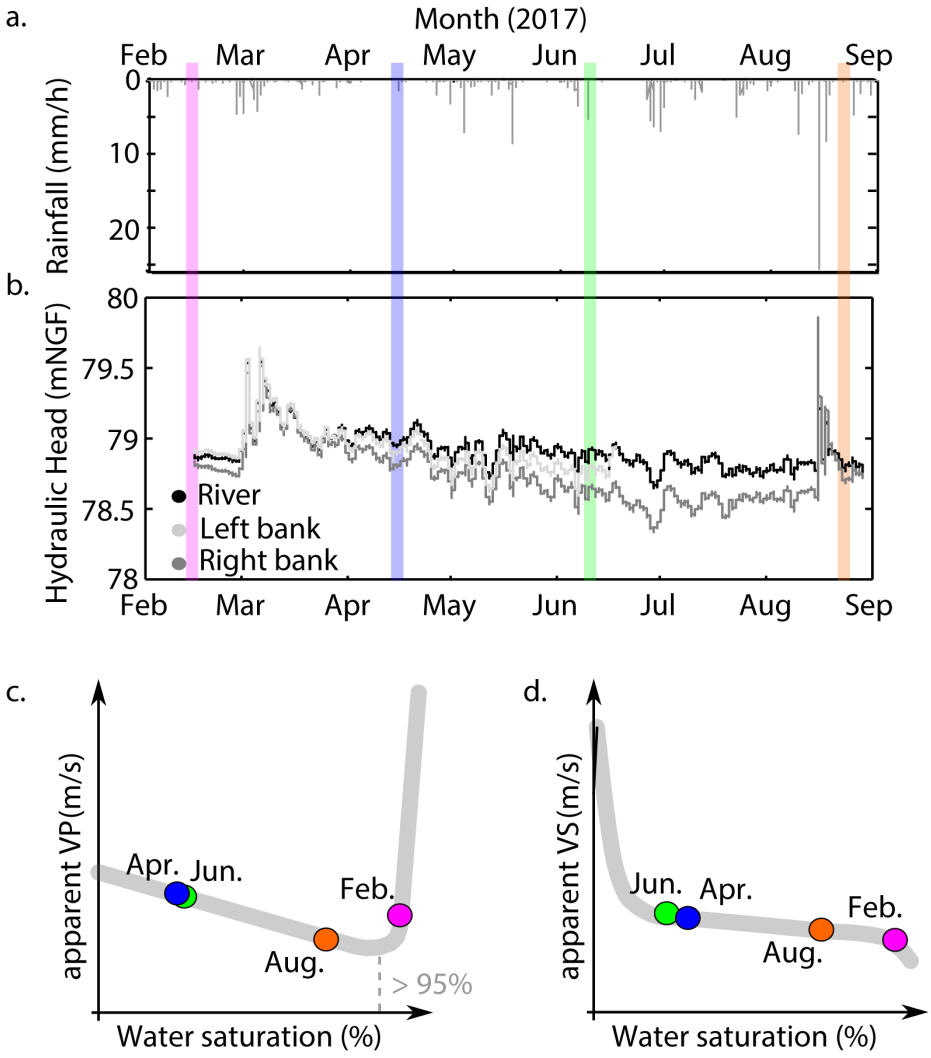

Figure 3.16: *(a) Rainfalls measured at the Boissy-le-Châtel meteorological station between February 14th, 2017 and August 28th, 2017 (date of first and last seismic acquisitions) (b) Hydraulic heads measured between February and August at the AvAv station in the river (black), as well as in right and left bank piezometers (dark and light gray respectively). The coloured rectangles indicates the dates of the seismic acquisitions (pink : February, blue : April, green : June and orange : August 2017). (c,d) Qualitative evolutions of the water saturation estimated from the apparent P-wave velocity (c) and apparent S-wave velocity (d) for each time step according to semi-empirical laws suggested by Bachrach and Nur (1998) and Cho and Santamarina (2001). Modified after Dangeard et al. (2017b); Dangeard (2019).*

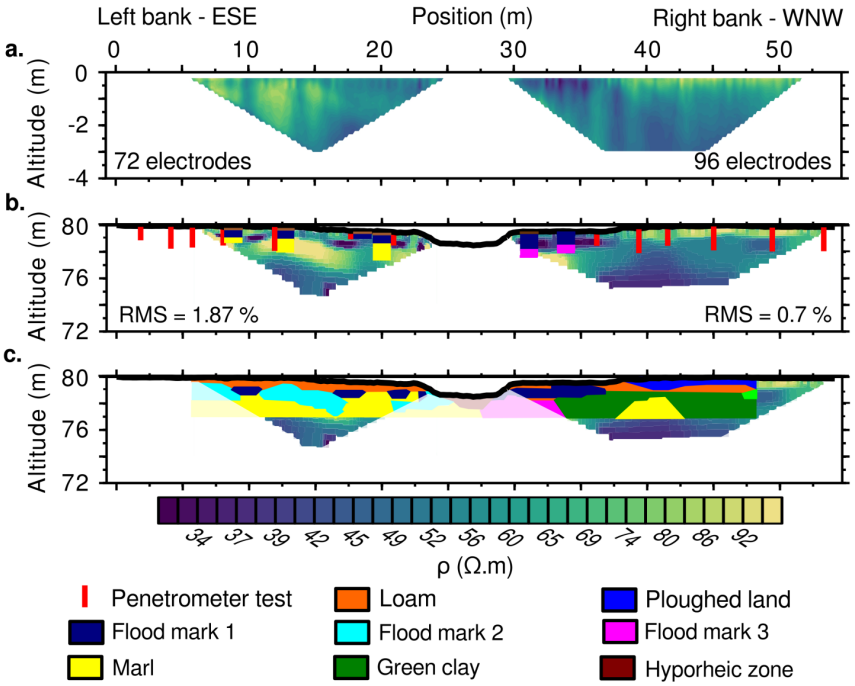

Figure 3.17: *Results of the ERT performed along the line perpendicular to the Avenelles using 72 electrodes (left bank) and 96 electrodes (right bank) with a 0.25-m spacing and a Wenner-Schlumberger array. (a) Apparent and (b) interpreted resistivities after inversion. The red lines represent the location of dynamic penetrometer tests. The results of auger sampling are presented by logs. (c) Definition of the zones corresponding to different lithologies. Modified after Dangeard et al. (2017b); Dangeard (2019).*

the studied profile. The recorded section is affected by a significant asymmetry between the two banks (Fig. 3.17). In addition, we performed 13 dynamic penetrometer tests (vertical red lines in Fig. 3.17b) and 4 auger soundings, about 1 m deep (color boxes in Fig. 3.17b). By comparing electrical resistivity variations to previous geological logs (Mouhri et al., 2013) and to the in situ geotechnical tests, we were able to identify each lithofacies of the site. The heterogeneities of the left bank can be related to frequent flood deposits and possible agricultural earthworks along the meander. On the contrary, the lithology of the right bank is relatively homogeneous and clayey. These structures and their important variations along the cross-section confirm the contrasted dynamic observed in the hydrological data (Fig. 3.16). It also confirms that the two piezometers located in the vicinity of the stream cannot be used as references to describe the water table spatial variations in time.

Thorough inversions

VP is estimated by tomographic inversion of first arrival times, initialised with a gradient model. VS is estimated by a 1D inversions of the surface-wave dispersion data collected along the lines. For each time step, theses inversion are performed independently. In addition, no constraints are imposed to the parametrization, neither in space nor in time, and it remains the same at each time step. Initial models, error and perturbation evolutions with iterations, final models etc are systematically controlled and compared for each time step (see Dangeard (2019) for more

details). The Poisson's ratio is then calculated from VP and VS models, as presented in Fig. 3.18. The high values (in blue) indicate a saturated medium, in contrast to the low values (in yellow) that correspond to an unsaturated medium, highlighting spatial variations (when 1D examples on Fig. 3.18a clearly show temporal changes). On these sections, the Poisson's ratio is close to 0.5 (in blue on Fig. 3.18) below the water table and do not longer vary with depth (at least above the DOI). At each time step, among Poisson's ratio lower than 0.48, we searched for zero values of its gradient with depth. We assumed that below such threshold, the medium was actually completely saturated.

However, the inversion methods used to estimate the seismic velocity models involve a limited number of layers and cannot describe the continuous variations of the water saturation. Water table depth values are thus interpolated to better correspond to the continuous variations of this property in the natural environment (using an approach previously implemented by Maineult (2016), imposing the hydraulic head measured in the river and in the piezometers as constraints). The depth of the water table at each time step (coloured lines on Fig. 3.18) is then clearly more variable on the left bank than on the right bank, linked to (1) the lithological heterogeneities described earlier in space, (2) to the hydrological observation in time, as well as (3) to the fluctuations of the stream-aquifer exchanges.

3.4.4. Take away message

Estimating evolution of exchanges within the stream-aquifer interface is frequently tackled with the help of numerical models. Yet, the definition of boundary conditions is generally based on poorly constrained assumptions and restrained to the location of piezometers. We suggested here to stretch the modelling domain and build stronger constraints, both in space and time, by using a multi-method approach. On a hotspot of the Orgeval Critical Zone observatory (France), we showed how a thorough interpretation of high-resolution geophysical images, combined with geotechnical data, helped describing the spatial heterogeneities of the aquifer. It provided a detailed distribution of hyro-facieses, valuable prior information about the associated hydrodynamic properties and made it possible to expand the modelling window in space. We showed how the local temporal dynamic of the water table can be captured with high resolution time-lapse seismic acquisitions. Time-lapse variations of collected seismic data were discriminated from noise or measurement errors thanks to the technique developed by Dangeard et al. (2018); Dangeard (2019). They were interpreted, regarding hydrological observations, as temporal changes of the saturated-unsaturated zone continuum. Each seismic snapshot was then thoroughly inverted to extrapolate the water table outside the boundaries defined by the piezometers, within the expanded modelling domain. This posterior geophysical information was eventually injected as initial and boundary conditions of a finite volume model in order to calibrate plausible ranges of hydraulic parameters (to simulate the piezometric surfaces and estimate the stream-aquifer exchanges).

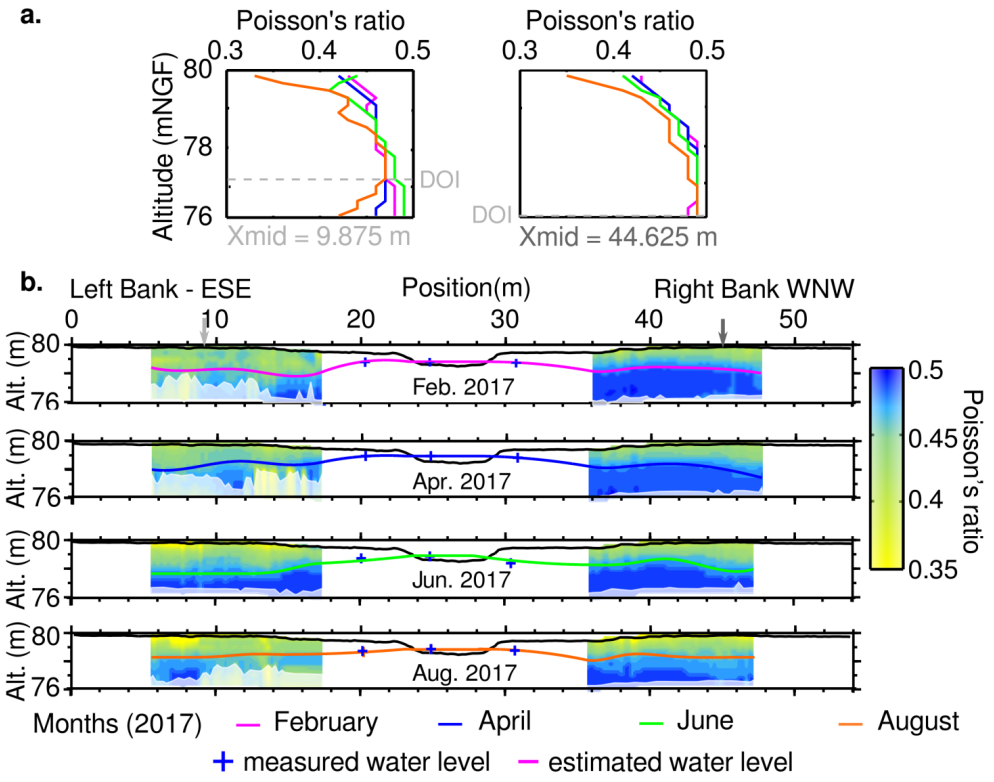

Figure 3.18: *(a) An example of 1D Poisson's ratio calculated on the left bank (at 9.875 m) and on the right bank (at 44.625 m) for each time step: February (pink), April (blue), June (green) and August (orange). The dashed gray line corresponds to the maximum DOI of the method. (b) Pseudo-sections of Poisson's ratio for each time step. The pink (February), blue (April), green (June) and orange (August) lines correspond to the piezometric levels estimated from the Poisson's ratio values interpolation using algorithm proposed by Maineult (2016). The blue crosses indicate the measured water levels in the river and in the bank piezometers. A white mask hide inversion results below the maximum DOI. Modified after Dangeard et al. (2017b); Dangeard (2019).*

3.5. Conclusions, current applications and further developments

3.5.1. CRITEX's seismic

P-wave refraction tomography and surface-wave dispersion inversion can be performed along coincident profiles to simultaneously estimate 2D VP and VS sections (Konstantaki et al., 2013). In the framework of both the CRITEX equipment excellency project and the PIREN-Seine program, we thus suggested the approach to be included in the hydrogeophysics' toolbox. Based on previous studies by West and Menke (2000); Duranteau (2010); Valois (2011), the idea of combining P- and sufrace-wave measurements and interpretations has been tested and validated on two CZ observatories with distinct hydrogeological characteristics: a continuous multi-layered hydrosystem and a fractured environment with strong discontinuities (Pasquet, 2014). On both sites, we were able to image spatial variations of VP/VS ratio, whose evolution was strongly associated to the water content observed locally (Pasquet et al., 2015a,b). The approach appeared successful in other contexts as well as for various application scales: from the laboratory on partially saturated glass beads (Pasquet et al., 2016a), to the field on a hydrothermal site (Pasquet et al., 2016b; Pasquet and Bodet, 2017). Tow major issues however remain:

1. The involved inversion processes yet use a small number of layers that cannot properly describe the continuous variations of the subsurface hydrological properties (see exemple on Fig 3.19).
2. The combined use of P-wave traveltime tomography and surface-wave dispersion inversion involve distinct characteristics of the wavefield and different assumptions about the medium, thus providing VP and VS models of different sensitivity, resolution, investigation depth and posterior uncertainties.

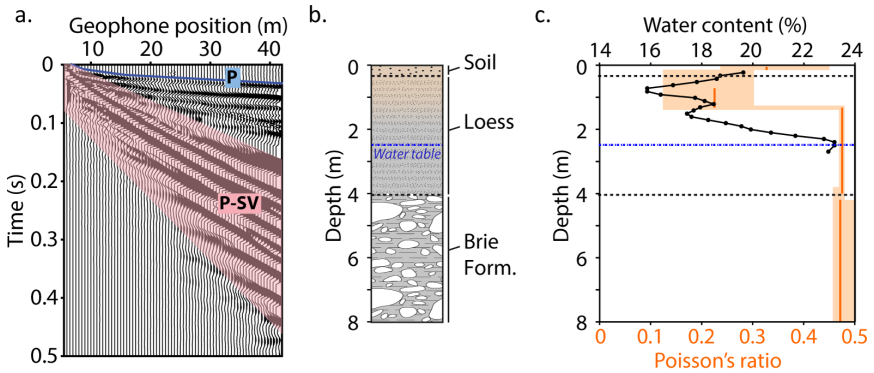

Figure 3.19: *A simple sketch presenting the CRITEX's seismic approach basically suggesting to retrieve the near surface Poisson's ratio from a single acquisition. (a) First arrival times and surface-wave dispersion are picked to be inverted for VP and VS, based on (b) strong prior information. (c) Estimated Poisson's ratio compared to actual saturation profile with depth. It clearly illustrates that near surface mechanical properties and saturation frequently vary on a continuous manner while the inversion of seismic data mainly yields discrete layers. This brings the need to use petrophysical models to build alternative forward modelling tools and improve inversion processes.*

Estimated VP and VS have thus to be interpreted separately with care before deriving any parameter of interest (e.g. VP/VS or Poisson's ratio, as shown in Dangeard et al. (2017b); Dangeard

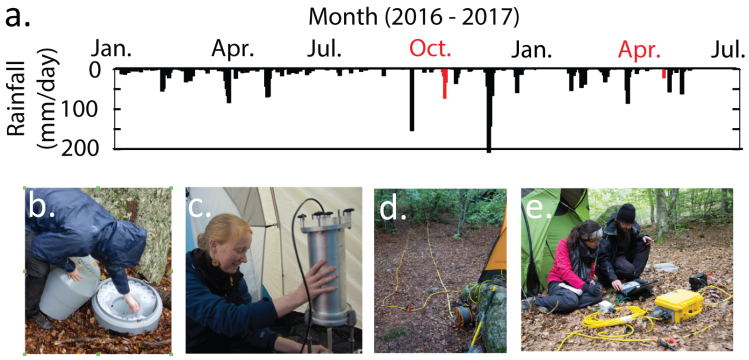

Figure 3.20: *Time-lapse experiment were performed on the the Mont Lozère (OHMCV) in October 2016 and April 2017 (a, red lines) in the framework of a RBV project on 'the influence of groundwater fluctuations on river chemistry – When Li isotopes meet geophysics!'. (b,c) Marie Kuessner (PhD in geochemistry, IPGP) collected water samples before, during and after strong rain events. (d,e) In the meantime, Marine Dangeard was recording seismic data to perform both seasonal and short-term time-lapse analyses, as presented on Fig. 3.21. Modified after Dangeard et al. (2017a); Dangeard (2019).*

(2019)). Such incompatibilities bring the need to revise our forward models, inversion tools and, more generally, our imaging approaches. That is why we aim at pushing to go from structural and static property imaging to process-based imaging approaches.

An alternative strategy was then first to consider the information carried by seismic data, instead of trying to invert them as for instance suggested by Bergamo et al. (2016a,b). We also wanted to precisely quantify their temporal variability, of great importance to understand the hydrosystems dynamics. We thus developed a 'time-lapse' implementation of our approach (again in the framework of both the CRITEX and PIREN-Seine programs), associated to a processing workflow to thoroughly estimate P-wave first arrivals and surface-wave dispersion picking errors (Dangeard et al., 2018; Dangeard, 2019). Similar time-lapse experiments and analyses were then for instance applied to several CZ observatories, such as the Mont Lozère in October 2016 and April 2017 (see Fig. 3.20). Seismic acquisitions with a time-step of 24 hours (before and after rainfalls, see Fig. 3.21) helped catching the dynamics of this pristine and poorly characterized site (Kuessner et al., 2017; Dangeard et al., 2017a; Dangeard, 2019), on which it was impossible to perform high resolution imaging (remote location, in a rather dense forest with difficult access to the site, granite boulders at the surface etc).

An other important aspect of these time-lapse studies was the idea to provide updated constraints, as well as initial and boundary conditions, to the hydrodynamic models (Dangeard et al., 2017b; Dangeard, 2019) by interloping and/or extrapolating point continuous data (as shown earlier, see e.g. Fig 3.18). By developing time-lapse seismic techniques articulated with other geophysical methods, hydrological monitoring, geotechnical soundings or geochemical sampling and analyses (Dangeard et al., 2017a), we aim at developing a fully integrated approach that can result in more quantitative studies of hydrogeological processes in the subsurface, as it is actually now classically recommended for the imaging and understanding of the CZ (Binley et al., 2015; Parsekian et al., 2015). Even if joint inversion of geophysical data is encouraged (e.g. Gallardo and Meju (2004); Linde and Doetsch, 2016; Shi et al. (2017)), such combined interpretations remain

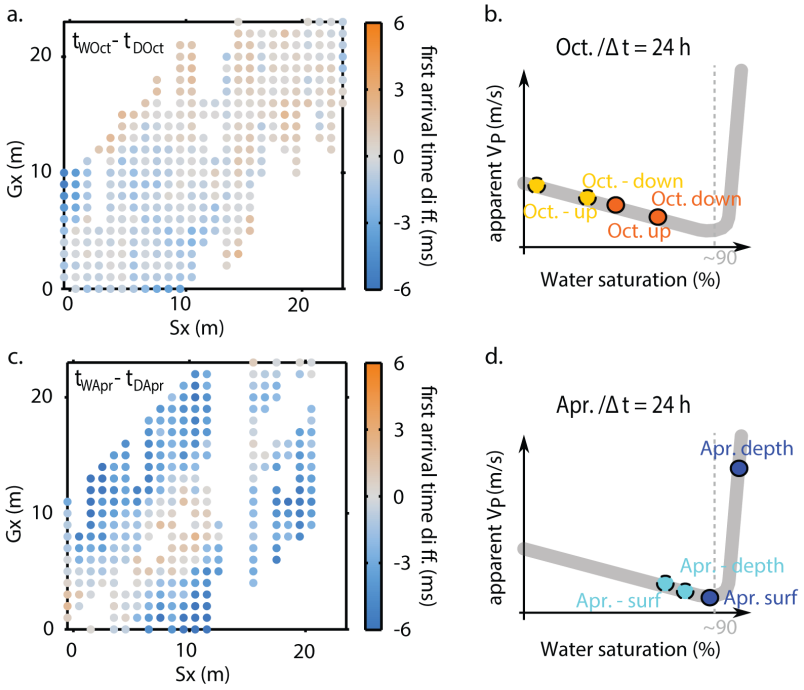

Figure 3.21: *Interpretations of the effect of strong rain events at both high-water (April 2017) and low-water (October 2016) periods on 'La Sapine' catchment. Time-lapse seismic acquisitions were performed with a time-step of 24 hours, before (D) and after (W) rainfalls and helped catching the dynamics of this pristine and poorly characterized site (Kuessner et al., 2017; Dangeard et al., 2017a; Dangeard, 2019).*

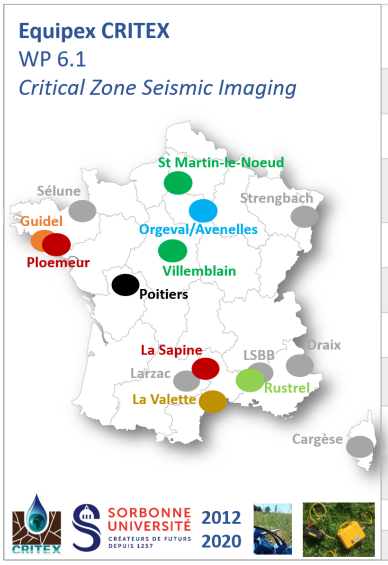

Sites	Main Partners	Funding/Frame-work (along with CRITEX)	Main scientific domains and approaches	Main targets	Max depth (m)	Multi-methods	Main seismic info
Ploemeur (cryst./WL)	U. Rennes	INSU / H+	Geophy. (methodo)	Heterogeneity / Water table	50	ERT	VP&VS models
Orgeval (alluv.)	Mines ParisTech	INSU / PIREN-Seine	Geophy. (methodo)	Water table	8	ERT	VP&VS models
Avenelles (Soli/VZ)	Mines ParisTech / IRSTEA Boissy	PIREN-Seine	Hydrogeophy. / Hydrogeol. (methodo. & modelling & appli.)	Heterogeneity / Water table & Saturation / Hydrodynamics	3	ERT / DCP	Time-lapse data Time lapse VP&VS models
Guidel (cryst./WZ)	U. Rennes / U. Nantes	OSUNA / ENIGMA ITN	Hydrogeophy. (appli.) Teaching / Workshop	Saturation / Dynamics	3	ERT / EM / DCP / TDR	VP&VS models Time-lapse data
La Sapine (crist./WL)	IPGP	RBV	Geophy / Hydro (appli.) / Geochem.	Structure / Saturation / Dynamics	15	ERT / EM / DCP / GPR	VP&VS models Time-lapse data
Rustrel (karst)	U. Avignon	INSU / H+	Hydrogeophy. (methodo.)	Heterogeneity / Partially sat. zone	50	ERT / NMR	NA (work in progress)
St Martin (karst)	CEREMA	INSU / R2DS	Hydrogeophy. (appli.)	Structure / Partially sat. zone / Infiltration	20	ERT / EM / SP / IR	VP&VS models (work in progress)
La Valette (soil)	IRSTEA Montpellier	NA	Geophy. / Agro. (appli.)	Heterogeneity / Water saturation / Dynamics	3	GPR / EM / ERT	VP&VS models (work in progress)
Villemblain (karst)	U. Orléans / BRGM	OZNS	Hydrogeophy. (methodo.)	Anisotropy / Water saturation	20	ERT	NA (work in progress)
Poitiers	U. Rennes / Silixa	H+	Teaching / Workshop	NA	NA	FO Temp.	NA
Cargèse	ENIGMA ITN	SU	Teaching / Workshop	NA	NA	NA	NA

Figure 3.22: *The Tour de France of CRITEX's seismic involved various hyrogeological contexts (in colour on the map): crystalline rocks (cryst.) with weathered layers (WL) of various thickness and fractured areas; alluvial catchments (alluv.) of continuous lithologies with interest in the vadose zone (VZ); soils and agricultural contexts (soil); heterogeneities in porosity and anisotropy in carbonates (karst). Several sites were used as natural laboratories to develop and validate our methodological approaches, depending on targets of interests: structure of the near-surface and heterogeneities of the porous medium; depth of the water table; spatial variations of saturation; temporal dynamics of the hydrosystems at various scales; infiltration processes; exchanges thorough the stream-aquifer continuum etc. Every studies systematically involved hydrogeological data and multi-geophysical/geotechnical surveys (Electrical Resistivity Tomography, Electro-Magnetic mapping/profiling; Ground Penetrating Radar; Nuclear Magnetic Resonance soundings; Infra-red thermography; Self-Potential mapping; Time Domain Reflectometry; Fiber-Optic distributed temperature sensing; Auger soundings; Dynamic Cone Penetrometer tests...). Some sites were also used for pedagogical purposes in the framework of workshops and summer schools. More recently, CRITEX's seismic has become popular in the framework of the OZCAR network and been deployed in several sites for various type of applications (in gray on the map).*

limited to specific acquisition configurations and are not operational yet. In parallel, efforts have to be made in the construction of strong physical and/or statistical links between the two methods and parameters of interest (de Pasquale et al., 2019; de Pasquale, 2017). That is why CRITEX's seismic is currently involved in both national and European projects [5] to find new ways to exploit the full wealth of seismic signals for the hydrogeophysical study of the CZ (see Fig 3.22).

3.5.2. Finding appropriate links between seismic properties and hydrodynamic parameters

The interpretation of the near surface mechanical properties and the definition of their quantitative links with hydrodynamic parameters remains complex. The typical theoretical framework for studying connections between rocks hydrodynamic parameters and seismic properties is poroelasticity Pride (2005). But most sites of interests on CZ observatories and associated hydrosystems not only involve 'hard rocks' but also –and almost systematically– unconsolidated and partially

5. www.critex.fr, http://www.ozcar-ri.org, https://enigma-itn.eu/

saturated soils. This issue has first to be tackled through the systematic and thorough exploration of existing petrophysical models and the suggestion of alternative relationships (Cho and Santamarina, 2001; Sawangsuriya et al., 2008, 2009; Heitor et al., 2012). We are currently investigating the theories behind wave propagation velocities in poorly consolidated media and how they are affected by water content, focusing on the partially saturated response. A field case was first studied, for which we used a Hertz-Mindlin based rock physics model to estimate water saturation from VP and VS from seismic data, as for instance recommended by Hollbrook et al. (2014). The model was able to distinguish between dry and fully saturated areas at two distinct hydrological periods, but failed in identifying partially saturated areas in both cases. This work underlines the need for more elaborated models to infer hydrodynamic properties from seismic data (Blazevic et al., 2018, 2020).

3.5.3. Exploiting the full wealth of seismic signals and extracting information from temporal variations

As mentionned earlier, 'the important spatial variability of subsurface materials dry properties is frequently of greater influence on seismic-wave velocities than the variation of water content itself'. We assumed the water content changes (hence the hydrological conditions) are the major factors of temporal variations of near-surface mechanical properties in hydrosystems (as far as seismic waves are concerned). The time-lapse applications we then developed (Dangeard, 2019) mainly focused on changes in the phase of 1-component seismic signals (mainly on apparent propagation velocities). Multi-component acquisitions should be considered and variations in amplitudes should (of course!) be exploited as well, by 'simply' studying the complex behaviour of attenuation with saturation in unconsolidated materials (Barrière et al., 2012) or for instance by developing full-waveform inversion approaches, as recently suggested for near-surface targets (e.g. Athanasopoulos and Bohlen, 2017b,a; Groos et al., 2017; Pan et al., 2019).

Controlled experiments are currently carried out (infiltration tests, pumping tests, see Ploemeur and Sélune sites on Fig 3.22) to focus on controlled dynamic processes and to enable quantitative comparisons with GPR and/or ERT. In September 2018, for instance, we carried out an infiltration experiment in the micaschist zone of Ploemeur. During the course of two days, 3.3 m^3 of water were infiltrated and 11 electrical resistivity and seismic acquisitions were performed on two orthogonal lines crossing the infiltration area (see Fig 3.23a). Adjacent to it, TDR probes previously installed in the subsurface (Jiménez-Martínez et al., 2013) provided real time water content throughout the experiment. Such study should provide means to understand how geophysical observations relate to each other and to the water content data, and perspectives on how to quantify the observed changes in terms of hydrodynamic processes. In this context joint inversion methods cited earlier should be implemented. Existing time-lapse inversion methods could be adapted as well, as recently suggested by Bergamo et al. (2016a,b) or Ikeda et al. (2017) for instance (e.g. seismic monitoring in the industry (Arts et al., 2004) or in soil sciences (Blum et al., 2004); Kalman filters such as in Nenna et al. (2011); focused time-lapse inversion like in Rosas-Carbajal et al. (2012) or other various studies such as Doetsch et al. (2010); Klotzsche et al. (2014); Singha et al. (2015); Suzaki et al. (2017).

Seismic noise interferometry has recently emerged as a promising tool to monitor VS continuously, even in hydrogeological context (Meier et al., 2010; Tsai, 2011; Le Feuvre et al., 2015; Lecocq et al., 2017; Fores et al., 2018). CRITEX plans to deploy semi-permanent broadband 3-component sensors to adapt the previously cited approaches to the local scale, in parallel to time-lapse active

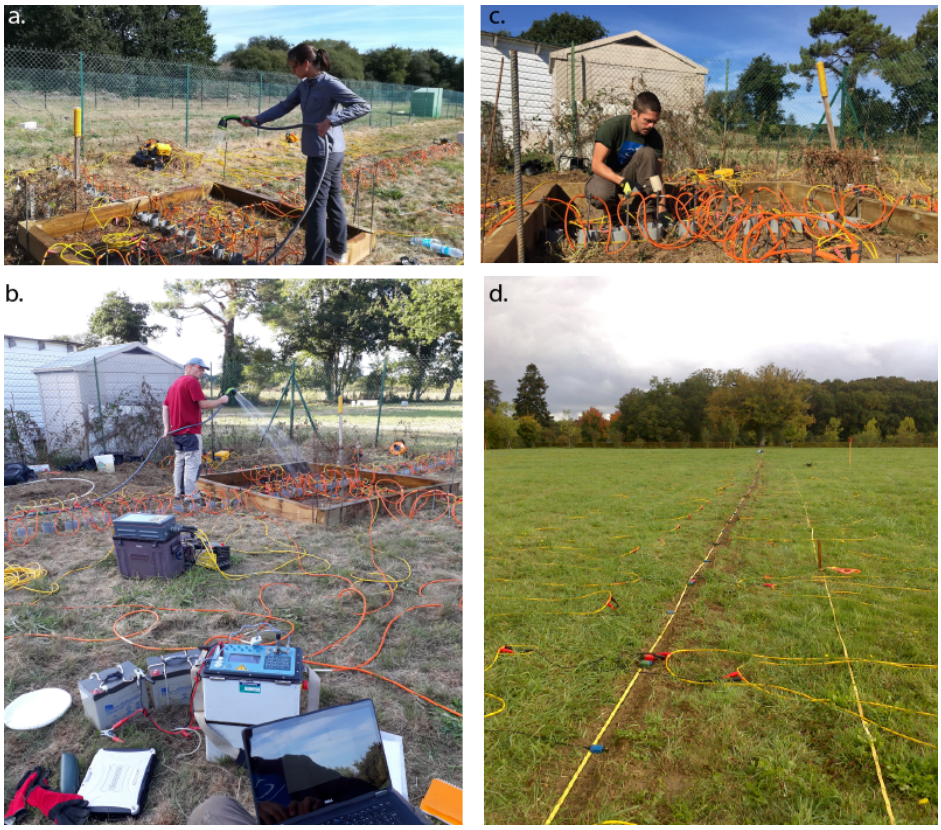

Figure 3.23: *(a, b, c) Lara Blazevic (PhD thesis, ITN ENIGMA, Sorbonne Université 2017-2020), Laurent Longuevergne and Sylvain Pasquet (Post-Doc OZCAR 2018-2020) performing an infiltration experiment monitored by time-lapse seismic and electrical methods as well as underground TDR probes. (d) Experimental set-up designed to perform comparisons between 3-component seismic acquisition with Fiber Optic Distributed Acoustic Sensing, the fiber-optic cable being buried in a trench below the geophones (CRITEX/H+ Workshop in Poitiers, Oct. 2015).*

methods and soil moisture observations (Guidel site on Fig 3.22). We will, depending on instruments availability and cost [6], evaluate the potential of Distributed Acoustic Sensing (see Ciocca et al. (2017)) for continuous monitoring of subsurface water content over long distances (see recent advances in Ajo-Franklin et al. (2017)).

3.5.4. Short term perspectives and recommendations

For the past ten years, with the help of PhD students and thanks to fruitful transdisciplinary cooperation, I have been developing alternative ways to image the heterogeneities of the CZ, to describe the dynamics of its hydrosystems and to add seismic prospecting techniques to the hydrogeophysics' toolbox. In the framework of my research projects, I actively involved the applied geophysics team at METIS in various environmental science programs such as the PIREN-Seine, the equipex CRITEX, the H+ and RBV networks etc, and the approach is becoming popular at

6. We actually performed preliminary tests in 2015, see Fig 3.23b.

an international level. But with the rise of long-term observation infrastructures in this domain (such as OZCAR), the tools we developed tend to be considered as state-of-the-art geophysical characterisation methods mainly deployed to enrich the observatories and networks data-bases (see Fig 3.22). A major issue here is that these geophysical results are most of the time just sets of parameters, in other words 'models', inferred from sparse datasets and ill-posed problems. They certainly cannot be considered as data by the observatories. Yet, with the work of Dangeard (2019), we confirmed that valuable 'hydrogeological' information is obviously carried by most geophysical data from which only interpretations can be suggested.

In order to transport information from the data to models that could be safely exploitable by non-geophysicists, we need: to increase both the extent and yield of our surveys; to optimise our acquisition set-ups with respect to target of interest; to highly increase our space and time sampling abilities [7]; to automatise our fastidious processing workflows, and; to improve or actually totally revise our inversion tools. As for the development of seismic methods on hydrogeological observatories in particular, I would recommend the following key points to be addressed in the very near future.

Machine aided semi-automatic processing.

— implementing automatic windowing and stacking of surface waves (based on the toolbox by Pasquet & Bodet, 2017);
— implementing multi-method P-wave first arrival picking based on recent developments by the METIS team (Khalaf et al., 2018) as well as on recent machine-learning approaches developed in seismology (Perol et al., 2018);
— building an automated version of Dangeard et al. (2018) to enable systematic error analysis;
— considering the full dispersion image (secular function with its real and complex parts) to include P-guided modes in the inversion (Maraschini et al., 2010; Boiero et al., 2013).

Better implementation and appraisal of standard inversion approaches.

— performing parametric studies to define how picking errors propagates into combined inverted models;
— selecting adapted petrophysical models to estimate the sensitivity of data to changes in saturation, depending on involved lithologies;
— suggesting sets of benchmarks to find ways to combine dramatically different resolutions and DOI.

Time-lapse acquisitions and constraints from other geophysical and geotechnical measurements.

— extracting dynamics from point continuous observations to constraint time-lapse inversions;
— developing spatial interpolation with geophysical models as suggested by Dangeard (2019);
— using low-costs and sparse acquisitions between high-resolution snapshots to perform interpolation of the datasets with machine learning approaches.

After that we will be able to include results of seismic prospecting in the data-bases of hydrogeological observatories. And only after that, we will be able to suggest strong coupling laws between hydrogeological properties and seismic observations. In the meantime, an alternative strategy should be: to thoroughly find which hydrological information is carried by which part of the signal;

7. As soon as fiber-optic, wireless permanent sensors and similar techniques will be of decent cost for academic environmental sciences...

to define how the hydrogeological objectives and targets should allow for a systematic and pertinent selection of adapted geophysical observables and acquisition set-ups, and; to better articulate geophysical and hydrological measurements (Marçais and de Dreuzy, 2017; Ferré, 2017; Dangeard, 2019), the hydrogeological properties being themselves rather models than data. Aren't they ?

Bibliography

Abraham, O., Chammas, R., Cote, P., Pedersen, H. A., Semblat, J.-F., 2004. Mechanical characterization of heterogeneous soils with surface waves: experimental validation on reduced-scale physical models. Near Surface Geophysics 2 (4), 249–258.

Abraham, O., Piwakowski, B., Villain, G., Durand, O., 2012. Non-contact, automated surface wave measurements for the mechanical characterisation of concrete. Construction and Building Materials 37, 904–915.

Ajo-Franklin, J., Dou, S., Daley, T., Freifeld, B., Robertson, M., Ulrich, C., Wood, T., Eckblaw, I., Lindsey, N., Martin, E., Wagner, A., 2017. Time-lapse surface wave monitoring of permafrost thaw using distributed acoustic sensing and a permanent automated seismic source. SEG Technical Program Expanded Abstracts 2017, pp. 5223 – 5227.

Aleshin, V., Gusev, V., Tournat, V., 2007. Acoustic modes propagating along the free surface of granular media. J. Acoust. Soc. Am. 121 (5), 2600–2611.

Andreotti, B., 2012. Sonic sands. Reports on Progress in Physics 75 (2), 026602.

Arran, M. I., Vriend, N., Muyzert, E., 2018. Seismic ground roll absorption and reemission by sand dunes. Journal of Geophysical Research: Solid Earth 123, 5675–5689.

Arts, R., Eiken, O., Chadwick, A., Zweigel, P., van der Meer, L., Zinszner, B., 2004. Monitoring of CO2 injected at Sleipner using time-lapse seismic data. Energy 29 (9), 1383–1392.

Athanasopoulos, N., Bohlen, T., 2017a. Aquifer characterization using elastic full-waveform inversion. In: 23rd European Meeting of Environmental and Engineering Geophysics.

Athanasopoulos, N., Bohlen, T., 2017b. Field data application of sequential full-waveform inversion of refracted and rayleigh waves. In: 79th EAGE Conference and Exhibition 2017.

Bachrach, R., Avseth, P., 2008. Rock physics modeling of unconsolidated sands: Accounting for nonuniform contacts and heterogeneous stress fields in the effective media approximation with applications to hydrocarbon exploration. Geophysics 73 (6), E197–E209.

Bachrach, R., Dvorkin, J., Nur, A., 1998. High-resolution shallow-seismic experiments in sand, Part II: Velocities in shallow unconsolidated sand. Geophysics 63 (4), 1234–1240.

Bachrach, R., Dvorkin, J., Nur, A., 2000. Seismic velocities and Poisson's ratio of shallow unconsolidated sands. Geophysics 65 (2), 559–564.

Bachrach, R., Nur, A., 1998. High-resolution of shallow-seismic experiments in sand; Part 1, Water table, fluid flow, and saturation. Geophysics 63 (4), 1225–1233.

Baker, G. S., Steeples, D. W., Schmeissner, C., 1999. In-situ, high-frequency P-wave velocity measurements within 1 m of the Earth's surface. Geophysics 64 (2), 323–325.

Barrière, J., Bordes, C., Brito, D., Sénéchal, P., Perroud, H., 2012. Laboratory monitoring of P waves in partially saturated sand. Geophysical Journal International 191 (3), 1152–1170.

Bauer, K., Moeck, I., Norden, B., Schulze, A., Weber, M., Wirth, H., 2010. Tomographic p wave velocity and vertical velocity gradient structure across the geothermal site groß schönebeck (NE german basin): Relationship to lithology, salt tectonics, and thermal regime. Journal of Geophysical Research: Solid Earth 115 (B8), B08312.

Bauer, K., Schulze, A., Ryberg, T., Sobolev, S. V., Weber, M. H., 2003. Classification of lithology from seismic tomography: A case study from the messum igneous complex, namibia. Journal of Geophysical Research: Solid Earth 108 (B3), 2152.

Bear, J., 1972. Dynamics of fluids in porous media. Elsevier, New York.

Bergamo, P., 2012. Surface wave analysis in laterally varying media. Ph.D. thesis, Politecnico di Torino.

Bergamo, P., Bodet, L., Socco, L. V., Mourgues, R., Tournat, V., 2014. Physical modelling of a surface-wave survey over a laterally varying granular medium with property contrasts and velocity gradients. Geophys. J. Internat. 197 (1).

Bergamo, P., Boiero, D., Socco, L. V., 2012. Retrieving 2D structures from surface-wave data by means of space-varying spatial windowing. Geophysics 77 (4), EN39–EN51.

Bergamo, P., Dashwood, B., Uhlemann, S., Swift, R., Chambers, J., Gunn, D., Donohue, S., 2016a. Time-lapse monitoring of climate effects on earthworks using surface waves. Geophysics 81 (2), EN1–EN15.

Bergamo, P., Dashwood, B., Uhlemann, S., Swift, R., Chambers, J. E., Gunn, D. A., Donohue, S., 2016b. Time-lapse monitoring of fluid-induced geophysical property variations within an unstable earthwork using P-wave refraction. Geophysics 81 (4), EN17–EN27.

Bergamo, P., Socco, L., 2016. P- and S-wave velocity models of shallow dry sand formations from surface wave multimodal inversion. Geophysics 81 (4), R197–R209.

Binley, A., Cassiani, G., Deiana, R., 2010. Hydrogeophysics: opportunities and challenges. Bollettino di Geofisica Teorica ed Applicata 51 (4).

Binley, A., Hubbard, S. S., Huisman, J. A., Revil, A., Robinson, D. A., Singha, K., Slater, L. D., 2015. The emergence of hydrogeophysics for improved understanding of subsurface processes over multiple scales. Water resources research 51 (6), 3837–3866.

Bishop, A. W., 1959. The principle of effective stress. Teknisk ukeblad 39, 859–863.

Bitri, A., Bégat, S. L., Baltassat, J. M., 1998. Shear wave velocity determination of soils from *in situ* Rayleigh waves measurements. In: Procc. 4th Meeting EEGS, Barcelona, Spain. Environmental and Engineering Geophysical Society, pp. 503–506.

Blazevic, L., Bodet, L., Pasquet, S., Linde, N., Jougnot, D., Longuevergne, L., 2020. Time-lapse seismic and electrical monitoring of the vadose zone during a controlled infiltration experiment at the Ploemeur hydrological observatory, france. in preparation for Water.

Blazevic, L. A., Bodet, L., Jougnot, D., Longuevergne, L., 2018. Finding appropriate rocks physics models to interpret seismic data in hydrogeophysics applications. In: AGU Fall Meeting, December 2018.

Blum, A., Flammer, I., Friedli, T., Germann, P., 2004. Acoustic tomography applied to water flow in unsaturated soils. Vadose Zone Journal 3, 288–299.

Blum, T. E., van Wijk, K., 2010. Advances in laboratory modeling of wave propagation. In: SEG Technical Program Expanded Abstracts 2010.

Blum, T. E., van Wijk, K., Pouet, B., Waertelle, A., 2011a. Multicomponent wavefield characterization with a novel scanning laser interferometer. Review of scientific instruments 81, 073101.

Blum, T. E., van Wijk, K., Snieder, R., Willis, M. E., 2011b. Laser excitation of a fracture source for elastic waves. Physical Review Letters 107, 275501.

Blum, T. E., van Wijk, K., Snieder, R., Willis, M. E., 2011c. Theory and laboratory experiments of elastic wave scattering by dry planar fractures. Journal of Geophysical Research 116, B08218.

Bocquet, L., Charlaix, E., Ciliberto, S., Crassous, J., 1998. Moisture-induced ageing in granular media and the kinetics of capillary condensation. Nature 396 (24/31), 735–737.

Bodet, L., 2005. Limites théoriques et expérimentales de l'interprétation de la dispersion des ondes de rayleigh: apport de la modélisation numérique et physique. Ph.D. thesis, École Centrale de Nantes et Université de Nantes, Nantes, France.

Bodet, L., Abraham, O., Clorennec, D., 2009a. Near-offsets effects on Rayleigh-wave dispersion measurements: Physical modelling. J. Appl. Geophys. 68 (1), 95–103.

Bodet, L., Bergamo, P., Dhemaied, A., Mourgues, R., Socco, L. V., Tournat, V., 2013. Laser-Doppler probing of granular materials involved in physical and analogue modelling. In: Measuring By Light, International Meeting on Optical Measurement Techniques and Industrial Applications, Shell Rijswijk, The Nederland, 20-21 November 2013 (invited presentation).

Bodet, L., Bergamo, P., Dhemaied, A., Mourgues, R. M. R., Pasquet, S., Socco, F. R. L. V., Tournat, V., 2014a. Surface-wave analyses in unconsolidated granular models with increasing degrees of complexity. In: 75th EAGE Conference Exhibition. EAGE, Amsterdam, Netherlands (invited keynote).

Bodet, L., Dhemaied, A., Martin, R., Mourgues, R., Rejiba, F., Tournat, V., 2014b. Small-scale physical modeling of seismic-wave propagation using unconsolidated granular media. Geophysics 79 (6), T323–T339.

Bodet, L., Dhemaied, A., Mourgues, R., Tournat, V., Rejiba, F., 2012. Laser-Doppler acoustic probing of granular media with in-depth property gradient and varying pore pressures. In: International Congress on Ultrasonics (ICU), University of Gdansk, Poland, September 5-8, 2011, AIP Conf. Proc. 1433. pp. 147–150.

Bodet, L., Dhemaied, A., Pasquet, S., Rejiba, F., Guérin, R., 2014c. Caractérisation mécanique de la plateforme ferroviaire par méthodes géophysiques : estimation des vitesses de cisaillement par ondes de surface. Tech. rep., Rapport interne, SNCF.

Bodet, L., Galibert, P., Dhemaied, A., Camerlynck, C., Al-Zoubi, A., 2010a. Surface-wave profiling for sinkhole

hazard assessment along the eastern Dead Sea shoreline, Ghor Al–Haditha, Jordan. In: 72nd EAGE Conference and Exhibition incorporating SPE EUROPEC 2010.

Bodet, L., Jacob, X., Tournat, V., Mourgues, R., Gusev, V., 2009b. Surface-wave dispersion inversion in an unconsolidated granular medium. In: 71^{st} EAGE Conference & Exhibition, Amsterdam, The Netherlands, 8-11 June 2009.

Bodet, L., Jacob, X., Tournat, V., Mourgues, R., Gusev, V., 2010b. Elasticity profile of an unconsolidated granular medium inferred from guided waves: Toward acoustic monitoring of analogue models. Tectonophysics 496, 99–104.

Bodet, L., Pasquet, S., Bergamo, P., Martin, R., Mourgues, R., Tournat, V., 2015. Experimental illustrations of seismic-wave properties of interest for hydrogeological studies. In: AGU Fall Meeting, San Francisco Calif., USA 14-18 December 2015 (invited presentation).

Bodet, L., Rahmania, I., Kyrkou, K., Wacquier, L., Dangeard, M., Pasquet, S., Vitale, Q., Dhemaied, A., Boisson-Gaboriau, J., Nebieridze, S., 2017. Estimation in situ des variations de propriétés mécaniques de la plateforme ferroviaire par ondes sismiques de surface. Tech. rep., Rapport interne, SNCF.

Bodet, L., van Wijk, K., Bitri, A., Abraham, O., Côte, P., Grandjean, G., Leparoux, D., 2005. Surface-wave inversion limitations from laser-Doppler physical modeling. J. Env. and Eng. Geophys. 10 (2), 151–162.

Bohlen, T., Kugler, S., Klein, G., Theilen, F., 2004. 1.5D inversion of lateral variation of Scholte-wave dispersion. Geophysics 69 (2), 330–344.

Boiero, D., Socco, L. V., 2010. Retrieving lateral variations from surface wave dispersion curves. Geophysical Prospecting 58 (6), 977–996.

Boiero, D., Socco, L. V., 2011. The meaning of surface wave dispersion curves in weakly laterally varying structures. Near Surface Geophysics 9 (6), 561–570.

Boiero, D., Wiarda, E., Vermeer, P., 2013. Surface- and guided-wave inversion for near-surface modeling in land and shallow marine seismic data. The Leading Edge 32 (6), 638–646.

Boisson-Gaboriau, J., Dhemaied, A., Rahmania, I., Bodet, L., Pasquet, S., Brand, L., Calon, N., Terpereau, J.-M., Kahil, S., 2016. Etude géophysique, géotechnique et historique d'une voie ferrée sur sol tourbeux. In: Journées Nationale de Géotechnique et de Géologie de l'Ingénieur.

Bonneau, L., Andreotti, B., Clément, E., 2008. Evidence of Rayleigh-Hertz surface waves and shear stiffness anomaly in granular media. Phys. Rev. Lett. 101 (11), 118001.

Bonneau, L., Andreotti, B., Clément, E., 2007. Surface elastic waves in granular media under gravity and their relation to booming avalanches. Physical Review E 75 (1), 016602.

Bradford, J. H., Sawyer, D. S., 2002. Depth characterization of shallow aquifers with seismic reflection, Part II—Prestack depth migration and field examples. Geophysics 67 (1), 98–109.

Bretaudeau, F., Brossier, R., Leparoux, D., Abraham, O., Virieux, J., 2013. 2D elastic full-waveform imaging of the near-surface: application to synthetic and physical modelling data sets. Near Surface Geophysics 11 (3), 307–316.

Bretaudeau, F., Leparoux, D., Durand, O., Abraham, O., 2011. Small-scale modeling of onshore seismic experiment: A tool to validate numerical modeling and seismic imaging methods. Geophysics 76, T101–T112.

Brunet, T., 2006. Etude des milieux granulaires secs et mouillés à l'aide des ondes ultrasonores. Ph.D. thesis, Ecole Doctorale : Mécanique, Thermique et Génie Civil.

Brunet, T., Jia, X., Mills, P., 2008. Mechanisms for acoustic absorption in dry and weakly wet granular media. Physical review letters 101 (13), 138001.

Buddensiek, M.-L., 2009. Seismic imaging of sandbox models. Ph.D. thesis, Freien Universität Berlin.

Buddensiek, M.-L., Krawczyk, C. M., Kukowski, N., Oncken, O., 2009. Performance of piezoelectric transducers in terms of amplitude and waveform. Geophysics 74 (2), T33–T45.

Cameron, A., Knapp, C. C. (Eds.), 2009. Geostatistical analysis of near-surface geophysical data : results from the P-Reactor Area at Savannah River Site, South Carolina. American Geophysical Union, Fall Meeting 2009.

Campman, X. H., van Wijk, K., Riyanti, K., Scales, J. A., Herman, G. C., 2004. Imaging scattered seismic surface waves. Near Surface Geophysics 2 (4), 223–230.

Campman, X. H., van Wijk, K., Scales, J. A., Herman, G. C., 2005. Imaging and suppressing near-receiver scattered surface waves. Geophysics 70 (2), V21–V29.

Chadwick, A., Williams, G., Delepine, N., Clochard, V., Labat, K., Sturton, S., Buddensiek, M.-L., Dillen, M., Nickel, M., Lima, A. L., Arts, R., Neele, F., Rossi, G., 2010. Quantitative analysis of time-lapse seismic monitoring data at the Sleipner CO2 storage operation. The Leading Edge 29 (2), 170–177.

Cho, G., Santamarina, J., 2001. Unsaturated particulate materials—particle-level studies. Journal of Geotechnical and Geoenvironmental Engineering 127 (1), 84–96.

Ciocca, F., Bodet, L., Simon, N., Karaulanov, R., Clarke, A., Abesser, A., Krause, S., Chalari, A., Mondanos, M., 2017. Towards the wetness characterization of soil subsurface using fibre optic distributed acoustic sensing. In:

AGU Fall Meeting. AGU, New Orleans, USA.

Dangeard, M., 2019. Développement d'une approche "time-lapse" des méthodes sismiques pour l'hydrogéophysique et la compréhension de la dynamique des hydrosystèmes. Ph.D. thesis, Sorbonne Université.

Dangeard, M., Bodet, L., Kuessner, M., Bouchez, J., Thiesson, J., Lucas, A., Gayer, E., Frick, D., 2017a. A multidisciplinary investigation of groundwater fluctuations and their control on river chemistry – Insights from time-lapse active seismic experiments during flood events. In: AGU Fall Meeting. AGU, New Orleans, USA.

Dangeard, M., Bodet, L., Pasquet, S., Thiesson, J., Guérin, R., Jougnot, D., Longuevergne, L., 2018. Estimating picking errors in near-surface seismic data to enable their time-lapse interpretation of hydrosystems. Near Surface Geophysics 16 (6), 613–625.

Dangeard, M., Pasquet, S., Bodet, L., Guérin, R., Longuevergne, L., Thiesson, J., 2016a. Temporal variations observed in near-surface seismic data at the ploemeur hydrogeological observatory. In: 43rd IAH International Congress. IAH, Montpellier, France.

Dangeard, M., Pasquet, S., Bodet, L., Guérin, R., Longuevergne, L., Thiesson, J., 2016b. Temporal variations of near-surface seismic data at the Ploemeur (France) hydrogeological observatory. In: Near Surface Geoscience 2016 – 22nd European Meeting of Environmental and Engineering Geophysics.

Dangeard, M., Rivière, A., Bodet, L., Schneider, S., 2019. Amélioration de la quantification des échanges nappe-rivière grâce aux time-lapse sismiques. Tech. rep., Rapport PIREN Seine.

Dangeard, M., Schneider, S., Bodet, L., Rivière, A., Guérin, R., Réjiba, F., Hovhannissian, G., 2017b. Vers une interpolation hydrogéophysique des propriétés hydrodynamiques de la subsurface : apports du « time-lapse » sismique. Tech. rep., Rapport PIREN-SEINE.

Danneels, G., Bourdeau, C., Torgoev, I., Havenith, H.-B., 2008. Geophysical investigation and dynamic modelling of unstable slopes: case-study of Kainama (Kyrgyzstan). Geophysical Journal International 175 (1), 17–34.

de Cacqueray, B., Roux, P., Campillo, M., Catheline, S., 2013. Tracking of velocity variations at depth in the presence of surface velocity fluctuations. Geophysics 78 (1), U1–U8.

de Cacqueray, B., Roux, P., Campillo, M., Catheline, S., Boue, P., 2011. Elastic-wave identification and extraction through array processing: An experimental investigation at the laboratory scale. Journal of Applied Geophysics 74, 81–88.

de Pasquale, G., 2017. Changing the prior model description in bayesian inversion of hydrogeophysics dataset. Groundwater 55 (5), 651–655.

de Pasquale, G., Linde, N., Doetsch, J., Holbrook, W. S., 2019. Probabilistic inference of subsurface heterogeneity and interface geometry using geophysical data. Geophysical Journal International 217 (2), 816–831.

Devi, M. S., Garambois, S., Brito, D., Dietrich, M., Poydenot, V., Bordes, C., 2018. A novel approach for seismoelectric measurements using multielectrode arrangements: II—Laboratory measurements. Geophysical Journal International 214 (3), 1783–1799.

Dewangan, P., Tsvankin, I., Batzle, M., van Wijk, K., Haney, M., 2006. PS-wave moveout inversion for tilted TI media: A physical-modeling study. Geophysics 71, D135–D143.

Dhemaied, A., 2011. Modélisation directe de la propagation d'ondes dans les milieux visco-élastiques : approche 2D par différences finies dans le domaine temporel. Ph.D. thesis, Université Pierre et Marie Curie-Paris 6.

Dhemaied, A., Cui, Y.-J., Tang, A. M., 2014a. Etude de la sensibilité de la raideur mécanique des sols supports à la variation de la teneur en eau. Rapports d'activité, ENPC/SNCF.

Dhemaied, A., Cui, Y.-J., Tang, A. M., Nebieridze, S., Terpereau, J.-M., Leroux, P., 2014b. Effet de l'état hydrique sur la raideur mécanique. In: GEORAIL 2014.

Dhemaied, A., Cui, Y.-J., Tang, A. M., Nebieridze, S., Terpereau, J.-M., Leroux, P., Bodet, L., Pasquet, S., 2014c. Caractérisation des sols prélevés in situ. In: GEORAIL 2014.

Dhemaied, A., Rejiba, F., Camerlynck, C., Bodet, L., Guérin, R., 2011. Seismic-wave propagation modeling in viscoelastic media using the auxiliary differential equation method. Bulletin of the Seismological Society of America 101 (1), 413–420.

Di Stefano, R., Aldersons, F., Kissling, E., Baccheschi, P., Chiarabba, C., Giardini, D., 2006. Automatic seismic phase picking and consistent observation error assessment: application to the italian seismicity. Geophysical Journal International 165 (1), 121–134.

Doetsch, J., Linde, N., Binley, A., 2010. Structural joint inversion of time-lapse crosshole ERT and GPR traveltime data. Geophysical Research Letters.

Domenico, S., 1977. Elastic properties of unconsolidated porous sand reservoirs. Geophysics 42 (7), 1339–1368.

Donohue, S., Forristal, D., Donohue, L. A., 2013. Detection of soil compaction using seismic surface waves. Soil and Tillage Research 128, 54–60.

Donohue, S., Gunn, D. A., Bergamo, P., Hughes, E., Dashwood, B., Uhlemann, S., Chambers, J. E., Ward, D., 2014.

Assessing climate effects on railway earthworks using MASW. In: Near Surface Geoscience 2014-20th European Meeting of Environmental and Engineering Geophysics.

Duranteau, M., 2010. Ondes de surface et caractéisation sismique des réservoirs hydrologiques. Mémoire de master 2, Université du Maine.

Ekanem, A., Wei, J., Li, X.-Y., Chapman, M., Main, I., 2013. P-wave attenuation anisotropy in fractured media: A seismic physical modelling study. Geophysical Prospecting 61, 420–433.

Endrun, B., Meier, T., Lebedev, S., Bohnhoff, M., Stavrakakis, G., Harjes, H.-P., 2008. S velocity structure and radial anisotropy in the aegean region from surface wave dispersion. Geophysical Journal International 174 (2), 593–616.

Ezersky, M. G., Bodet, L., Akawwi, E., Al-Zoubi, A. S., Camerlynck, C., Dhemaied, A., Galibert, P.-Y., 2013. Seismic Surface-wave Prospecting Methods for Sinkhole Hazard Assessment along the Dead Sea Shoreline. Journal of Environmental & Engineering Geophysics 18 (4), 233–253.

Fauchard, C., Pothérat, P., 2004. Détection de cavités souterraines par méthodes géophysiques. Techniques et méthodes des laboratoires des ponts et chaussées.

Ferré, T. P., 2017. Revisiting the relationship between data, models, and decision-making. Groundwater 55 (5), 604–614.

Filippi, C., 2019. Etude des observables sismiques en ondes de surface pour la détection et caractérisation de cavités souterraines : approches numérique et expérimentale. Ph.D. thesis, Université de Nantes.

Forbriger, T., 2003a. Inversion of shallow-seismic wavefields: I. Wavefield transformation. Geophys. J. Internat. 153 (3), 719–734.

Forbriger, T., 2003b. Inversion of shallow-seismic wavefields: II. Inferring subsurface properties from wavefield transforms. Geophys. J. Internat. 153 (3), 735–752.

Fores, B., Champollion, C., Mainsant, G., Albaric, J., Fort, A., 2018. Monitoring saturation changes with ambient seismic noise and gravimetry in a karst environment. Vadose Zone J. 17, 170163.

Foti, S., 2000. Multistation methods for geotechnical characterisation using surface waves. Ph.D. thesis, Politecnico di Torino.

Foti, S., Lancellotta, R., Lai, C. G., 2002. Porosity of fluid-saturated porous media from measured seismic wave velocities. Géotechnique 52 (5), 359–373.

Fratta, D., Alshibli, K. A., Tanner, W. M., Roussel, L., 2005. Combined TDR and P-Wave velocity measurements for the determination of in situ soil density–experimental study. Geotechnical Testing Journal 28 (6).

Fredlund, D., Morgenstern, N. R., Widger, R., 1978. The shear strength of unsaturated soils. Canadian geotechnical journal 15 (3), 313–321.

Gabriels, P., Snieder, R., Nolet, G., 1987. In situ measurements of shear-wave velocity in sediments with higher-mode Rayleigh waves. Geophysical Prospecting 35 (2), 187–196.

Gallardo, L. A., Meju, M. A., 2004. Joint two-dimensional dc resistivity and seismic travel time inversion with cross-gradients constraints. Journal of Geophysical Research: Solid Earth 109 (B3).

Garnier, V., Piwakowski, B., Abraham, O., Villain, G., C., P., J.F., C., 2012. Acoustical techniques for concrete evaluation: improvements, comparisons and consistencies. Construction and Building Materials 37, 598–613.

Gassmann, F., 1951. Elastic waves through a packing of spheres. Geophysics 16, 673–685.

Géli, L., Bard, P., Schmitt, D. P., 1987. Seismic wave propagation in a very permeable wave-saturated surface layer. Journal Of Geophysical Research 92 (B8), 7931–7944.

George, L. A., Dewoolkar, M. M., Znidarcic, D., 2009. Simultaneous laboratory measurement of acoustic and hydraulic properties of unsaturated soils. Vadose Zone Journal 8 (3), 633.

Grandjean, G., Bitri, A., 2006. 2M-SASW : multifold multichannel seismic inversion of local dispersion of Rayleigh waves in laterally heterogeneous subsurfaces: application to the Super-Sauze earthflow, France. Near Surface Geophysics 4 (6), 367–375.

Grelle, G., Guadagno, F. M., 2009. Seismic refraction methodology for groundwater level determination: "Water seismic index". Journal of Applied Geophysics 68 (3), 301–320.

Gressier, J.-B., Mourgues, R., Bodet, L., Mathieu, J.-Y., Galland, O., Cobbold, P. R., 2010. Control of pore fluid pressure on depth of emplacement of magmatic sills: an experimental approach. Tectonophysics 489, 1–13.

Groos, L., Schäfer, M., Forbriger, T., Bohlen, T., 2017. Application of a complete workflow for 2D elastic full-waveform inversion to recorded shallow-seismic Rayleigh waves. Geophysics 82 (2), R109–R117.

Gunn, D., Chambers, J., Dashwood, B., Lacinska, A., Dijkstra, T., Uhlemann, S., Swift, R., Kirkham, M., Milodowski, A., Wragg, J., Donohue, S., 2018. Deterioration model and condition monitoring of aged railway embankment using non-invasive geophysics. Construction and Building Materials 170, 668 – 678.

Gunn, D., Chambers, J., Uhlemann, S., Wilkinson, P., Meldrum, P., Dijkstra, T., Haslam, E., Kirkham, M., Wragg,

J., Holyoake, S., et al., 2015. Moisture monitoring in clay embankments using electrical resistivity tomography. Construction and Building Materials 92, 82–94.

Gunn, D., Dashwood, B. A., Bergamo, P., Donohue, S., 2016. Aged embankment imaging and assessment using surface waves. Proceedings of the Institution of Civil Engineers-Forensic Engineering 169 (4), 149–165.

Gusev, V., Aleshin, V., Tournat, V., 2006. Acoustic waves in an elastic channel near the free surface of granular media. Phys. Rev. Lett. 96 (214301).

Gusev, V., Tournat, V., 2008. How acoustic waves are guided in buried subsurface channels in unconsolidated granular media. Physical Review E 78 (036602).

Haines, S. S., 2007. A hammer-impact, aluminium, shear-wave seismic source. Tech. Rep. OF 07-1406, United States Geological Survey.

Haskell, N. A., 1953. The dispersion of surface waves on multilayered media. Bullettin of the Seismologicol Society of America 43, 17–346.

Hayashi, K., Nishizawa, O., 2001. Laboratory studies of surface waves using a laser Doppler vibrometer. In: 5^{th} Int. Symp. on Recent Advances in Exploration Geophysics in Kyoto. pp. 1–8.

Hayashi, K., Suzuki, H., 2004. CMP cross-correlation analysis of multi-channel surface-wave data. Exploration Geophysics 35 (1), 7–13.

Heisey, J. S., II, K. H. S., Meyer, A. H., 1982. Moduli pavements systems from spectral analysis of surface waves. Transp. Res. Rec. 852, 22–31.

Heitor, A., Indraratna, B., Rujikiatkamjorn, C., Golaszewski, R., 2012. Characterising compacted fills at penrith lakes development site using shear wave velocity and matric suction. In: 11th Australia - New Zealand Conference on Geomechanics: Ground Engineering in a Changing World. Melbourne, Australia, pp. 1262–1267.

Hejazi Nooghabi, A., Boschi, L., Roux, P., de Rosny, J., 2017. Coda reconstruction from cross-correlation of a diffuse field on thin elastic plates. Phys. Rev. E 96, 032137.

Heraibi, R., 2019. Optimisation du profilage par ondes de surface pour la reconnaissance des plateformes ferroviaires. Master's thesis, Sorbonne Université.

Hubbard, S. S., Linde, N., 2011. Hydrogeophysics. Treatise on Water Science. Elsevier.

Hugenschmidt, J., Kasa, C., Kato, H., 2013. GPR for the inspection of industrial railway tracks. Near Surface Geophysics 11 (1988).

Hévin, G., Abraham, O., Pedersen, H., Campillo, M., 1998. Characterization of surface cracks with rayleigh waves: a numerical model. NDT & E International 31 (4), 289 – 297, non-destructive Testing in Civil Engineering.

Hwang, H.-J., Park, H.-C., 2014. Evaluation of condition of gravel ballast layer on high-speed railway using surface wave method based on harmonic wavelet analysis of waves. NDT & E International 68, 78–87.

Ikeda, T., Tsuji, T., Matsuoka, T., 2013. Window-controlled CMP crosscorrelation analysis for surface waves in laterally heterogeneous media. Geophysics 78 (6), EN95–EN105.

Ikeda, T., Tsuji, T., Takanashi, M., Kurosawa, I., Nakatsukasa, M., Kato, A., Worth, K., White, D., Roberts, B., 2017. Temporal variation of the shallow subsurface at the Aquistore CO2 storage site associated with environmental influences using a continuous and controlled seismic source. Journal of Geophysical Research: Solid Earth 122 (4), 2859–2872.

Jacob, X., Aleshin, V., Tournat, V., Leclaire, P., Lauriks, W., Gusev, V. E., 2008. Acoustic probing of the jamming transition in an unconsolidated granular medium. Phys. Rev. Lett. 100 (158003).

Jacqueline, D., 2015. Caractérisation de la compacité du ballast ferroviaire par méthodes sismiques. Ph.D. thesis, École doctorale Sciences, Ingénierie et Environnement, Université Paris-Est.

Jacqueline, D., Fauchard, C., Semblat, J.-F., Magnan, J.-P., 2017. Caractérisation de la compacité du ballast ferroviaire par méthodes sismique. In: GEORAIL 2017.

Jacqueline, D., Hemmati, S., Vinceslas, G., Dimnet, E., 2014. Mesure et simulation de la propagation de vibrations à travers une couche de ballast. In: GEORAIL 2014.

Jia, X., Caroli, C., Velicky, B., 1999. Ultrasound propagation in externally stressed granular media. Phys. Rev. Lett. 82 (9), 1863–1866.

Jiao, L., Moon, W. M., 2000. Detection of seismic refraction signals using a variance fractal dimension technique. Geophysics 65 (1), 286–292.

Jiménez-Martínez, J., Longuevergne, L., Le Borgne, T., Davy, P., Russian, A., Bour, O., 2013. Temporal and spatial scaling of hydraulic response to recharge in fractured aquifers: Insights from a frequency domain analysis. Water Resources Research 49 (5), 3007–3023.

Jongmans, D., Demanet, D., 1993. The importance of surface waves in vibration study and the use of Rayleigh waves for estimating the dynamic characteristics of soils. Engineering Geology 34 (1–2), 105–113.

Jongmans, D., Demanet, D., Horrent, C., Campillo, M., Sanchez-Sezma, F. J., 1996. Dynamic soil parameters

determination by geophysical prospecting in Mexico City : implication for site effect modeling. Soil Dyn. and Earth. Eng. 15, 549–559.

Jougnot, D., Linde, N., Haarder, E. B., Looms, M. C., 2015. Monitoring of saline tracer movement with vertically distributed self-potential measurements at the HOBE agricultural test site, Voulund, Denmark. Journal of Hydrology 521, 314 – 327.

Karl, L., Fechner, T., Schevenels, M., François, S., Degrande, G., 2011. Geotechnical characterization of a river dyke by surface waves. Near Surface Geophysics 9 (6), 515 – 527.

Kaslilar, A., 2007. Inverse scattering of surface waves: imaging of near-surface heterogeneitie. Geophys. J. Internat. 171, 352–367.

Khakiev, Z., Shapovalov, V., Kruglikov, A., Yavna, V., 2014. GPR determination of physical parameters of railway structural layers. Journal of Applied Geophysics 106, 139–145.

Khalaf, A., Camerlynck, C., Florsch, N., Schneider, A., 2018. Development of an adaptive multi-method algorithm for automatic picking of first arrival times: application to near surface seismic data. Near Surface Geophysics 16 (5), 507–526.

Khidas, Y., Jia, X., 2012. Probing the shear-band formation in granular media with sound waves. Physical Review E 85, 051302.

Köhn, D., Meier, T., Fehr, M., De Nil, D., Auras, M., 2016. Application of 2D elastic Rayleigh waveform inversion to ultrasonic laboratory and field data. Near Surface Geophysics 14, 461 – 476.

Kim, G., Kim, J.-Y., Kurtis, K. E., Jacobs, L. J., Pape, Y. L., Guimaraes, M., 2016. Quantitative evaluation of carbonation in concrete using nonlinear ultrasound. Materials and Structures 49, 399–409.

Klotzsche, A., van der Kruk, J., Bradford, J., Vereecken, H., 2014. Detection of spatially limited high-porosity layers using crosshole gpr signal analysis and full-waveform inversion. Water Resour. Res. 50.

Komatitsch, D., Martin, R., 2007. An unsplit convolutional Perfectly Matched Layer improved at grazing incidence for the seismic wave equation. Geophysics 72 (5), SM155–SM167.

Konstantaki, L. A., Carpentier, S. F. A., Garofalo, F., Bergamo, P., Socco, L. V., 2013. Determining hydrological and soil mechanical parameters from multichannel surface-wave analysis across the Alpine Fault at Inchbonnie, New Zealand. Near Surface Geophysics 11 (4), 435–448.

Krawczyk, C. M., Buddensiek, M.-L., Oncken, O., Kukowski, N., 2013. Seismic imaging of sandbox experiments – laboratory hardware setup and first reflection seismic sections. Solid Earth 4, 93–104.

Kuessner, M., Bouchez, J., Dangeard, M., Bodet, L., Julien, T., Didon-Lescot, J.-F., Grard, N., Domergue, J.-M., Guérin, R., Gaillardet, J., 2017. A multidisciplinary investigation of groundwater fluctuations and their control on river chemistry – insights from river dissolved concentrations and li isotopes during flood events.

Kyrkou, K., 2016. Characterization of the mechanical properties of a railway embankment through seismic surface-waves: Application on a classic line. Rapport de Master 2 - Univ. Paris 7.

Lai, C. G., Rix, G. J., Foti, S., Roma, V., 2002. Simultaneous measurement and inversion of surface wave dispersion and attenuation curves. Soil Dynamics and Earthquake Engineering 22 (9–12), 923–930.

Le Feuvre, M., Joubert, A., Leparoux, D., Côte, P., 2015. Passive multi-channel analysis of surface waves with cross-correlations and beamforming. application to a sea dike. Journal of Applied Geophysics 114, 36 – 51.

Lecocq, T., Longuevergne, L., Pedersen, H. A., Brenguier, F., Stammler, K., 2017. Monitoring ground water storage at mesoscale using seismic noise: 30 years of continuous observation and thermo-elastic and hydrological modeling. Scientific Reports.

Lee, J., Santamarina, J., 2005. Bender elements: Performance and signal interpretation. Journal of Geotechnical and Geoenvironmental Engineering 131 (9), 1063–1070.

Legland, J.-B., Tournat, V., Dazel, O., Novak, A., Gusev, V., 2012. Linear and nonlinear Biot waves in a noncohesive granular medium slab: Transfer function, self-action, second harmonic generation. Journal of the Acoustical Society of America 131 (6), 4292–4303.

Liu, C.-H., Nagel, S. R., 1992. Sound in sand. Phys. Rev. Lett. 68, 2301–2304.

Longuevergne, L., Florsch, N., Boudin, F., Oudin, L., Camerlynck, C., 2009. Tilt and strain deformation induced by hydrologically active natural fractures: application to the tiltmeters installed in Sainte-Croix-aux-Mines observatory (France). Geophysical Journal International 178 (2), 667–677.

Lorenzo, J. M., Smolkin, D. E., White, C., Chollett, S. R., Sun, T., 2013. Benchmark hydrogeophysical data from a physical seismic model. Computers & Geosciences 50, 44–51.

Lu, L., Chekroun, M., Abraham, O., Maupin, O., Villain, G., 2011. Mechanical properties estimation of functionally graded materials using surface waves recorded with a laser interferometer. NDTE 44 (2), 169–177.

Lu, N., Likos, W. J., 2004. Unsaturated soil mechanics. Wiley.

Lu, Z., 2014. Feasibility of using a seismic surface wave method to study seasonal and weather effects on shallow

surface soils. Journal of Environmental and Engineering Geophysics 19 (2), 71–85.
Lu, Z., Sabatier, J. M., 2009. Effects of soil water potential and moisture content on sound speed. Soil Science Society of America Journal 73 (5), 1614–1625.
Lumley, D., Landro, M., Vasconcelos, I., Eisner, L., Hatchell, P., Li, Y., Saul, M., Thompson, M., 2015. Advances in time-lapse geophysics — introduction. Geophysics 80, WAi–WAii.
Maillot, B., 2013. A sedimentation device to produce uniform sand packs. Tectonophysics 593, 85–94.
Maineult, A., 2016. Estimation of the electrical potential distribution along metallic casing from surface self-potential profile. Journal of Applied Geophysics 129, 66–78.
Makse, H. A., Gland, N., Johnson, D. L., Schwartz, L. M., 1999. Why effective medium theory fails in granular materials. Phys. Rev. Lett. 83 (24).
Makse, H. A., Gland, N., Johnson, D. L., Schwartz, L. M., 2004. Granular packings: Nonlinear elasticity, sound propagation, and collective relaxation dynamics. Physical Review E 70.
Marçais, J., de Dreuzy, J.-R., 2017. Prospective interest of deep learning for hydrological inference. Groundwater 55 (5), 688–692.
Maraschini, M., Ernst, F., Foti, S., Socco, L. V., 2010. A new misfit function for multimodal inversion of surface waves. Geophysics 75 (4), G31–G43.
Mari, J.-L., Arens, G., Chapellier, D., Gaudiani, P., 2004. Géophysique de gisement et de génie civil. Technip.
Martin, R., Bodet, L., Tournat, V., Rejiba, F., 2018. Seismic wave propagation in nonlinear viscoelastic media using the auxiliary differential equation method. Geophysical Journal International 216 (1), 453–469.
Martin, R., Komatitsch, D., 2009. An unsplit convolutional perfectly matched layer technique improved at grazing incidence for the viscoelastic wave equation. Geophys. J. Internat. 179 (1), 333–344.
Martin, R., Komatitsch, D., Ezziani, A., 2008. An unsplit convolutional perfectly matched layer improved at grazing incidence for seismic wave equation in poroelastic media. Geophysics 73 (4), T51–T61.
Matthews, M. C., Hope, V. S., Clayton, C. R. I., 1996. The use of surface waves in the determination of ground stiffness profiles. Geotechnical Eng. 119, 84–95.
McMechan, G. A., Yedlin, M. J., 1981. Analysis of dispersive waves by wave field transformation. Geophysics 46, 869–874.
Meier, U., Shapiro, N., Brenguier, F., 2010. Detecting seasonal variations in seismic velocities within los angeles basin from correlations of ambient seismic noise. Geophys. J. Int. 181, 985–996.
Mikesell, T. D., van Wijk, K., Otheim, L. T., Marshall, H.-P., Kurbatov, A., 2017. Laser ultrasound observations of mechanical property variations in ice cores. Geosciences 7 (3).
Miller, R. D., Xia, J., Park, C. B., Ivanov, J., 1999. Multichannel analysis of surface waves to map bedrock. The Leading Edge 18 (12), 1392–1396.
Mindlin, R., 1949. Compliance of elastic bodies in contact. J. Appl. Mech., ASME 16, 259–268.
Mokhtar, T. A., Herrmann, R. B., Russell, D. R., 1988. Seismic velocity and Q model for the shallow structure of the Arabian shield from short-period Rayleigh waves. Geophysics 53, 1379–1387.
Mouhri, A., Flipo, N., Rejiba, F., de Fouquet, C., Bodet, L., Kurtulus, B., Tallec, G., Durand, V., Jost, A., Ansart, P., Goblet, P., 2013. Designing a multi-scale sampling system of stream–aquifer interfaces in a sedimentary basin. Journal of Hydrology 504, 194–206.
Mourgues, R., Bureau, D., Bodet, L., Gay, A., Gressier, J., 2012. Formation of conical fractures in sedimentary basins: Experiments involving pore fluids and implications for sandstone intrusion mechanisms. Earth and Planetary Science Letters 313, 67–78.
Mourgues, R., Cobbold, P., 2003. Some tectonic consequences of fluid overpressures and seepage forces as demonstrated by sandbox modelling. Tectonophysics 376, 75–97.
Mourgues, R., Cobbold, P., 2006. Sandbox experiments on gravitational spreading and gliding in the presence of fluid overpressures. Journal of Structural Geology 28 (5), 887 – 901.
Mourgues, R., Gressier, J., Bodet, L., Bureau, D., Gay, A., 2011. "basin scale" versus "localized" pore pressure/stress coupling–implications for trap integrity evaluation. Marine and Petroleum Geology 28 (5), 1111–1121.
Murillo, C., Thorel, L., Caicedo, B., 2009. Ground vibration isolation with geofoam barriers: Centrifuge modeling. Geotextiles and Geomembranes 27, 423–434.
Nazarian, S., Stokoe II, K. H., 1984. In situ shear wave velocity from spectral analysis of surface waves. Proc. 8th Conf. on Earthquake Eng, S. Francisco 3, 31–38.
Nebieridze, S., Leroux, P., 2012. Geotechnics, geophysics; a help to the earthworks diagnosis example: The excavation of Versigny. In: Journées Nationales de Géotechnique et de Géologie de l'Ingénieur JNGG2012–Bordeaux 4-6 juillet 2012.
Neducza, B., 2007. Stacking of surface waves. Geophysics 72 (2), V51–V58.

Nenna, V., Pidlisecky, A., Knight, R., 2011. Application of an extended Kalman filter approach to inversion of time-lapse electrical resistivity imaging data for monitoring recharge. Water Resources Research.

Nishizawa, O., Kitagawa, G., 2007. An experimental study of phase angle fluctuation in seismic waves in random heterogeneous media: time-series analysis based on multivariate AR model. Geophys. J. Internat. 169, 149–160.

Nishizawa, O., Satoh, T., Lei, X., Kuwahara, Y., 1997. Laboratory studies of seismic wave propagation in inhomogeneous media using a laser Doppler vibrometer. Bull. Seism. Soc. Am. 87, 809–823.

O'Donovan, J., O'Sullivan, C., Marketos, G., 2012. Two-dimensional discrete element modelling of bender element tests on an idealised granular material. Granular Matter 14 (6), 733–747.

O'Neill, A., 2003. Full-waveform reflectivity for modelling, inversion and appraisal of seismic surface wave dispersion in shallow site investigations. Ph.D. thesis, The University of Western Australia, School of Earth and Geographical Sciences.

O'Neill, A., Dentith, M., List, R., 2003. Full-waveform P-SV reflectivity inversion of surface waves for shallow engineering applications. Expl. Geophys. 34 (3), 158–173.

O'Neill, A., Matsuoka, T., 2005. Dominant higher surface-wave modes and possible inversion pitfalls. J. Env. and Eng. Geophys. 10 (2), 185–202.

Palermo, A., Krödel, S., Matlack, K. H., Zaccherini, R., Dertimanis, V. K., Chatzi, E. N., Marzani, A., Daraio, C., 2018. Hybridization of guided surface acoustic modes in unconsolidated granular media by a resonant metasurface. Physical Review Applied 9, 054026.

Pan, Y., Gao, L., Bohlen, T., 2019. High-resolution characterization of near-surface structures by surface-wave inversions: From dispersion curve to full waveform. Surveys in Geophysics.

Park, C. B., Miller, R. D., Xia, J., 1999. Multichannel analysis of surface waves. Geophysics 64 (3), 800–808.

Parsekian, A., Singha, K., Minsley, B. J., Holbrook, W. S., Slater, L., 2015. Multiscale geophysical imaging of the critical zone. Reviews of Geophysics 53 (1), 1–26.

Pasquet, S., 2014. Apport des méthodes sismiques à l'hydrogéophysique : importance du rapport V_P/V_S et contribution des ondes de surface. Ph.D. thesis, Université Pierre et Marie Curie, Paris, France.

Pasquet, S., Bodet, L., 2017. SWIP: An integrated workflow for surface-wave dispersion inversion and profiling. Geophysics 82 (6), WB47–WB61.

Pasquet, S., Bodet, L., Bergamo, P., Guérin, R., Martin, R., Mourgues, R., Tournat, V., 2016a. Small-scale seismic monitoring of varying water levels in granular media. Vadose Zone Journal 15 (7).

Pasquet, S., Bodet, L., Dhemaied, A., Mouhri, A., Vitale, Q., Rejiba, F., Flipo, N., Guérin, R., 2015a. Detecting different water table levels in a shallow aquifer with combined P-, surface and SH-wave surveys: insights from Vp/Vs or poisson's ratios. Journal of Applied Geophysics 113, 38–50.

Pasquet, S., Bodet, L., Longuevergne, L., Dhemaied, A., Camerlynck, C., Rejiba, F., Guérin, R., 2015b. 2D characterization of near-surface VP/VS: surface-wave dispersion inversion versus refraction tomography. Near Surface Geophysics 13 (4), 315–331.

Pasquet, S., Holbrook, W. S., Carr, B. J., Sims, K. W. W., 2016b. Geophysical imaging of shallow degassing in a Yellowstone hydrothermal system. Geophysical Research Letters 43 (23), 2016GL071306.

Perol, T., Gharbi, M., Denolle, M., 2018. Convolutional neural network for earthquake detection and location. Science Advances 4 (2), e1700578.

Piatti, C., Socco, L., Boiero, D., Foti, S., 2013. Constrained 1D joint inversion of seismic surface waves and P-refraction traveltimes. Geophysical Prospecting 61 (1), 77–93.

Polom, U., Alrshdan, H., Al-Halbouni, D., Holohan, E. P., Dahm, T., Sawarieh, A., Atallah, M. Y., Krawczyk, C. M., 2018. Shear wave reflection seismic yields subsurface dissolution and subrosion patterns: application to the Ghor Al-Haditha sinkhole site, Dead Sea, Jordan. Solid Earth 9 (5), 1079–1098.

Prasad, M., 2002. Acoustic measurements in unconsolidated sands at low effective pressure and overpressure detection. Geophysics 67 (2), 405–412.

Pride, S. R., 2005. Relationships between Seismic and Hydrological Properties. Springer Netherlands, Dordrecht, pp. 253–290.

Rhamania, I., 2015. Caractérisation mécanique de la plateforme ferroviaire par sismique ondes de surface : application à une ligne classique. Rapport de Master 2 - UPMC.

Rix, G. J., Lai, C. G., Foti, S., 2001. Simultaneous measurement of surface wave dispersion and attenuation curves. Geotechnical testing journal 24 (4), 350–358.

Rosas-Carbajal, M. R., Linde, N., Kalscheuer, T., 2012. Focused time-lapse inversion of radio and audio magnetotelluric data. Journal of Applied Geophysics 84, 29–38.

Rubin, Y., et al., 1999. The handbook of groundwater engineering.

Ruiz, A., Nagy, P. B., 2004. Laser-ultrasonic surface wave dispersion measurements on surface-treated metals. Ultra-

sonics 42, 665–669.
Russel, D. R., 1987. Multi-channel processing of dispersed surface waves. Ph.D. thesis, Saint Louis University, Saint Louis, Missouri, USA.
Rydén, N., Ulriksen, P., Park, C. B., 2004. Surface waves in inversely dispersive media. Near Surface Geophysics 2 (4), 187–197.
Rydén, N., Ulriksen, P., Park, C. B., Miller, R. D., Xia, J., Ivanov, J., 2001. High frequency MASW for non-destructive testing of pavements–accelerometer approach. In: Symposium on the Application of Geophysics to Engineering and Environmental Problems. Environmental and Engineering Geophysical Society, pp. 1–12.
Sabbione, J. I., Velis, D., 2010. Automatic first-breaks picking: New strategies and algorithms. GEOPHYSICS 75 (4), V67–V76.
Sambridge, M., 1999. Geophysical inversion with a neighbourhood algorithm—I. Searching a parameter space. Geophysical Journal International 138 (2), 479–494.
Santamarina, J., Rinaldi, V., Fratta, D., Klein, K., Wang, Y., Cho, G., Cascante, G., 2005. 4. A Survey of Elastic and Electromagnetic Properties of Near-Surface Soils. In: Near-Surface Geophysics. Investigations in Geophysics. Society of Exploration Geophysicists, pp. 71–88.
Saragiotis, C. D., Hadjileontiadis, L. J., Panas, S. M., 2002. PAI-S/K: A robust automatic seismic P phase arrival identification scheme. IEEE Transactions on Geoscience and Remote Sensing 40 (6), 1395–1404.
Saussine, G., Dhemaied, A., Delforge, Q., Benfeddoul, S., 2017. Statistical analysis of cone penetration resistance of railway ballast. Georail 2017, Marne-La-Vallee, France 140, 16011.
Sawangsuriya, A., Edil, T. B., Bosscher, P. J., 2008. Modulus-suction-moisture relationship for compacted soils. Canadian Geotechnical Journal 45 (7), 973–983.
Sawangsuriya, A., Edil, T. B., Bosscher, P. J., 2009. Modulus-suction-moisture relationship for compacted soils in postcompaction state. Journal of Geotechnical and Geoenvironmental Engineering 135 (10), 1390–1403.
Scales, J. A., Malcolm, A. E., 2003. Laser characterization of ultrasonic wave propagation in random media. Physical Review E E 67, 046618–046624.
Scales, J. A., van Wijk, K., 1999. Multiple scattering attenuation and anisotropy of ultrasonic surface waves. Applied Physics Letters 74, 3899–3901.
Schmelzbach, C., Green, A., Horstmeyer, H., 2005. Ultra-shallow seismic reflection imaging in a region characterized by high source-generated noise. Near Surface Geophysics 3 (16).
Schneider, S., 2017. Geophysical interpolation of hydrodynamic properties in the vadoze zone. Master's thesis, Université de Rennes 1.
Schon, J. H., 1996. Physical properties of rocks: Fundamentals and Principles of Petrophysics (Handbook of Geophysical Exploration Series). Elsevier.
Schuite, J., Longuevergne, L., Bour, O., Boudin, F., Durand, S., Lavenant, N., 2015. Inferring field-scale properties of a fractured aquifer from ground surface deformation during a well test. Geophysical Research Letters 42 (24), 10–696.
Schuster, G. T., Quintus-Bosz, A., 1993. Wavepath eikonal traveltime inversion: Theory. Geophysics 58 (9), 1314–1323.
Scruby, C. B., 1989. Some applications of laser ultrasound. Ultrasonics 27, 195–209.
Senkaya, M., Karsli, H., 2014. A Semi-Automatic Approach to Identify First Arrival Time: the Cross-Correlation Technique (CCT). Earth Sciences Research Journal 18, 107 – 113.
Sheriff, R. E., Geldart, L. P., 1995. Exploration seismology. Cambridge university press.
Sherlock, D. H., 1999. Seismic imaging of sandbox models. Ph.D. thesis, Curtin University of Technology.
Sherlock, D. H., Evans, B. J., 2001. The development of seismic reflection sandbox modelling. AAPG Bulletin 85, 1645–1659.
Shi, Z., Hobbs, R. W., Moorkamp, M., Tian, G., Jiang, L., 2017. 3-D cross-gradient joint inversion of seismic refraction and DC resistivity data. Journal of Applied Geophysics 141, 54 – 67.
Shirley, D. J., Hampton, L. D., 1978. Shear-wave measurements in laboratory sediments. The Journal of the Acoustical Society of America 63 (2), 607–613.
Sidler, R., Carcione, J. M., Holliger, K., 2010. Simulation of surface waves in porous media. Geophysical Journal International 183 (2), 820–832.
Singha, K., Day-Lewis, F. D., Johnson, T., Slater, L. D., 2015. Advances in interpretation of subsurface processes with time-lapse electrical imaging. Hydrological Processes 29 (6), 1549–1576.
Sivaji, C., Nishizawa, O., Kitagawa, G., Fukushima, Y., 2002. A physical-model study of the statistics of seismic waveform fluctuations in random heterogeneous media. Geophys. J. Internat. 148, 575–595.
Socco, L., Foti, S., Boiero, D., 2010. Surface-wave analysis for building near-surface velocity models—established

approaches and new perspectives. Geophysics 75 (5), 75A83–75A102.
Socco, L. V., Boiero, D., Foti, S., Wisén, R., 2009. Laterally constrained inversion of ground roll from seismic reflection records. Geophysics 74 (6), G35–G45.
Socco, L. V., Strobbia, C., 2004. Surface-wave method for near surface characterization: a tutorial. Near Surface Geophysics 2 (4), 165–185.
Solymosi, B., Favretto-Cristini, N., Monteiller, V., Komatitsch, D., Cristini, P., Arntsen, B., Ursin, B., 2018. How to adapt numerical simulation of wave propagation and ultrasonic laboratory experiments to be comparable—a case study for a complex topographic model. Geophysics 83 (4), T195–T207.
Souloumiac, P., Krabbenhøft, K., Leroy, Y. M., Maillot, B., 2010. Failure in accretionary wedges with the maximum strength theorem: numerical algorithm and 2D validation. Computers & Geosciences 14, 793–811.
Souloumiac, P., Maillot, B., Leroy, Y. M., 2012. Bias due to side wall friction in sand box experiments. Journal of Structural Geology 35, 90–101.
Spetzler, J., Sivaji, C., Nishizawa, O., Fukushima, Y., 2002. A test of ray theory and scattering theory based on a laboratory experiment using ultrasonic waves and numerical simulation by finite-difference method. Geophys. J. Internat. 148, 165–178.
Steinel, H., Hausmann, J., Werban, U., Dietrich, P., 2014. Reliability of MASW profiling in near-surface applications. Near Surface Geophysics 12 (2046).
Sussmann Jr, T., Thompson II, H., Stark, T., Wilk, S., Ho, C., 2017. Use of seismic surface wave testing to assess track substructure condition. Construction and Building Materials 155, 1250–1255.
Suzaki, A., Minato, S., Ghose, R., Konishi, C., Sakai, N., 2017. Modelling time-lapse shear-wave velocity changes in an unsaturated soil embankment due to water infiltration and drainage. First Break 35, 81–90.
Talfumiere, V., Nebieridze, S., 2008. Detection of cavities using ambient noise as seismic source – gare de l'est. In: Journées Nationales de Géotechnique et de Géologie de l'Ingénieur JNGG'08 - Nantes, 18-20 juin 2008.
Terzaghi, K. v., 1936. The shearing resistance of saturated soils and the angle between the planes of shear. In: First international conference on soil Mechanics, 1936. Vol. 1. pp. 54–59.
Thomson, W. T., 1950. Transmission of elastic waves through a stratified solid medium. J. Appl. Phys. 21 (2), 89–93.
Tournat, V., Gusev, V., 2010. Acoustics of uncosolidated "model" granular media: an overview of recent results and several open problems. Acta Acustica united with Acustica 96.
Tsai, V. C., 2011. Understanding the amplitudes of noise correlation measurements. Journal of Geophysical Research: Solid Earth 116 (B9).
Turesson, A., 2007. A comparison of methods for the analysis of compressional, shear, and surface wave seismic data, and determination of the shear modulus. Journal of Applied Geophysics 61 (2), 83–91.
Uhlemann, S., Chambers, J., Wilkinson, P., Maurer, H., Merritt, A., Meldrum, P., Kuras, O., Gunn, D., Smith, A., Dijkstra, T., 2017. Four-dimensional imaging of moisture dynamics during landslide reactivation. Journal of Geophysical Research: Earth Surface 122 (1), 398–418.
Uhlemann, S., Hagedorn, S., Dashwood, B., Maurer, H., Gunn, D., Dijkstra, T., Chambers, J., 2016. Landslide characterization using P- and S-wave seismic refraction tomography — The importance of elastic moduli. Journal of Applied Geophysics 134, 64–76.
Uyanık, O., 2011. The porosity of saturated shallow sediments from seismic compressional and shear wave velocities. Journal of Applied Geophysics 73 (1), 16–24.
Valensi, R., Leparoux, D., Durand, O., Bretaudeau, F., Côte, P., 2015. Multicomponent reduced scale seismic modelling: upgrade of the musc laboratory with application to polarization observations. Geophysical Journal International 202 (3), 1993–2024.
Valois, R., 2011. Caractérisation structurale de morphologies karstiques superficielles et suivi temporel de l'infiltration à l'aide des méthodes électriques et sismiques. Thèse de doctorat, Université Pierre et Marie Curie, Paris, France.
Valverde, J. M., Castellanos, A., 2006. Random loose packing of cohesive granular materials. Europhysics Letters 75 (6), 985–991.
van Wijk, K., Hitchman, S., 2017. Apple seismology. Physics Today 70 (10).
van Wijk, K., Komatitsch, D., Scales, J. A., Tromp, J., 2004. Analysis of strong scattering at the micro-scale. J. Acoust. Soc. Am. 115 (3), 1006–1011.
van Wijk, K., Levshin, A. L., 2004. Surface wave dispersion from small vertical scatterers. Geophys. Res. Lett. 31, L20602.
Virieux, J., Asnaashari, A., Brossier, R., Métivier, L., Ribodetti, A., Zhou, W., 2017. 6. An introduction to full waveform inversion. pp. R1–1–R1–40.
Vriend, N. M., Hunt, M. L., Clayton, R. W., 2105. Linear and nonlinear wave propagation in booming sand dunes. Physics of Fluids 27 (10), 103305.

Vriend, N. M., Hunt, M. L., Clayton, R. W., Brennen, C. E., Brantley, K. S., Ruiz-Angulo, A., 2007. Solving the mystery of booming sand dunes. Geophys. Res. Lett. 34, L16306.

Wacquier, L., 2017. Caractérisation mécanique de la plateforme ferroviaire par sismique ondes de surface. Rapport de Master 2 - UR1.

Walton, K., 1978. The oblique compression of two elastic spheres. Journal of the Mechanics and Physics of Solids 26 (3), 139 – 150.

Wathelet, M., 2008. An improved neighborhood algorithm: Parameter conditions and dynamic scaling. Geophys. Res. Lett. 35, L09301.

Wathelet, M., Jongmans, D., Ohrnberger, M., 2004. Surface-wave inversion using a direct search algorithm and its application to ambient vibration measurements. Near Surface Geophysics 2 (4), 211–221.

West, M., Menke, W., 2000. Fluid-induced changes in shear velocity from surface waves. In: Symposium on the Application of Geophysics to Engineering and Environmental Problems 2000. Society of Exploration Geophysicists, pp. 21–28.

Xia, J., Miller, R. D., Park, C. B., 1999. Estimation of near-surface shear-wave velocity by inversion of Rayleigh waves. Geophysics 64 (3), 691–700.

Zimmer, M., Prasad, M., Mavko, G., Nur, A., 2007a. Seismic velocities of unconsolidated sands: Part 1 — pressure trends from 0.1 to 20 MPa. Geophysics 72 (1), E1–E13.

Zimmer, M., Prasad, M., Mavko, G., Nur, A., 2007b. Seismic velocities of unconsolidated sands: Part 2 — influence of sorting- and compaction-induced porosity variation. Geophysics 72 (1), E15–E25.

Zywicki, D., Rix, G., 2005. Mitigation of near-field effects for seismic surface wave velocity estimation with cylindrical beamformers. Journal of Geotechnical and Geoenvironmental Engineering 131 (8), 970–977.